PHOTOPRODUCTION OF POSITIVE PIONS FROM HYDROGEN NEAR THRESHOLD

Part II: Positron Decay Counting Method

by

Richard A. Carrigan and Edwin L. Goldwasser

Technical Report No. 32

Research in Nuclear Physics
at the University of Illinois
under Contract ONR 1834(05)

Physics Research Laboratory
Physics Department
University of Illinois
Urbana, Illinois

February, 1962

ACKNOWLEDGEMENTS

The High Energy Radiation Group at the National Bureau of Standards rendered substantial aid in the completion of this experiment. Dr. J. E. Leiss and Dr. S. Penner patiently explained many phases of their original experiment. They also suggested valuable improvements in the experiment described here. Dr. J. S. Pruitt and Mr. S. R. Domen made an important contribution to the entire betatron program with their help in recalibrating the betatron monitors. The authors wish to thank Dr. H. W. Koch for several useful discussions dealing with bremsstrahlung and for arranging a monitor calibration run at the National Bureau of Standards.

The active participation of Professor A. C. Odian in the design of the experiment and the first run was greatly appreciated.

The authors also wish to acknowledge helpful advice received from Professors A. O. Hanson and C. S. Robinson.

TABLE OF CONTENTS

I. INTRODUCTION

The study of the photoproduction of positive pions in the process

$$\gamma + p \longrightarrow \pi^+ + n$$

represents a clue to many of the problems of nuclear forces. For instance, measurement of the cross section near threshold should provide an accurate value of the renormalized pion-nucleon coupling constant. The threshold value of the photoproduction matrix element is related, through the Panofsky ratio, to the threshold amplitude for charge-exchange pion scattering.[1] Above the threshold region the 3.3 resonance exerts a strong and interesting effect on the cross section. For these reasons, the photoproduction interaction has been studied extensively in the past, both experimentally and theoretically. However because of the coupling of an electromagnetic process to a nuclear one the theoretical treatment of the problem is somewhat more difficult than that of meson scattering. Experimentally the photoproduction process is the more difficult one to study because of the necessity of using a bremsstrahlung spectrum.

Among the most complete experimental studies of charged meson photoproduction were those of Beneventano et al[2]. They analyzed their experimental results to obtain a value of the pion-nucleon coupling constant. In addition, the empirically extrapolated threshold value of the photoproduction matrix element was used to compare the photoproduction results with the scattering amplitudes through the Panofsky ratio and the π^-/π^+ photoproduction ratio. Some rather large discrepancies between various experiments, and

experiment and theory were found.

Cini et al.[3] noted that the theoretical analysis of the photopion process rested on very firm footing in the threshold region. There the theoretical treatment of the photoproduction process is extremely simple. Since most of the gamma ray energy goes into the production of meson mass, little angular momentum can be brought in. For this reason most of the final-state interaction is expected to be s state and consequently the differential cross section in the center of mass should be nearly constant with angle. Furthermore, in this region it is no longer necessary for the treatment to be completely relativistic. The "classical" terms of the theory should give a very good representation of the interaction. The effects of various resonances are expected to be small and the several unknown electric dipole contributions which have been mentioned in dispersion relation treatments are hopefully assumed to be negligible. Cini et al. therefore used the theoretically derived energy dependence of the matrix element near threshold and extrapolated the experimental data existing around 170 Mev to threshold. This procedure resulted in the disappearance of the previously suspected inconsistencies. It remained to justify the procedure experimentally.

Two measurements made by Barbaro et al.[4] at 160 and 219 Mev appeared to be consistent with the analysis of Cini et al. However the original data of a series of experiments very near threshold by Leiss, Penner, and Robinson [5,6] differed markedly from this analysis. Later several large corrections were applied by Leiss and Penner[7] to this data which brought it more in

accord with the Cini extrapolation. However in view of the strong dependence of the results obtained by this method upon the analytical techniques it seemed worthwhile to perform a similar set of measurements in a way that would provide some checks on the analytical methods to be applied. The experiment described in this thesis was undertaken with that purpose in mind.

Several severe limitations occur in the measurement of a cross section for pion photoproduction near threshold. The final neutron is, of course, difficult to detect. The pion comes off with very little kinetic energy. (The dynamics near threshold have been illustrated in Fig. 32 of Swanson's thesis.[8]) Typically at a laboratory gamma ray energy of 180 Mev and a laboratory angle of 90° the pion can travel about 8 cm in hydrogen and 1.1 cm in carbon of density 1.7. Below 180 Mev the situation is even worse. This restriction has limited direct counter detection of the pion to laboratory gamma ray energies of greater than 180 Mev.

A background problem also exists. The gamma rays impinging on the hydrogen target always make large numbers of positron-electron pairs. The number of particles due to the pair background decreases rapidly with increasing energy. However at 90° in the lab system there are roughly the same number of 40 Mev particles from pair production as there are from the pi-mu-electron chain and at 10° the pair cases are 1000 times as great. (See for example Miller [9].)

A third difficulty comes about because of the bremsstrahlung distribution of the gamma rays. There are some uncertainties

inherent in the determination of the energy flux in a gamma ray beam and there are further uncertainties involved in the knowledge of the partitioning of this flux into gamma rays of various energies.

Against the background of these limitations, several types of experiments have been attempted. Up to the present the most comprehensive have been those of Beneventano et al.[2] using photographic emulsions. The original results have been extended to lower energies by Barbaro et al.[4]. This was achieved by measuring the cross section at forward angles where the pions have more energy in the laboratory system. In order to accomplish this, measures had to be taken to lower the background. Outside of elaborate shielding the main method used was that of underdeveloping the emulsions to suppress the minimum ionizing tracks. Goldwasser[10] has observed that the cross sections of Beneventano et al. above 200 Mev should probably be lowered slightly due to the effect of the scattering of pions in the emulsions.

The results are in reasonable agreement with the Chew et al. dispersion relation theory. However the method is limited to pions of more than 10 Mev kinetic energy. Similar experiments in the same vein which produced comparable results have recently been performed by Gorzhevskaya et al.[11] using a thin organic target and Adamovich et al[12].

A second method, perfected by Lewis and Azuma[13], involved electronic detection utilizing the pi-mu signature. The pion was required to pass through a 10 mil dE/dx counter and then stop and decay in a second range counter. An oscilloscope was triggered

on a coincidence in time between the pi and mu pulses in the second counter and displayed both the pulses in the first and second counters. The kinetic energy of the pion was determined by pulse height analysis. The pulse heights were calibrated using the mu pulse height and the maximum energy pion that would just stop at the back of the range counter. Within the assigned errors, the experiment agreed with theory. This method is again limited to pions of at least five Mev kinetic energy. The background problem evidently could become acute at forward angles. It is also worthwhile to note that the Lewis and Azuma experiment used an organic rather than a hydrogen target. Recently Rutherglen et al.[14] have extended this method to lower and higher energies.

The fact that the results of this experiment are consistent with the others provides some assurance that the monitor calibrations are understood since it uses a different x ray monitor, the Wilson quantameter[15].

A third method employs a hydrogen bubble chamber in a gamma ray beam. Although no results have been reported, such experiments have been performed by Gates et al.[16] at Berkeley and Miller and Hill at General Electric. The bubble chamber represents an ideal detector for this process since the pion tracks range from less than a centimeter to 30 centimeters. Some difficulty occurs due to the pair background. Even at very low yield rates the region of the beam is almost totally obscured. The situation can be improved by employing a beam hardener but this in turn complicates the monitor problem. Eventually this method will

probably produce the best results.

The fourth method, developed by Leiss, Penner, and Robinson[5] and employed in this experiment, detects the positron from the decay of the mu meson. The pion is stopped in a carbon absorber surrounding the hydrogen target. Then it decays into a muon and in turn the muon decays into an energetic positron. The positrons are counted by a counter telescope. The cross section is obtained by the analysis of an activation curve as a function of gamma ray energy.

Table I is a tabulation of some of the experimental values of the positive pion photoproduction cross section in the threshold region. Some of the points have also been plotted in Fig. 1 along with the theoretical prediction of Chew et al.

Table I: Values of $\left.\frac{d\sigma^+}{d\Omega}\right|_{c.m.}$ and a_o obtained in several experiments in the threshold region. $\left.\frac{d\sigma^+}{d\Omega}\right|_{c.m.}$ is given in units of 10^{-30} cm^2/ster. Gamma ray energies are laboratory energies in Mev. a_o is given in units of 10^{-30} cm^2/ster.

A. Emulsion experiments.

1.) Beneventano et al.[2] (93° values are Bernardini and Goldwasser [17] with a more extensive scan.) Angles are center of mass angles.

a) Cross sections

E_γ	59°	93°	123°	159°
170	5.2 ± .4	5.4 ± .4		
180	6.5 ± .5	7.5 ± .4	7.6 ± .5	6.6 ± .9
190	7.2 ± .5	9.1 ± .5	8.7 ± .6	7.5 ± .6

b) $a_o = 14.8 \pm .2$

2.) Barbaro et al.[4]

E_γ	$\frac{d\sigma^+}{d\Omega}$ (50° - lab.)
160	4.6 ± .5

3.) Adamovich et al.[12] (Includes Gorzhevskaya et al.[11]) a_o evaluated from their $|K_p|^2$ assuming an isotropic angular distribution.

E	$\frac{d\sigma^+}{d\Omega}$ (120° - c.m.)	a_o
156.5	3.4 ± .6	19 ± 3
159.5	4.2 ± 1.7	16 ± 6.5
162.5	6.7 ± 1.5	
167.5	5.94 ± .97 ($\theta = 103°$)	
172.5	7.50 ± .58	

B. π - μ signature experiments.

1.) Lewis and Azuma[13]

E	$\frac{d\sigma^+}{d\Omega}$ (115° - lab.)	$\frac{d\sigma^+}{d\Omega}$ (90° - lab.)	a_o
170		4.8 ± 1.1	13.6 ± 3.0
175	6.0 ± 1.0	5.8 ± .9	14.1 ± 2.2
180	6.8 ± 1.0		
185		7.3 ± 1.1	14.2 ± 2.2

2.) Rutherglen et al[14]. a_o extrapolated from 50° lab. using angular distribution of Beneventano et al[2]. (Values taken from graph.)

E_γ	a_o
162	22 ± 3
171	18 ± 2
191	15.5 ± 1
200	15.5 ± 1

C. Positron detection experiments. $\frac{d\sigma^+}{d\Omega}$ c.m. obtained by assuming an isotropic angular distribution.

1.) Leiss [18]

E_γ	$\frac{d\sigma^+}{d\Omega}$ (90° - c.m.)
151.8	.28 ± .17
152.8	1.24 ± .29
154.8	2.15 ± .36
156.8	2.47 ± .32
158.8	3.70 ± .34
160.8	4.96 ± .36
162.8	4.69 ± .36
164.8	5.26 ± .40
166.8	5.55 ± .39
168.8	5.19 ± .48
170.8	6.05 ± .45
172.8	7.34 ± .59
174.8	6.63 ± .49
176.8	5.49 ± .62
178.7	6.27 ± .63

2.) Penner[19]

E_γ	$\frac{d\sigma^+}{d\Omega}$ (90° - c.m.)
156.6	2.41 ± .21
158.6	3.09 ± .27
160.6	3.70 ± .31
162.6	5.30 ± .39
164.7	5.12 ± .41
166.7	5.13 ± .52
168.7	4.62 ± .52
170.7	3.49 ± .64
172.7	6.60 ± .64
174.7	7.06 ± .78
176.7	5.53 ± .80
178.7	8.82 ± .88

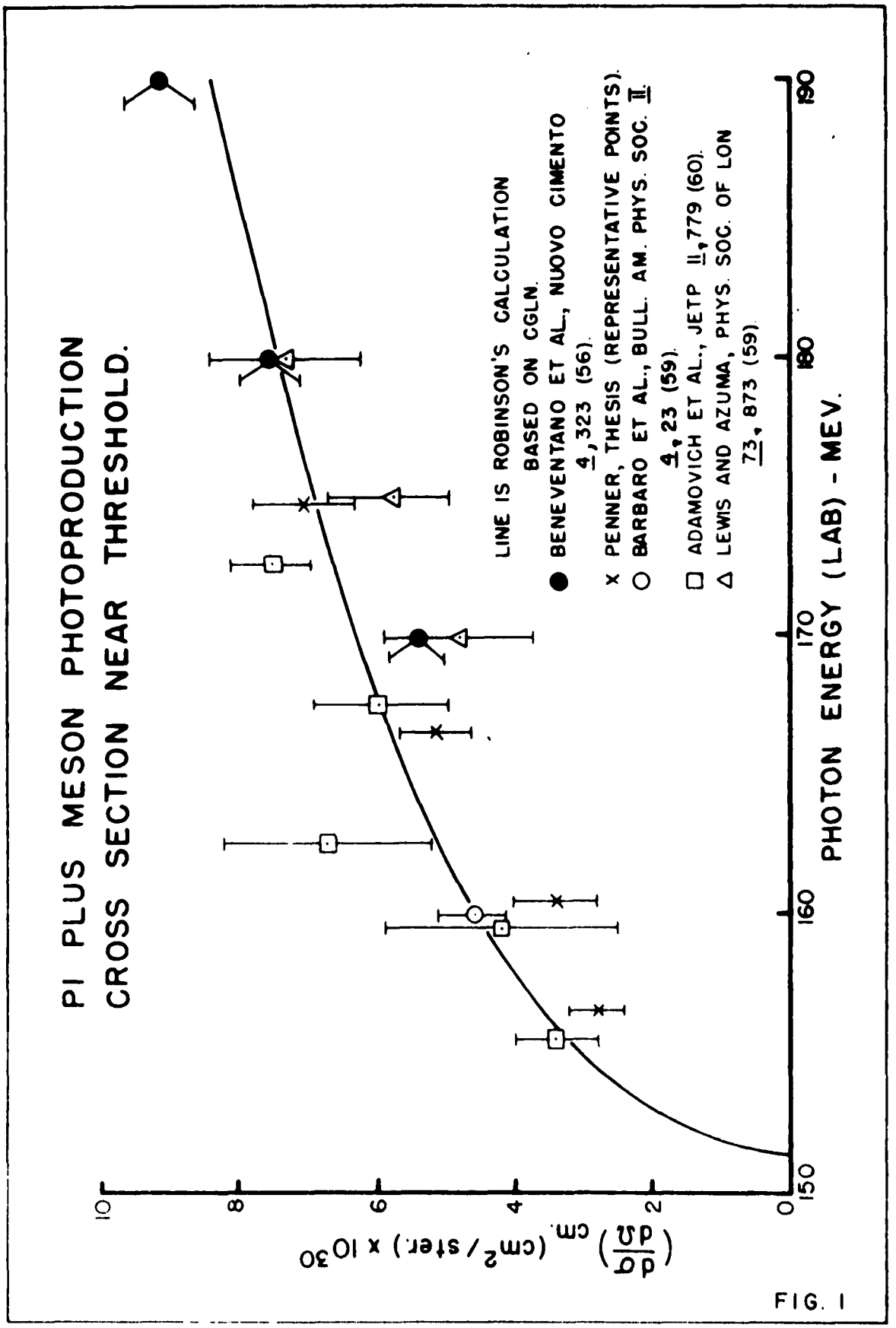
PI PLUS MESON PHOTOPRODUCTION
CROSS SECTION NEAR THRESHOLD.
LINE IS ROBINSON'S CALCULATION BASED ON CGLN.
● BENEVENTANO ET AL., NUOVO CIMENTO 4,323 (56).
× PENNER, THESIS (REPRESENTATIVE POINTS).
○ BARBARO ET AL., BULL. AM. PHYS. SOC. II. 4,23 (59).
□ ADAMOVICH ET AL., JETP 11,779 (60).
△ LEWIS AND AZUMA, PHYS. SOC. OF LON 73, 873 (59).
PHOTON ENERGY (LAB) - MEV.
150
160
170
180
190
0
2
4
6
8
10
(dσ/dΩ) cm. (cm²/ster.) x 10³⁰

FIG. 1

II. THEORY

Modern theories of pion-nucleon interactions are very complicated. The present, fairly successful, relativistic dispersion relation treatment due to Chew, Goldberger, Low and Nambu[20] (CGLN) employs a very abstract mathematical approach. The numerical evaluation of its predictions is a difficult procedure by itself. In addition, it relies on an earlier treatment, the cutoff model [21,22,23] as a guide. That too is difficult to understand. Both of these theories have roots in attempts to explain the success of thephenomenological model[24]. Baldin and Govorkov [25] have expressed the difficulty encountered in relating these theories to experiment by stating, "Comparison of the inferences from quantum field theory and the experimental data of π-meson physics is one of the most complex and stimulating problems." In view of this problem a discussion of the physical basis underlying some of the generally accepted terms in the photoproduction cross section is useful. Then the evaluation of the renormalized pion-nucleon coupling constant using the functional form of the cross section may be explained. Finally brief mention is made of recent attempts to generalize the dispersion relation method.

A naive picture of the photoproduction process might visualize the nucleon as being in some meson-nucleon state. If one or both of the particles were charged the system would possess a dipole moment. The photoproduction process would then be seen as the interaction of the photon with the electric dipole moment. For photoproduction from hydrogen the dipole moment of the π^+ -neutron

system is roughly seven times that of the π^o -proton case. Considering this simple model one would expect the π^+ cross section to be much greater than the π^o cross section. In general, however, more π^os are produced so that the simple picture must be rejected.

In the case of meson-nucleon scattering a phenomenological approach using charge independence and an $I = 3/2$, $J = 3/2$ resonance is very successful. Charge independence is based on the idea that nuclear forces are strong and independent of the weaker electromagnetic ones. Under these circumstances isotopic spin is assumed to be conserved. If the strong meson-nucleon interaction is assumed to occur in the $I = 3/2$ state the 9,1,2 ratio for the total cross sections for $p\pi^+$, $p\pi^-$, $p\pi^o$ scattering can be understood. In addition, the total cross section for scattering exhibits a resonance-like behavior near 200 Mev. The trailing edge of the resonance agrees well with the maximum cross section predicted for a $J = 3/2$ state.

Since photoproduction is an electromagnetic interaction conservation of isotopic spin is no longer necessary. It seems reasonable, however, that the resonance would still influence the final pion-nucleon state. For instance the proton must initially be in an $I = 1/2$ state. After the gamma ray interaction this could be transformed to an $I = 3/2$ state. The z component of isotopic spin must remain the same in any case since charge is conserved. In terms of isotopic spin wave functions:

(Using the notation employed by Fermi[26])

$$\psi^{1/2}_{1/2} \xrightarrow{\text{electromagnetic}} \psi^{1/2}_{3/2} = \sqrt{2/3}\ \text{po} + \sqrt{1/3}\ \text{n+}$$

For this particular case π^o production would be twice that of π^+ production and the cross section would be primarily p state in order that the $J = 3/2$ aspect of the resonance be satisfied. The cross section would be small near threshold since enough angular momentum would not be brought in to excite the p state. These phenomenological terms describe π^o photoproduction on hydrogen quite well, partly because the π^o in the final state cannot interact with the electromagnetic field.

This model does not adequately describe π^+ photoproduction. Even near the resonance the π^+ cross section is much more than half of the π^o cross section. Near threshold it is many times as great and increases in the manner expected of an S wave cross section[24], making it necessary to look elsewhere for an explanation of the π^+ cross section.

Since the pion is a pseudoscalar the pion-nucleon interaction must also be a pseudoscalar so that the Hamiltonian may be a scalar. For this reason a pseudoscalar, strong coupling interaction of the form $\vec{\sigma} \cdot \nabla$ was proposed--that is the spin of the nucleon interacting with the momentum of the pion. By itself this form is not gauge invariant and cannot be applied to photoproduction. It can be made gauge invariant by the standard recipe of letting $\nabla \longrightarrow \nabla - ie\vec{A}$. ($\vec{A}$ is the vector potential for the electromagnetic field.) The Hamiltonian is then reformed

into creation and destruction operators on the charged pions, leaving the π^0 production unchanged (in the static limit) but adding a new effect for π^+ production. The new contribution, the so called "gauge invariant" term, leads to a final S state. Using the "gauge invariant" term alone a π^+ total cross section near threshold of the form

$$\sigma = 8\pi \left(\frac{\hbar}{\mu c}\right)^2 \left(\frac{e^2}{\hbar c}\right) f^2 \frac{\eta}{k} \qquad \text{(II-1)}$$

is predicted[26]. (η is the meson momentum in the center of mass, k is the photon momentum, μ is the pion rest mass and f^2 is the renormalized meson-nucleon coupling constant.) Notice that it goes as the first power of the momentum. Here the cross section has been expressed as the square of the meson Compton wave length multipled by electromagnetic and meson coupling constants. The above expression was derived on the basis of a static nucleon. When appropriate kinematic and recoil terms are added it is about half as large.

Although the "gauge invariant" term plays the dominant role near threshold several other terms still have important effects on the energy dependence. Cini et al.[3] have exhibited this dependence explicitly by writing the cross section in the form:

$$\left.\frac{d\sigma}{d\Omega}\right|_{90^\circ} = \frac{2e^2f^2}{\mu^2} \frac{W(\omega)}{k\omega} \left[1 - \frac{v^2}{2k^2} - \frac{g_p + g_n}{M}\omega\left(1 - \frac{v^2}{2}\right) + \underline{P}'(\omega)\right] \qquad \text{(II-2)}$$

(Notice that the matrix element has already been squared.) Here ω is the total energy of the pion in the center of mass and v is the velocity of the pion. This form uses as a guide the very similar results from the cutoff model and dispersion relations. It should be pointed out that the Kroll-Ruderman theorem states that the quantity in the brackets approaches 1 as $\omega \longrightarrow 0$.

The third term of (II-2) in the brackets is a correction to the raw "gauge invariant" term that comes about because the nucleon has finite mass and can recoil so that its charge contributes to the dipole moment of the system. In the case of π^- photoproduction the recoil term has a positive sign and acts to increase the cross section. Such a term can be understood classically and gives rise to a different cross section for the photoproduction of π^- mesons from free neutrons and π^+ mesons from free protons. In fact the ratio π^-/π^+ is predicted to be about 1.3. One simple way to see this is to compare the dipole moment of the π^-, P system with that of the π^+, N system. When these dipole moments are squared they give a ratio of $1 + \frac{2\mu}{M}$ or about 1.3. Since pure neutron targets are not readily available experiments have explored this ratio by observing the π^-/π^+ ratio from deuterium.

The second term in the brackets is due to the direct interaction of the photon with the pion. It is analogous to the photoelectric effect in atomic physics. In terms of a diagram the interaction is [27]:

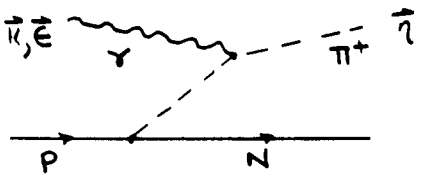

The diagram should be contrasted to the "gauge invariant" diagram for an s state:

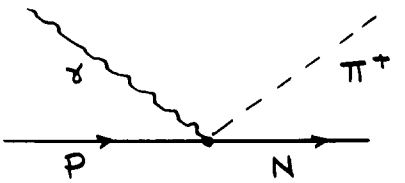

and the p state diagram:

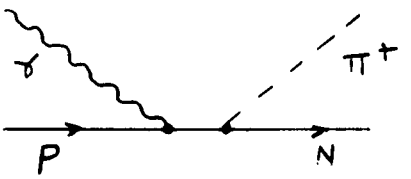

In the differential cross section the result of the direct interaction is a term of the form

$$\frac{-v^2 \sin^2 \theta}{2k^2 (1-\beta\cos\theta)^2} .$$

Physically the $1-\beta\cos\theta$ in the denominator comes about because the photon and meson can interact more when they are moving in the same direction. Moravcsik[28] has emphasized the importance of this term and pointed out that the $1-\beta\cos\theta$ in

the denominator leads to the possibility of all powers of cos Θ in the angular distribution. The effect of the direct interaction has been observed experimentally by Malmberg[29] and others as a slight increase in the cross section at very forward angles. At threshold the term is zero but at energies very near threshold it contributes appreciably, tending to lower the cross section.

$P'(\omega)$ is included in the brackets to account for the p wave contributions and their interference terms. These terms are partly analogous to the ones that dominate π^o photoproduction. Since π^o photoproduction is small near the threshold, a reasonable conclusion seems to be that $P'(\omega)$ represents a small contribution to the π^+ cross section near threshold.

$\overline{W}(\omega)$ includes terms due to the density of final states and the incident flux (See for instance Bernardini[30]). The incident flux in the center of mass is the flux in the laboratory system (c) times $(1 + \beta)$ where β is the velocity of the nucleon and is equal to $\frac{k}{E_i}$ (applying momentum conservation). The density of final states,

$$\rho = \frac{\eta^2}{2\pi^2} \quad d\eta/dE_f \quad , \tag{II-3}$$

can be found by noting that $E_f = \sqrt{\mu^2 + \eta^2} + \sqrt{M^2 + \eta^2}$.

From these two consideration $\overline{W}(\omega)/k\omega$ is found to be:

$$\frac{\overline{W}(\omega)}{k\omega} = \frac{\eta}{k} \quad \frac{1}{(1 + \frac{\omega}{E_n})(1 + \frac{k}{E_p})} \tag{II-4}$$

These kinematic terms can be applied for greater accuracy to the simple expression given for the cross section based on the "gauge invariant" term alone(II-1).

If the energy dependence of the quantity in brackets is known f^2 can be obtained by dividing the cross section by the kinematic factors and the bracket. In order to minimize the effects of the p wave and direct interaction terms an experimental value of the cross section near threshold is usually used and the cross section is extrapolated to threshold with the hypothetical energy dependence.

Bethe and DeHoffman[31] used this method by first extracting the S wave portion of the cross section and then extrapolating it to threshold using just the energy dependence of the "gauge invariant" term.

Beneventano et al.[2] used an empirical extrapolation method in which they extracted the isotropic portion of the cross section from an angular distribution analysis based on $\frac{d\sigma}{d\Omega} = A_o + A_1 \cos\theta + A_2 \cos^2\theta$ and then divided it by the phase factors. (Note that they did not strip out the $1/k\omega$ from the square of the matrix element.) They observed experimentally that this quantity, a_o, was constant over a wide range of energies. To evaluate f^2 they assumed that a_o was constant all the way to threshold. From this they obtained a value for f^2 of .067. This extrapolation procedure received some support from the original data of Leiss et al[5,6]. The Beneventano et al. extrapolation is illustrated in Fig. 2 as a dotted line.

Cini et al.[3] used experimental data at 170 Mev and the energy dependence given in formula(II-2). They obtained a value of $f^2 = .073$. The energy dependence they used is given in Fig. 2 as a solid line. At the time the extrapolation was performed it appeared to disagree with the original Leiss et al. points at low energy and the higher energy Beneventano et al. points. However reasonable corrections have been proposed for both sets of experimental data which would bring them into line with the energy dependence given.

The extrapolation procedure suggested by Cini et al. closely follows the energy dependence predicted by the CGLN dispersion relations. The recent experimental evidence of Barbaro et al.[4] and the corrected experimental values of Leiss and Penner[7] lend some weight to the Cini et al. extrapolation and in turn support the CGLN approach.

The CGLN method relied on several approximations. (These have been summarized by Baldin and Govorkov[25].) The dispersion integrals were evaluated by assuming that the 3-3 resonance represented the important contribution. In turn any high energy contributions were neglected. Recoil terms were included to order μ/M. Chew et al.[20] acknowledged these approximations in the original article but pointed out that since this type of theory neglected electromagnetic radiative effects, approximations to μ/M were sufficient. To emphasize this they noted that the same radiative corrections cause a 4% mass difference between the neutral and charged pions. In addition, the success of the cutoff model in a particular situation can be used as a guide to

a_0 COEFFICIENT VERSUS ENERGY

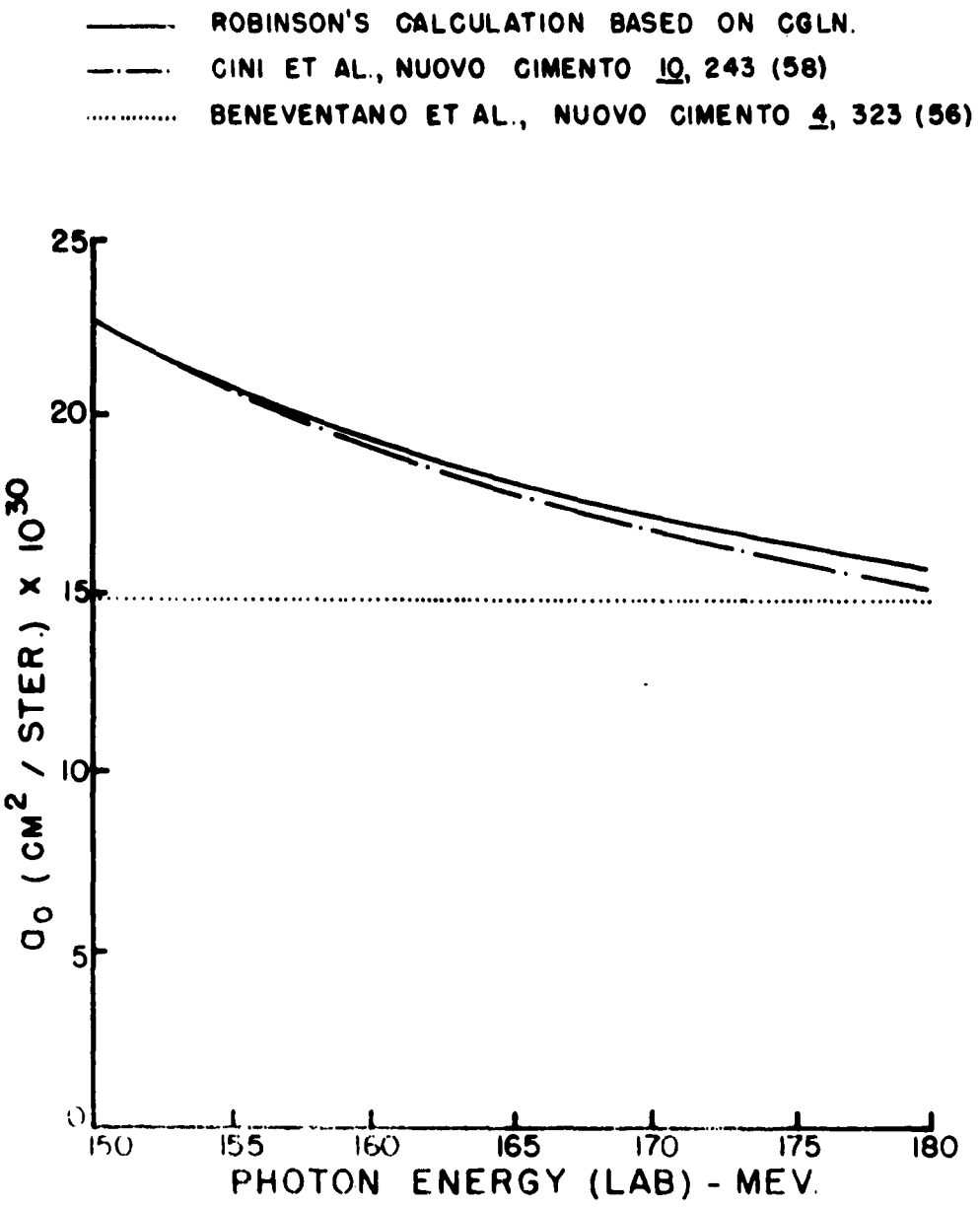

FIG. 2

the validity of neglecting high energy contributions to the dispersion integrals.

Recently however several attempts have been made to generalize the dispersion relation approach. Gartenhaus and Blankenbecler[32] and Höhler and Dietz[33] have devised dispersion integrals that account for the recoil effects exactly. Near threshold these give values very similar to CGLN. Jona-Lasinio and Munczek[34] make a "second approximation" on the dispersion relations by adding two of the Chew et al. integrals in such a way as to reduce the high energy contribution and emphasize the 3-3 resonance. Their form of the theory allows the possibility of a π^+ cross section that is somewhat smaller and has less energy dependence near threshold. Hamilton and Woolcock[35] have reviewed the situation near threshold and found it to be in good agreement with CGLN. They have also evaluated the cross section considering small negative values of the electric dipole amplitude. They find that the cross section decreases but the energy dependence does not change a great deal. They note that such a term would tend to change the π^-/π^+ ratio. Baldin[36] has pointed out the effect of the unphysical region (although his main point concerns π^o production) and indicated a small interval of energies and angles where it can be avoided. Near threshold the difficulty with the unphysical region tends to vanish.

Most of the generalizations can be summarized by stating that although they do make important contributions to such things as the S wave phase shifts in scattering (where Chew et al. feel

high energy effects would manifest themselves) they do not appreciably change the situation near the threshold of pion photoproduction.

III. DESCRIPTION OF THE EXPERIMENT

III-A. Introduction

At gamma ray energies near threshold pions have little kinetic energy and consequently very short ranges. The positron detection scheme relies on the fact that they soon decay by a sequence:

$$\pi^+ \longrightarrow \mu^+ + \nu \qquad (\tau = 2.55 \times 10^{-8}\text{s})$$

$$\mu^+ \longrightarrow e^+ + \nu + \bar{\nu} \qquad (\tau = 2.212 \times 10^{-6}\text{s})$$

The π^+ decay is a two body one. The resulting μ^+ carries off only 4.1 Mev of kinetic energy and even in liquid hydrogen has a range of just 1 cm. However the μ^+ decays into a positron which can carry off nearly half of the μ^+ rest mass as kinetic energy. The resulting positron can easily be detected with counters. The nearest competing pion decay mode is:

$$\pi^+ \longrightarrow e^+ + \nu$$

This occurs about 10^{-4} as frequently[37]. It is interesting to note that the 70 Mev positrons from the π-e decay would be detected somewhat more efficiently than those due to the μ^+ decay in this type of experiment. However even with this factor the direct decay mode is a negligible contamination.

Since the μ^+ decay is a three body decay the positrons do not have a fixed energy. Instead they are emitted with a momentum spectrum sometimes designated as a Michel spectrum. Dudziak et al.[38] give as the spectrum:

$$P(x) = \left\{1+h(x)\right\} \left\{12x^2(1-x) + 8\rho\, x^2 \left(\tfrac{4}{3}x - 1\right)\right\} \qquad \text{(III-1)}$$

where h(x) is a number small compared to 1 which includes the effect of radiative corrections, x is the momentum divided by the maximum momentum, P(x) is the number of positrons per unit momentum, and ρ is the Michel parameter. (This form neglects certain very small corrections.) The effect of the radiative corrections is to transfer probability from the upper to the lower portion of the spectrum. A large change in ρ makes very little change in the experimental spectrum. Before parity nonconservation was anticipated some experiments gave values of $\rho = .2$. Now it is generally accepted that $\rho \simeq 3/4$. In Fig. 3. (III-1) is plotted for $\rho = 3/4$ with and without radiative corrections and for $\rho = .60$ without radiative corrections (value used by Penner[19]).

In this experiment the pions were photoproduced in a cylindrical hydrogen target with its axis parallel to the x ray beam. The hydrogen was surrounded with a concentric cylindrical shell of carbon 3/4" thick. Most of the pions were stopped in this shell. These decayed into μ mesons which in turn were stopped. Finally the μ mesons decayed into positrons. The portion of the positrons with an energy greater than roughly 40 Mev was then detected by a thick, five-counter telescope. This method becomes unreliable above about 180 Mev. At this point the mesons begin to leak out of the target because their range exceeds the thickness of the absorber.

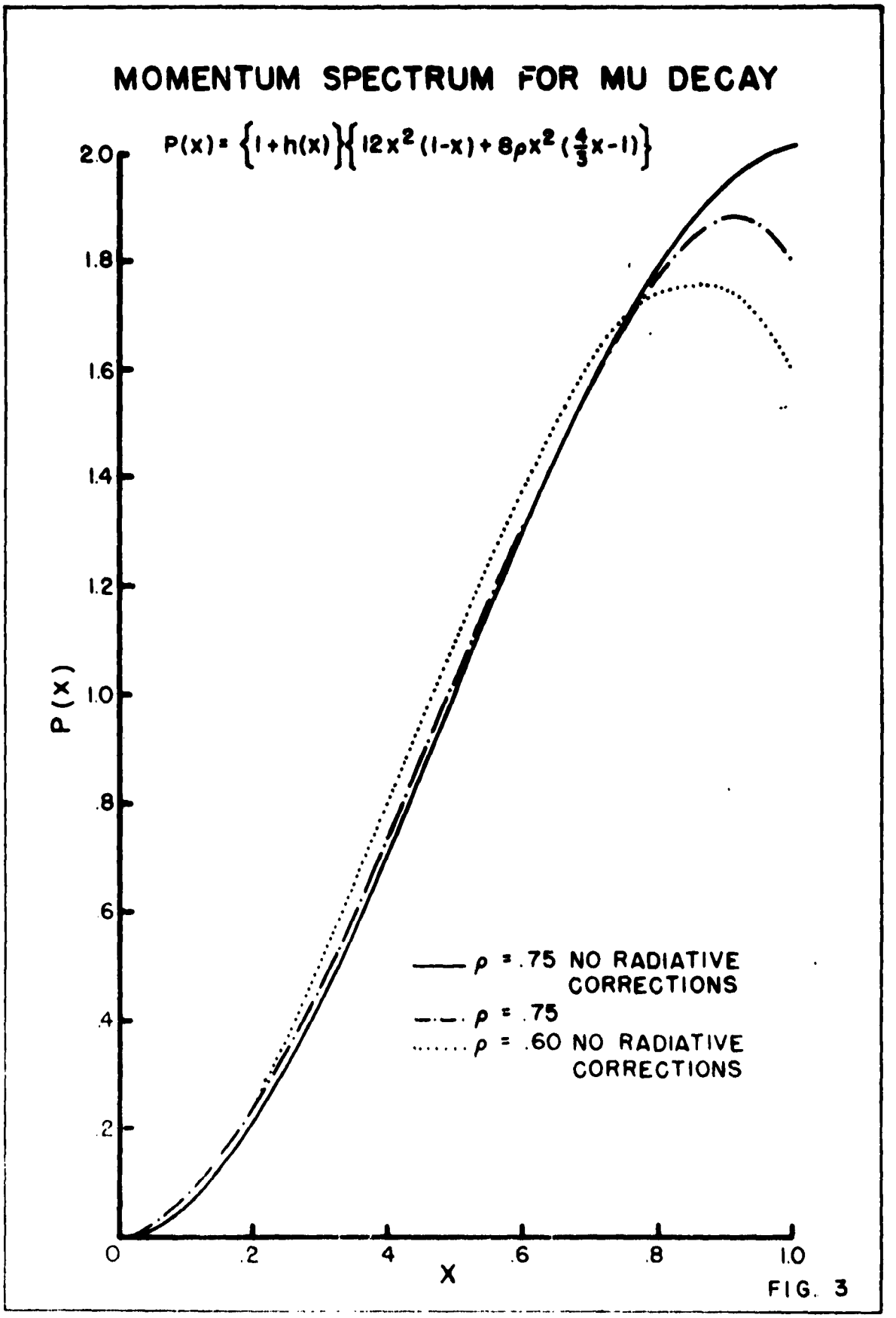
MOMENTUM SPECTRUM FOR MU DECAY
$P(x) = \{1 + h(x)\}\{12x^2(1-x) + 8\rho x^2(\frac{4}{3}x - 1)\}$
P(x)
X
2.0
1.8
1.6
1.4
1.2
1.0
.8
6
.4
.2
0
.2
4
.6
.8
1.0
ρ = .75 NO RADIATIVE CORRECTIONS
ρ = .75
ρ = .60 NO RADIATIVE CORRECTIONS

FIG. 3

High energy electrons and positrons are also produced in purely electromagnetic interactions by the incident x rays. These represent a source of background since they cannot be easily distinguished. (Malmberg[39] has distinguished the two sources by bringing out the x rays from the betatron in a burst of less than a microsecond and then turning the counters on after the burst.)

In the process of stopping the mesons all dynamical information is destroyed. This represents a serious loss because the incident x rays are from a continuous bremsstrahlung distribution having energies from the kinetic energy of the electron incident on the internal betatron target down to zero energy. As a result one can only say that a particular meson was produced by a photon below a certain energy. To overcome this difficulty activation curves are run by increasing the energy of the betatron in a series of small steps and counting at each energy. Then much of the increased counting rate at each energy is due to photons of that energy.

This type of operation can also be used to subtract the electromagnetic background by noting that below the meson threshold all the counts result from non-mesonic interactions. The "below threshold" energy dependence can then be extrapolated to the higher energies and subtracted from the counting rates above threshold.

An absolute cross section must be measured to evaluate the meson-nucleon coupling constant. Therefore the x ray monitor

must be well calibrated and the efficiency of the counting system known absolutely. (The calibration of the x ray monitor is discussed in an appendix.)

An absolute theoretical calculation of the efficiency of the counting system was made. Since positrons undergo a great deal of range straggling and multiple scattering the calculation is sensitive to the energy-loss parameters. Because of this an experimental measurement of the efficiency was also made by playing a collimated, monoenergetic beam of positrons over the face of the counter and measuring the fraction that counted as a function of energy*. In turn this fraction was compared to the theoretically predicted value.

In addition, the overall efficiency was changed drastically by substituting a copper absorber for the carbon one and thus greatly changing the effective thickness of the counting system. This gave some indication of the ability of the theoretical efficiency calculation to follow changes in the target-counter system.

This experiment yields a total cross section directly because mesons from all directions are stopped and counted on an equal basis. (Of course some angles do count less efficiently and a small forward cone is not counted at all at some energies.)

---

*NOTE: One proposed method that was not employed was to stop a known number of pions in an absorber located in the position of the target and note the fraction that counted.

III-B. Equipment

X ray beam: The x ray beam was produced by the circulating electron beam in the betatron striking an internal platinum target. The x rays then filtered through a porcelain doughnut and were collimated by a quarter-inch primary lead collimator. An appreciable portion (somewhere between one-half and three-quarters) of the x ray beam interacted with the primary collimator producing electron pairs and neutrons. A secondary lead collimator slighly larger than the beam and a boraffin neutron collimator were placed downstream from the primary collimator in order to remove part of these from the edge of the beam. From the secondary collimator to approximately 30 centimeters past the hydrogen target the x ray beam passed through a vacuum system. A 2,500 gauss sweeping field was placed in the vacuum system at the exit of the secondary collimator. The field was sufficient to deflect charged particles originating in the thin mylar window of the vacuum system away from the target. One meter past the clearing field was a liquid-hydrogen target 4.51 inches thick. At the hydrogen target the x ray beam was 2.2 centimeters in diameter. A calibrated x ray monitor, the bass drum ionization chamber, was placed several meters beyond the target. Directly after the monitor was a lead beam stop. A plan view of the target-counter area is given in Fig. 4.

Target: The hydrogen target system used in this experiment was similar to the one described by Whalin and Reitz[40].

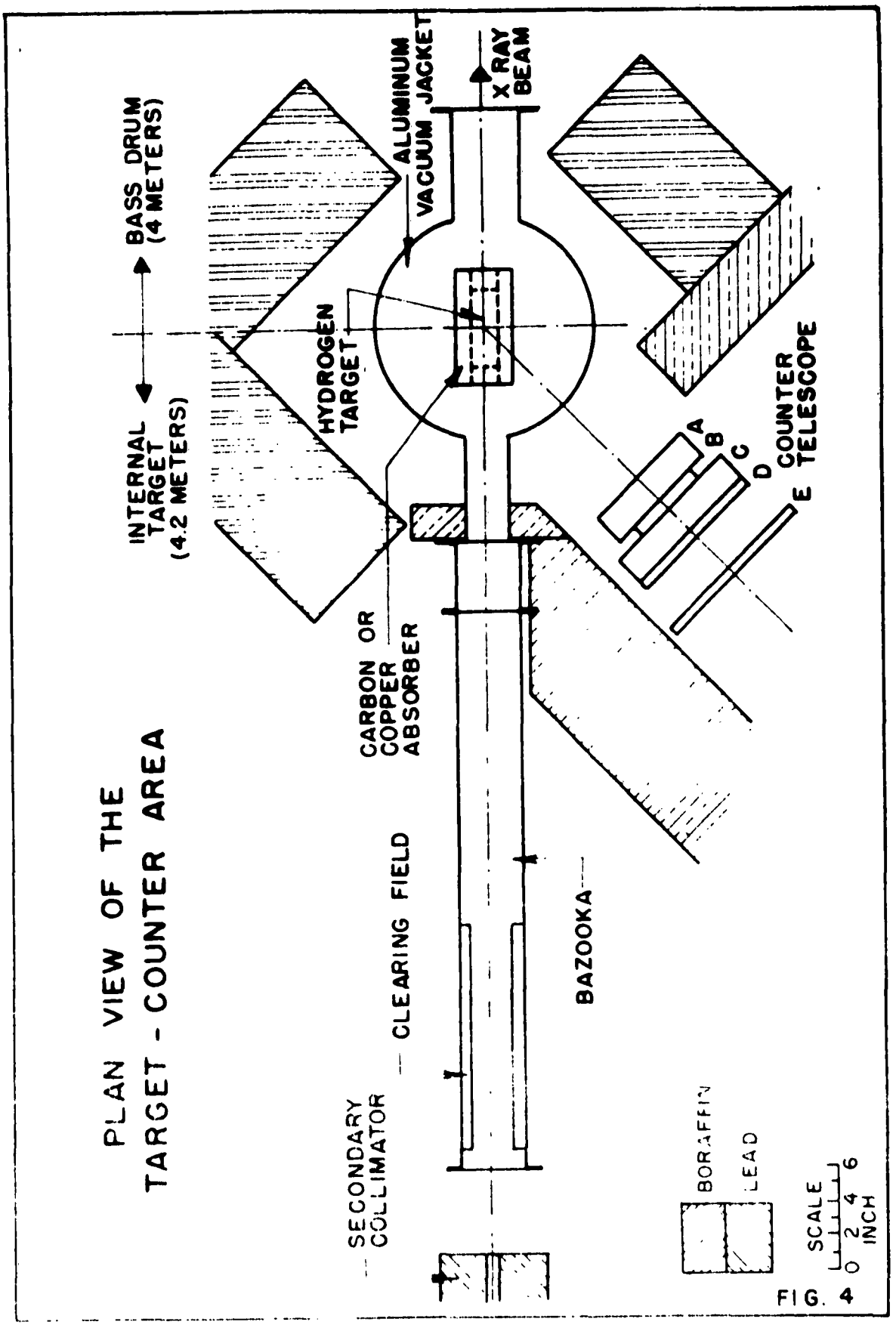
PLAN VIEW OF THE
TARGET - COUNTER AREA
BASS DRUM
(4 METERS)
INTERNAL
TARGET
(4.2 METERS)
HYDROGEN
TARGET
ALUMINUM
VACUUM JACKET
X RAY
BEAM
A
B
C
D
E
COUNTER
TELESCOPE
CARBON OR
COPPER
ABSORBER
CLEARING FIELD
BAZOOKA
SECONDARY
COLLIMATOR
PARAFFIN
LEAD
SCALE
0 2 4 6
INCH

FIG. 4

The actual target was a liquid hydrogen appendix with a liquid hydrogen reservoir six inches above it. The appendix was shielded by a radiation shield at nitrogen temperature and a second inner shield that floated at a temperature between nitrogen and hydrogen. The absorber and appendix system is illustrated in Fig. 5 and Fig. 6.

The design of the appendix and absorber was motivated by several factors. One important requirement was that few mesons leak out of the target and stop on places where they might count efficiently. To overcome this the absorber was made thick enough to stop all 180 Mev mesons. That is to say the range at 180 Mev times the sin of the production angle was never greater than the thickness of the absorber. Since mesons could leak out of the front end and the laboratory differential cross section is probably larger at small angles some attempt was made to remove material from the vacuum chamber in the forward direction by making a large snout on the vacuum chamber in the direction of the beam. In most cases mesons traveling at very large back angles were stopped by the hydrogen alone.

The electromagnetic background pairs go as $z(z+1)$ per atom. Then for a four-inch hydrogen target with 1-mil brass windows the pair background from the windows is one-fifth of that from the hydrogen. This meant that every effort had to be made to keep the windows thin. An attempt was made to use bonded mylar windows but for the small window area it proved impractical. Instead, 1-mil brass windows were used. These were really too thin because they distorted appreciably. In practice the empty target

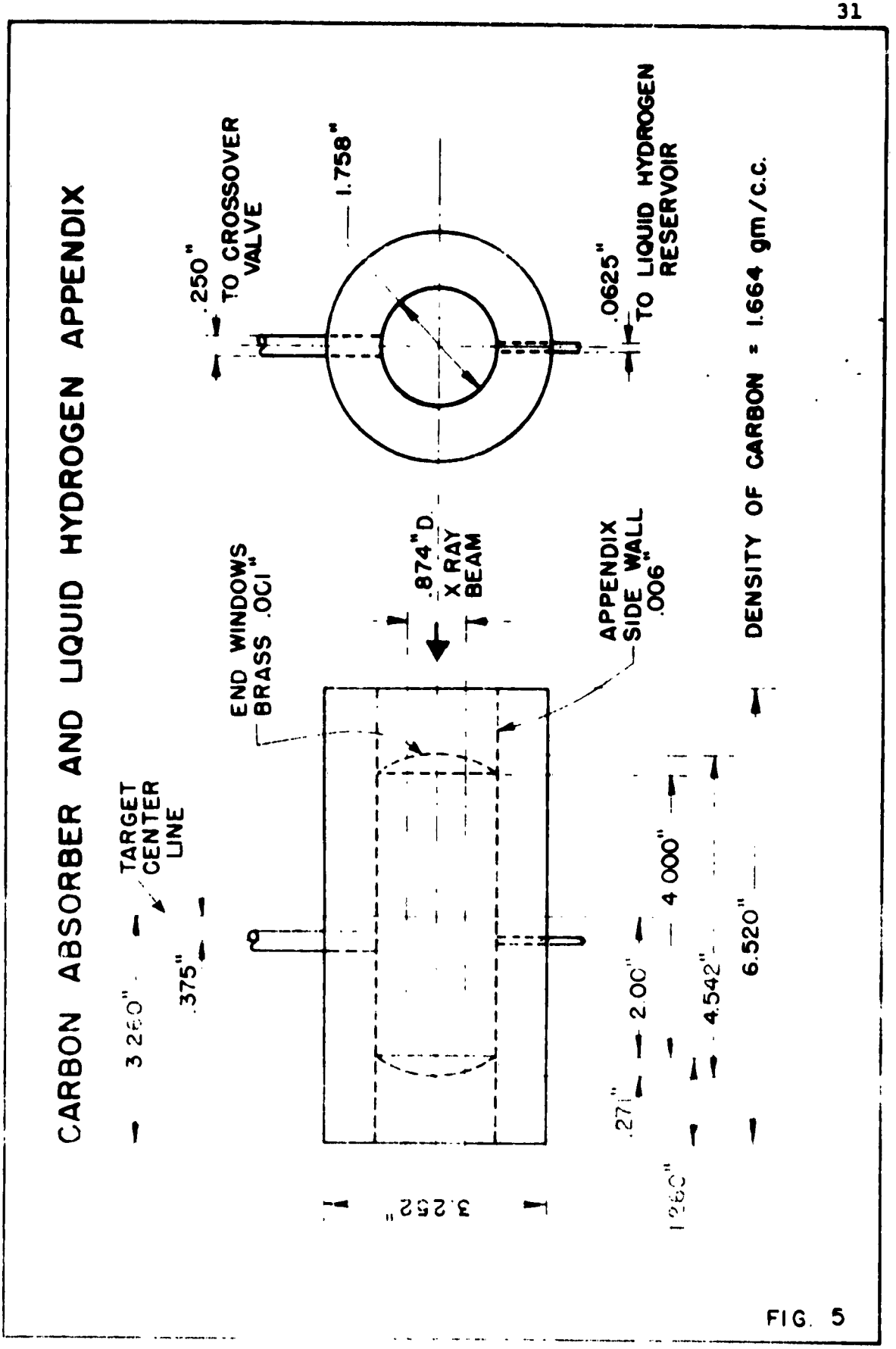
CARBON ABSORBER AND LIQUID HYDROGEN APPENDIX
.250" TO CROSSOVER VALVE
1.758"
.0625" TO LIQUID HYDROGEN RESERVOIR
END WINDOWS BRASS .001"
.874" D X RAY BEAM
APPENDIX SIDE WALL .006"
DENSITY OF CARBON = 1.664 gm/c.c.
TARGET CENTER LINE
3.260"
.375"
3.252"
.271"
2.00"
4.000"
4.542"
6.520"
1.260"

FIG. 5

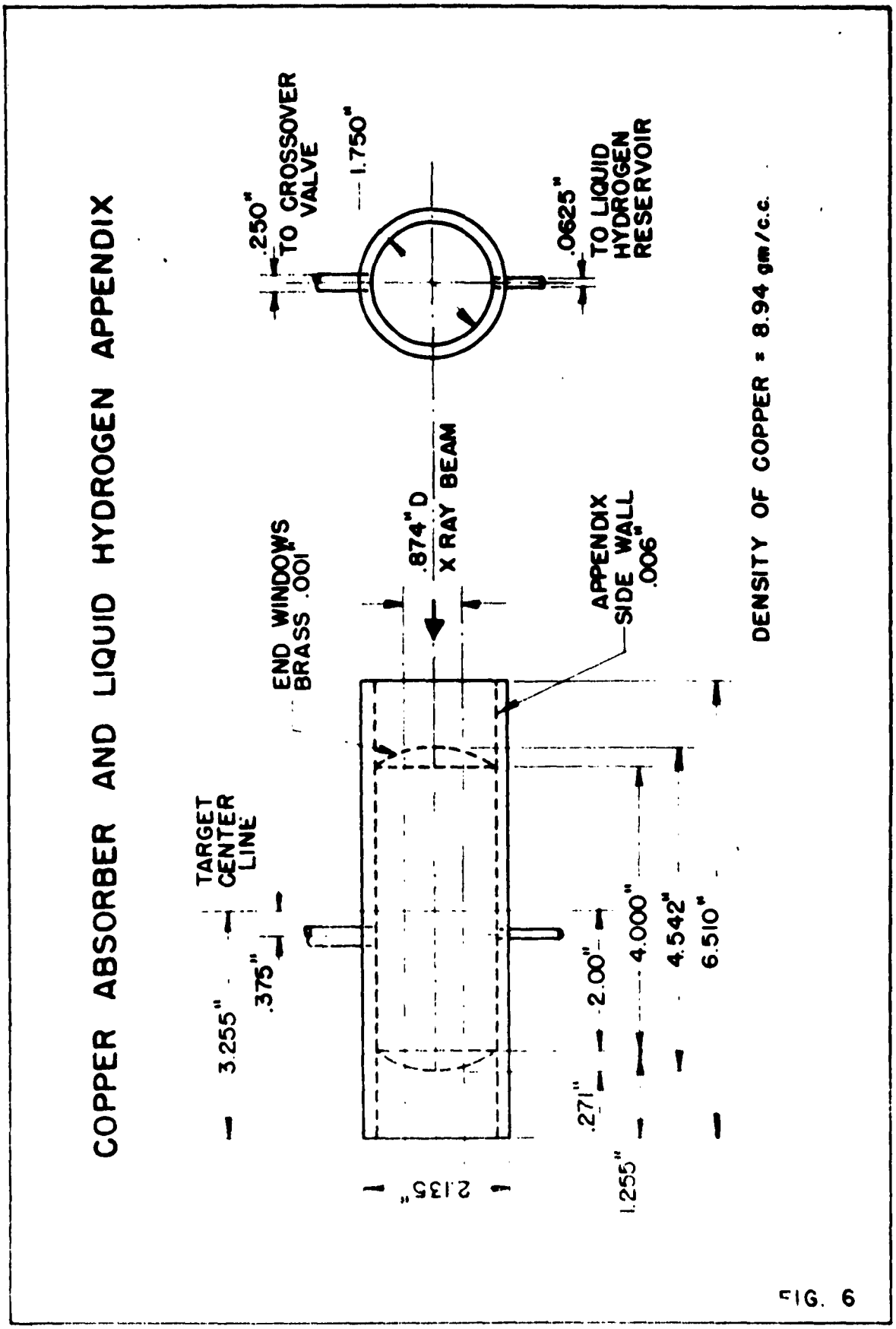
COPPER ABSORBER AND LIQUID HYDROGEN APPENDIX
.250" TO CROSSOVER VALVE
1.750"
.0625" TO LIQUID HYDROGEN RESERVOIR
.874" D X RAY BEAM
END WINDOWS BRASS .001
APPENDIX SIDE WALL .006
DENSITY OF COPPER = 8.94 gm/c.c.
TARGET CENTER LINE
3.255"
.375"
2.135"
.271"
2.00"
4.000"
4.542"
6.510"
1.255"

FIG. 6

background was half of the full target background. Part of this was due to the added effect of the carbon absorber.

The gamma ray beam grazing the carbon absorber was thought to cause a good deal of the pair background in earlier experiments. Therefore it seemed desirable to make the diameter of the hydrogen appendix large, but if this was done more mesons would escape from the front end. In part this effect could be compensated by making the absorber overhangs on the front and back ends larger. For the experiment the hole size was made large enough to clear the beam halo observed on a beam photograph taken in a preliminary run and allow for a 1/16-inch misalignment.

On previous appendices used with the Whalen and Reitz target system, larger fill tubes had been employed. However in this experiment the fill tube represented a slight perturbation in that some mesons could leak out through the hole. To minimize this source of leakage the fill tube was reduced from the usual half-inch brass tube to a quarter-inch copper tube thereby reducing the conducting area by a factor of two. Use of copper increased the conductivity sufficiently to compensate for the loss in area. Unfortunately the softer copper was somewhat more troublesome to align.

Carbon was used for the absorber for several reasons. One important point was the lower multiple scattering for lower z. A second point was one of convenience. Since the counters were

also mainly carbon the efficiency calculation was simplified to some extent. In order to obtain more information on the effect of the absorber, a copper absorber was also used. The meson range criterion was also used to determine the thickness of the copper absorber. Of course radiation effects are more important in copper so that the escaping positron is degraded in energy more (on the average) than in the carbon absorber, resulting in a lower counting rate.

Counters: The construction of the counters is illustrated in Fig. 7. Table II contains a tabulation of some of the counter parameters. The rather complicated structure was dictated by several considerations.

1) The basic solid angle should be approximately the one used by Leiss and Penner in order to utilize their efficiency calculations for preliminary analysis of the data.

2) The effects of multiple scattering should be minimized by equalizing in and out scattering.

3) The electromagnetic background should be suppressed relative to the pion counts.

The primary solid angle of the telescope was determined by the thin, small counter B. B was made thin so that few counts would cut through an edge. The neighboring counters, A and C, covered a much larger area. Counter A was made wide enough so that the number of trajectories through A and B was only 5% less than the number there would have been for an infinite counter A. Likewise C was made wide enough so that only 5% of the counts through B could scatter out of C. (Counter C is larger than A

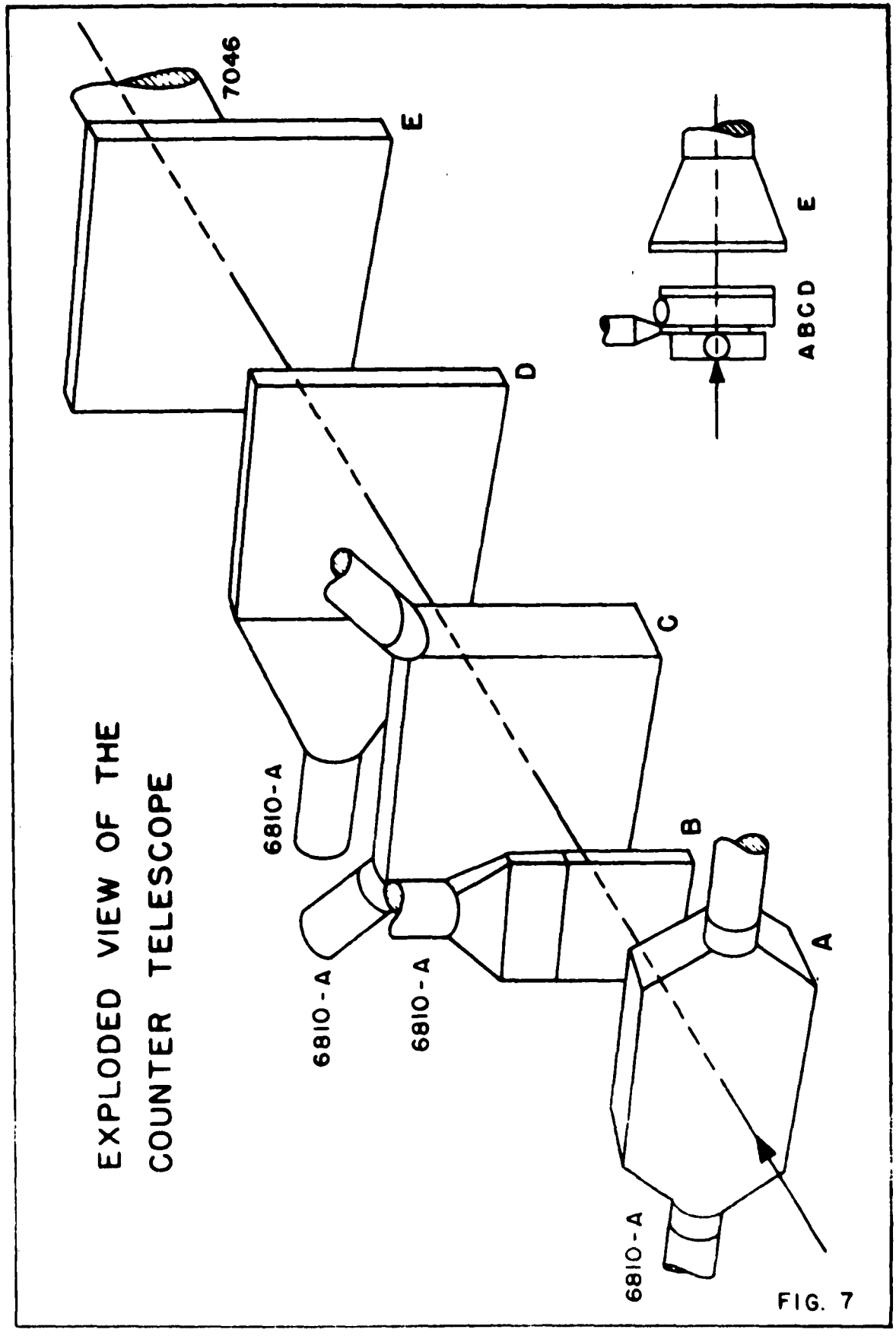
EXPLODED VIEW OF THE
COUNTER TELESCOPE
7046
E
D
C
B
A
6810-A
6810-A
6810-A
6810-A
ABCD
E

FIG. 7

TABLE II: ABSORBING MATERIAL IN THE TARGET AND COUNTER TELESCOPE

(Compare to Table I in Penner's Thesis).

Item	Material	Density $\frac{g}{cm^3}$	Approximate Dimensions In Inches	Thickness $\frac{g}{cm^2}$	Thickness $\frac{g}{cm^2}$ (of carbon equivalent)
Absorber	Carbon	1.664	.75 (thick)	3.26	3.26
Vacuum jacket, Radiation shields	Aluminum	2.70	.093	.65	.87
Cerenkov Counter A	Lucite	1.185	7x7x2	6.10	6.59
Scintillator B	Pilot B	1.02	4.5x4.5x1/4	.84	.92
Cerenkov Counter C	Lucite	1.185	8.5x8.5x2	6.10	6.59
Scintillator D	Pilot B	1.02	8.5x8.5x1/2	1.54	1.70
Scintillator E	Pilot B	1.02	10x10x1/2		

Counter wrappings are included on the item just before each counter.

because of the lower average energy and increased multiple scattering expected in it.) Under these circumstances there is very little net transfer of trajectories from the solid angle determined by B and it can be considered to be the aperture counter. Placing the aperture in the middle of the telescope has the effect of minimizing the area of the other counters. In practice A was used as a secondary aperture in counting ACD. Since A was not compensated for in and out scattering it was expected to behave much less cleanly. The forth counter, D, was made thin so that relatively few of the μ decay positrons would stop in it. The fifth counter, E, was arranged so that absorbers could be placed between it and D in order to test the effect of changes of depth on the efficiency.

The ratio of true pion counts to electromagnetic background counts depends critically on the overall thickness of the counter telescope. The spectrum of the electromagnetic background drops very rapidly with energy (Miller[9]). The Michel spectrum is rising with energy almost to the peak positron energy. Therefore one would expect the ratio of pion counts to background to rise rapidly with increasing depth then fall again at the depth where the highest energy positron can no longer penetrate. The counter thickness to the frontface of D plus the carbon in the target was chosen to maximize the ratio of pion counts divided by background counts. That it did can be seen by noting that the ratio $R = \frac{\text{Counting Rate (180 Mev)} - \text{Counting Rate (150 Mev)}}{\text{Counting Rate (150 Mev)}}$ had the following dependence:

Counter	R	Depth (Including target)
ABC	2.3	13.0 grams (Carbon equivalent)
ABCD	10.0	19.6 grams
ABCDE	9.2	21.3 grams

Although making the counter fairly deep does have this desirable effect it also cuts down the counting rate. In designing such a system a better criterion might have been to minimize the change in counting rate with depth subject to some constraint on the pion-background ratio.

Since the positrons from μ decay are distributed isotropically the beam telescope could have been located at any angle to the beam. However the electromagnetic background was strongly peaked in the forward direction. In order to minimize the effect of the pair background, the telescope was placed at an angle of 135° to the gamma ray beam. That represented the maximum back angle obtainable with adequate shielding. Fig. 8 illustrates the angular dependence of the background found in a preliminary run and compares it with a theoretical angular distribution based on Miller's article[9].

A four-counter telescope was employed in order to reduce the number of accidentals due to background counts which might trigger a double. It also had the effect of ruling out most events where the positron turned into a gamma ray through bremsstrahlung then reappeared later as a pair.

Counters A and C were Cerenkov counters. They were employed with the idea of eliminating pulses from proton recoils

ABCD EMPTY TARGET BACKGROUND AS A FUNCTION OF THE COUNTER ANGLE IN THE LABORATORY OBTAINED IN A PRELIMINARY RUN. (SWEEPING MAGNET ON.)

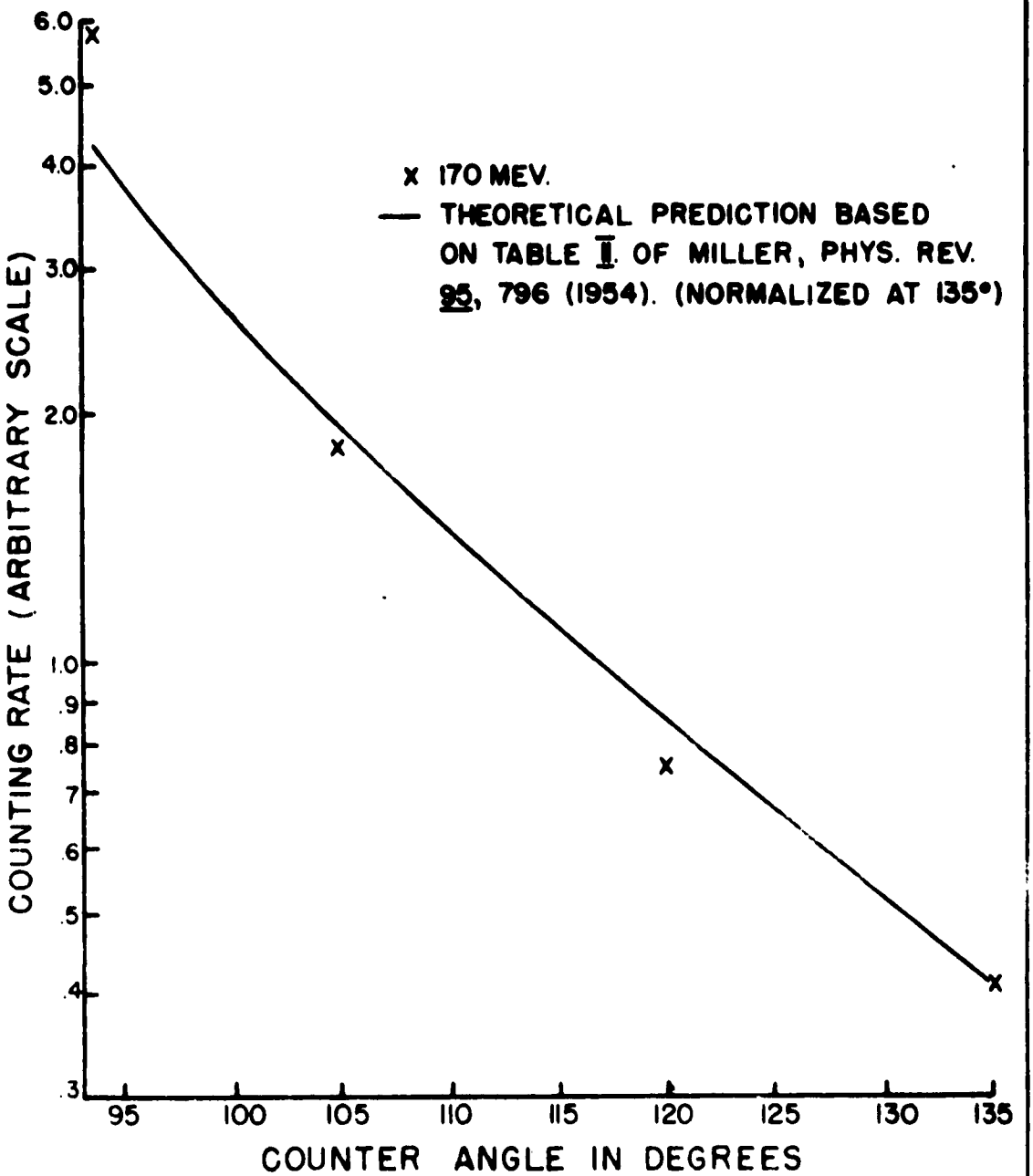

FIG. 8

due to fast neutrons and very low energy electrons. The Cerenkov counters were constructed of lucite. The index of refraction of lucite is 1.5 so that the light cone from Cerenkov radiation goes off at approximately 45°. This made it quite easy to collect the light at the side of the radiator. The radiator thickness was four to ten times the thickness of scintillating crystals normally employed because of the expected lower light yield. In the case of counter A the radiator was tapered in order to provide light piping. Light piping for C was provided by locating the photomultipliers at the corners of a square. Two photomultipliers were used on each radiator. They were coupled using a circuit:

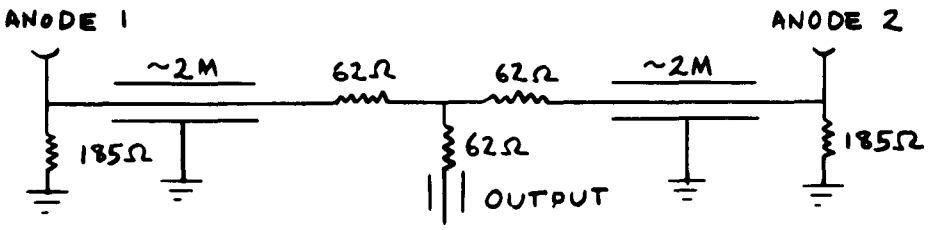

Because of the method of coupling the output pulses, two tubes provided no increase in pulse height relative to one tube. However two tubes did provide some increase in resolution. One disadvantage of two photomultiplier operation in such a system is that the number of noise pulses is doubled (although they are all reduced in pulse height by a factor of two).

The scintillation counters employed air light pipes to eliminate the possibility of Cerenkov counts in lucite pipes.

The counters in the ABCD portion of the telescope were

held rigidly in place by a masonite frame and enclosed in an iron box. The box was rigidly attached to the same frame that held the target. The side of the counter housing closest to the x ray beam was shielded with eight inches of lead while the top , bottom, and sides were shielded with two to four inches of lead. In addition eight inches of boraffin or paraffin was placed on the sides nearest the x ray beam and the top.

The individual counters were tested for resolving power and uniformity of response with cosmic rays. A small probe counter was positioned directly above a particular area of the counter under study. A lead absorber, six inches thick, was placed below the counter being tested. Below the absorber was a large counter which formed a coincidence with the small probe counter. The net effect was to give a μ meson beam of energy greater than 230 Mev with an angular spread in the counter under test of roughly that expected in the experiment. The energy requirement guaranteed that all the μ mesons would give Cerenkov radiation and also be minimum ionizing. For this system a typical counting rate was one count per minute. The pulse for each cosmic ray coincidence count was photographed for the counter being studied. Then a pulse height distribution was plotted based on the order of one to two hundred counts. These indicated that the maximum variation of average pulse height over the face of the counter was 15% except in the case of B where it was half that. The resolutions of the counters (full width at half maximum) were about 16% for the D counter, 30%

for the Cerenkov counters, and 45% for B. The poor resolution on B was probably due to the long light pipe.

Electronic counting system: The electronic system used in this experiment was built along the lines of conventional betatron counting arrangements. Such systems are designed mainly to achieve the very short resolving time necessary because of the low duty cycle of the betatron. Their general operation has been adequately described in the theses of Leiss[18], Mills[41], and Jones[42], and in an article by Schoenwetter[43]. Therefore only the newer features used in this experiment will be covered here. Fig. 9 is the block diagram of the electronics system. Many of the individual circuits are illustrated in Appendix A.

The basic photomultiplier employed was the RCA 6810A. It was felt that the increased gain provided by these tubes would in part offset the poor light yield expected from the counters. The dynode voltage distribution employed was that of the RCA low-light, high-gain circuit. The focusing electrode on each tube was peaked individually using a pulsed light or a Po^{210} scintillator source. The voltage of the focusing electrode was usually 10% to 15% of the way from the first dynode to the photocathode. Proper peaking did result in improved gain with no appreciable loss in resolution. The accelerating grid voltage was also peaked but in most cases it had less than a 10% effect on the pulse height. Some trouble was experienced with a long, ragged trailing edge on the output pulse when

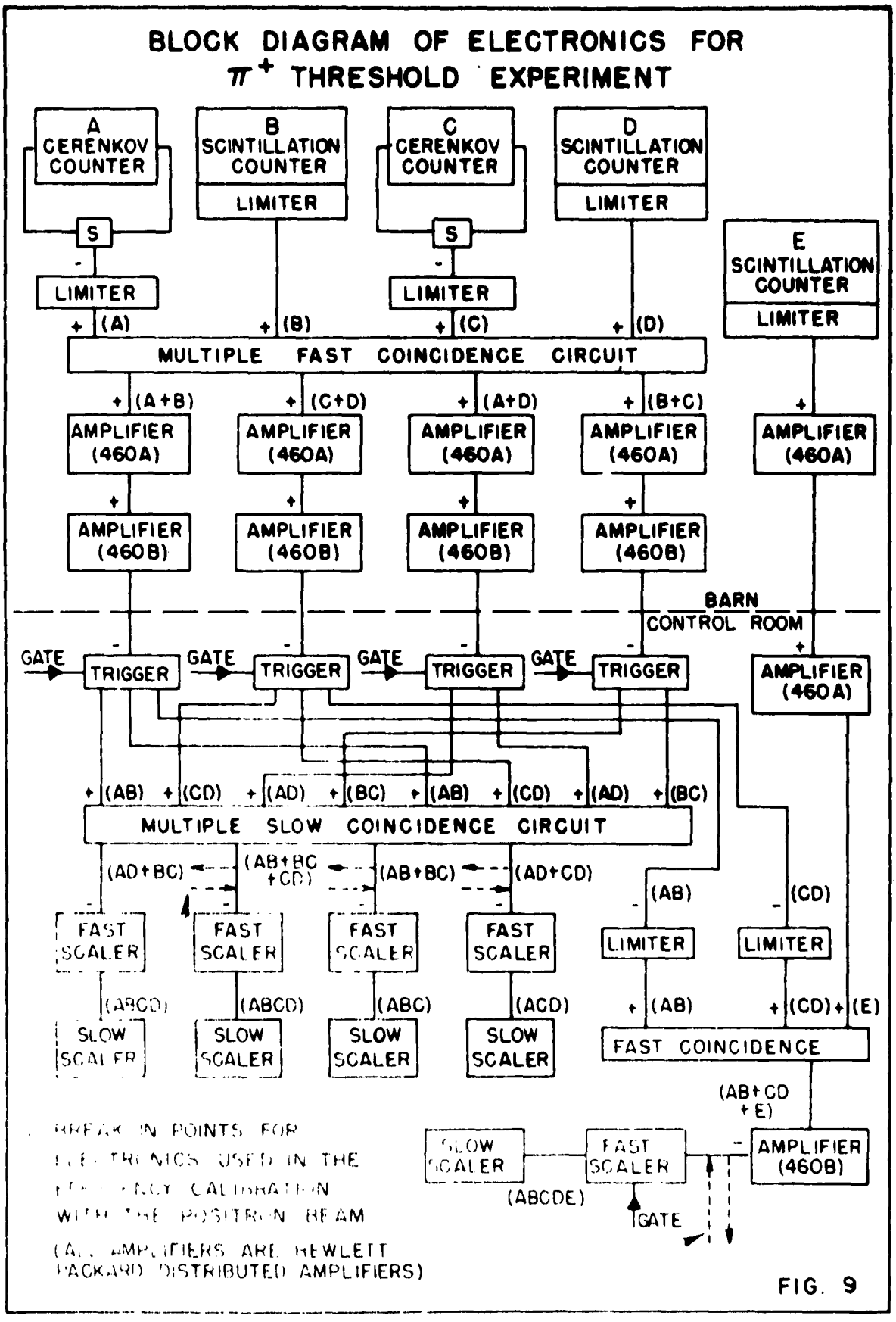
BLOCK DIAGRAM OF ELECTRONICS FOR
π+ THRESHOLD EXPERIMENT
A CERENKOV COUNTER
B SCINTILLATION COUNTER
C CERENKOV COUNTER
D SCINTILLATION COUNTER
E SCINTILLATION COUNTER
LIMITER
S
(A)
(B)
(C)
(D)
MULTIPLE FAST COINCIDENCE CIRCUIT
(A+B)
(C+D)
(A+D)
(B+C)
AMPLIFIER (460A)
AMPLIFIER (460B)
BARN
CONTROL ROOM
GATE
TRIGGER
(AB)
(CD)
(AD)
(BC)
MULTIPLE SLOW COINCIDENCE CIRCUIT
(AD+BC)
(AB+BC +CD)
(AB+BC)
(AD+CD)
FAST SCALER
SLOW SCALER
(ABCD)
(ABC)
(ACD)
(AB)
(CD)
(E)
FAST COINCIDENCE
(AB+CD +E)
(ABCDE)
GATE
BREAK IN POINTS FOR
ELECTRONICS USED IN THE
EFFICIENCY CALIBRATION
WITH THE POSITRON BEAM
(ALL AMPLIFIERS ARE HEWLETT PACKARD DISTRIBUTED AMPLIFIERS)

FIG. 9

certain of these tubes were operated at too high a voltage. Several alternative voltage distributions were tried to diminish the effect but the eventual solution was to select tubes which showed the least trouble.

The conventional 6AH6 pentode limiter was replaced by a very similar 6688 limiter. The 6688, a special, high-transconductance tube, can be cut off with less voltage and provides 10% to 25% larger output voltage pulses than the 6AH6 depending on the cutoff voltage used. In addition the 6688 has the advantage of a long life.

Transitron 570 diodes replaced the G7A's used in earlier coincidence circuits and performed quite well.

Some care was taken to terminate at least one end of every line with its characteristic impedance. In some cases near the front end, both ends were terminated.

The counting system was gated on only during a millisecond period bracketing the x ray yield. The most important effect of this was to reduce the background due to cosmic rays to a very small fraction of the total counting rate.

All possible doubles counting channels were tried at one time or another. The combinations eventually employed paired a Cerenkov counter with a scintillator giving four doubles; AB, CD, AD, and BC. These were in turn used to form four multifolds: ABC, ACD, and ABCD in two different ways. The two different methods of forming ABCD provided some degree of cross check on the counting system. ABC provided a counting rate for a thinner

telescope while ACD provided a larger solid angle.

The E counter was not integrated directly into the main system of doubles but instead formed what amounted to a fast coincidence with ABCD. This was made possible in part by the ABCD counting rate being relatively low and the fact that E was provided with better shielding because of its location in the counter telescope.

It should be emphasized that the experiment was designed and run on the basis of the ABCD coincidence. The other channels were not expected to perform as well because of such things as a higher background (ABC) or a poorly defined solid angle (ACD).

X ray monitor: The x ray monitor employed in this experiment was a flat-plate, open-to-air ionization chamber, the bass drum. The charge collected from the chamber was monitored by a vibrating-reed electrometer. The bass drum was periodically calibrated against a standard ionization chamber such as the Edwards and Kerst chamber or the N.B.S. Dural chamber. In turn these standards had been calibrated against some primary standard and thus indicated the amount of energy brought in by the x ray beam for a certain ion chamber current.

Since the experimentally measured cross section depended directly on the response of the bass drum some care was taken in calibrating it. The monitor calibration is discussed in more detail in Appendix B.

III-C. Experimental Method

Before the experimental apparatus was placed in the x ray beam the primary and secondary collimators were aligned. First the alignment of the primary and secondary bull's-eyes and the x ray hotspot was checked with x ray pictures. Then the primary collimator was installed and fine adjustments on the secondary collimator position were made to better than 1/32 inch. Next a telescope was sighted in on the axis defined by the collimators and used to roughly position the target and sweeping magnet. The target was positioned to better than 1/16 inch by using the bull's-eyes again to give a complete x ray picture of the appendix and absorber. It was necessary to position the target accurately because of the large background associated with the possibility of the beam grazing the absorber.

At this point the electronic counting system was roughly aligned in the normal way by a series of discriminator and high voltage runs. Then shielding was stacked around the counters and in the vicinity of the target. The shielding was arranged to reduce empty-target doubles counts in AB and CD as much as possible. At the same time several different sweeping magnet currents were tried. A magnet current of 25 amps or more did result in a reduction of background. During the data-gathering portion of the experiment the triple count rates always increased noticeably if the sweeping magnet was left off. When the shielding was in place the target position was rechecked with an x ray picture.

The systematic alignment of the counters in the experiment was complicated by the fact that a spectrum of pulse heights was expected in each counter. As a result flat discriminator curves of individual doubles channels were hard to obtain. The difficulty could be somewhat alleviated by using multifold coincidences in which the counter being adjusted was followed by another counter. This arrangement assured in most cases that the particle had traveled all the way through the counter under consideration and given a uniform pulse height. However for D (neglecting E) this was not possible. In many cases when the discriminator curves were made, two sets of doubles were observed along with a triple and quadruple. The doubles discriminator curves were also improved by subtracting the empty target counting rate which was very steeply sloping.

The high voltage curves were done in the conventional manner. As the high voltage in a channel was increased extra delay was usually added to compensate the decreased transit time in the photomultiplier. In the case of A and C a difference between the two photomultiplier voltages was found initially and then held constant throughout later runs. Delay curves were also performed. The delays were carefully established because of the way in which each channel was connected to two double-coincidence circuits. In the later stages of the experiment ABCD was formed in two ways--by a triple, and a double coincidence of doubles channels. The counting rates obtained by the two methods could rarely be brought into exact agreement.

Part of the effect could be explained on the basis of accidentals. In comparison with counters A, B, C, and D, very little attention was paid to the alignment of E.

During the time in which the final data were gathered several miscellaneous runs were made. The doubles were checked occasionally along with the doubles accidentals. The accidentals in the multifold channels were determined by increasing the yield rate and by delays in individual channels. One run was also made to roughly establish the singles counting rates.

The stability of the counting system was maintained by several methods. The gains on the amplifiers were adjusted about once a day by bringing in a standard mercury pulser voltage pulse to the front end of the fast coincidence circuit and adjusting the gain on each channel until it just fired. Large changes in the gain were considered suspect. At the same time a radium source in a standard position was monitored on each counter and any change from the previous counting rate noted. The high voltages on the photomultipliers were frequently checked with a galvanometer. Cosmic ray counts were taken several times to enable corrections to be made for them. The vibrating-reed electrometer leakage rate was checked about once a week. The leakage was never considered large enough to require a correction on the data. Finally a pocket dosimeter was occasionally placed about 25° from the beam on the target vacuum jacket to give an independent monitor on whether or not the hydrogen target was full.

For part of the runs the hydrogen was removed from the appendix to obtain information on the empty-target background. Runs were also made with a copper absorber replacing the carbon one.

Energy calibration. Precise information on the peak photon energy of the machine is necessary in this type of experiment. Since the cross section changes rapidly with energy near threshold it is important to know the absolute energy. The step interval in the activation curve must also be known exactly since the cross section will depend linearly on its size.

Three independent methods were used to estimate the peak energy of the x rays in the experiment. The threshold break in the activation curve for the pion experiment provided a distinct point in the region of 150 Mev. The betatron integrator circuit provided a precise measurement of the flux through the electron orbit which could be related to proton resonance magnetometer data for the magnetic field at the x ray target and in turn to the peak x ray energy. An electron spin resonance magnetometer was in the early stages of development and provided some direct information on the field at the target.

The details of the interrelationships between the various methods of energy measurement are contained in Appendix C. The integrator gave an energy several Mev higher than the meson threshold data. The electron spin resonance apparatus also gave approximately the same value for the energy as the other two methods but had not yet been improved to the point where

accurate comparison was possible.

For the individual activation points the betatron was adjusted to give a three-hundred-microsecond yield pulse. Mark II was set at a calibrated energy point. Then Mark III was adjusted to fire at the same time. Since Mark III appeared to have less jitter it was sometimes used as the reference during a run on a particular point and Mark II was referred to only occasionally. The relation between the two integrators appeared to be quite good. Some attention was paid to proper setting of the pre bias, 90° on the scope, and the integrator standard voltage. The operators were cautioned not to allow the integrator pip to wander more than 50 μs (.4 Mev).

III-D. Equipment for Counter Efficiency Calibration With a Positron Beam

Positrons were pair-produced using a photon beam with peak bremsstrahlung energy of 250 Mev on an aluminum or tungsten target. The pairs were separated and momentum analyzed by a magnetic field. The positron beam was bent through 90° on a 33.6 cm radius. The aperture was initially defined by the two-inch separation of the magnet pole pieces and a one-inch wide brass channel. Thirty centimeters beyond the exit of the magnet the beam passed through a vertical half-cm lead slit. A second, gold, knife-edge slit 1.2 cm wide was placed 130 cm beyond the lead slit. Sixty centimeters beyond the gold slit was a wide, thick, tertiary lead collimator. In the region of the collimators the positron beam was transported in a helium gas bag

at atmospheric pressure.

A beam probe, consisting of two 1.3 x 1.3-cm scintillators each 1/8-inch thick and separated by 50 cm, was placed behind the tertiary collimator to define the positron beam. The scintillators were made as thin as possible to minimize the energy loss in them and, in the case of the second one, to minimize multiple scattering so that the positron beam would not spread. The first counter was surrounded by a lead and iron mask one-half-inch thick to suppress positrons which might in turn cause accidentals in the counter telescope. The beam probe was aligned on the central positron ray. The counter telescope was placed directly behind the beam probe so that the positron beam would strike it at the desired position and angle. A plan view of the positron beam layout is given in Fig. 10. (A similar apparatus was used by Parker[44] for this type of calibration.)

A "positron" was taken as a coincidence between the two scintillators in the beam telescope. The double coincidence was put into slow coincidence with each of the multifold channels from the counter telescope and these coincidences were counted by scalers. The efficiency was given by the number of multifold coincidences for a particular channel divided by the number of double coincidences. The original electronics (up to the slow coincidence outputs) was used for forming the multifolds to insure that the efficiency would not be changed by the electronic parameters. A block diagram of the electronics

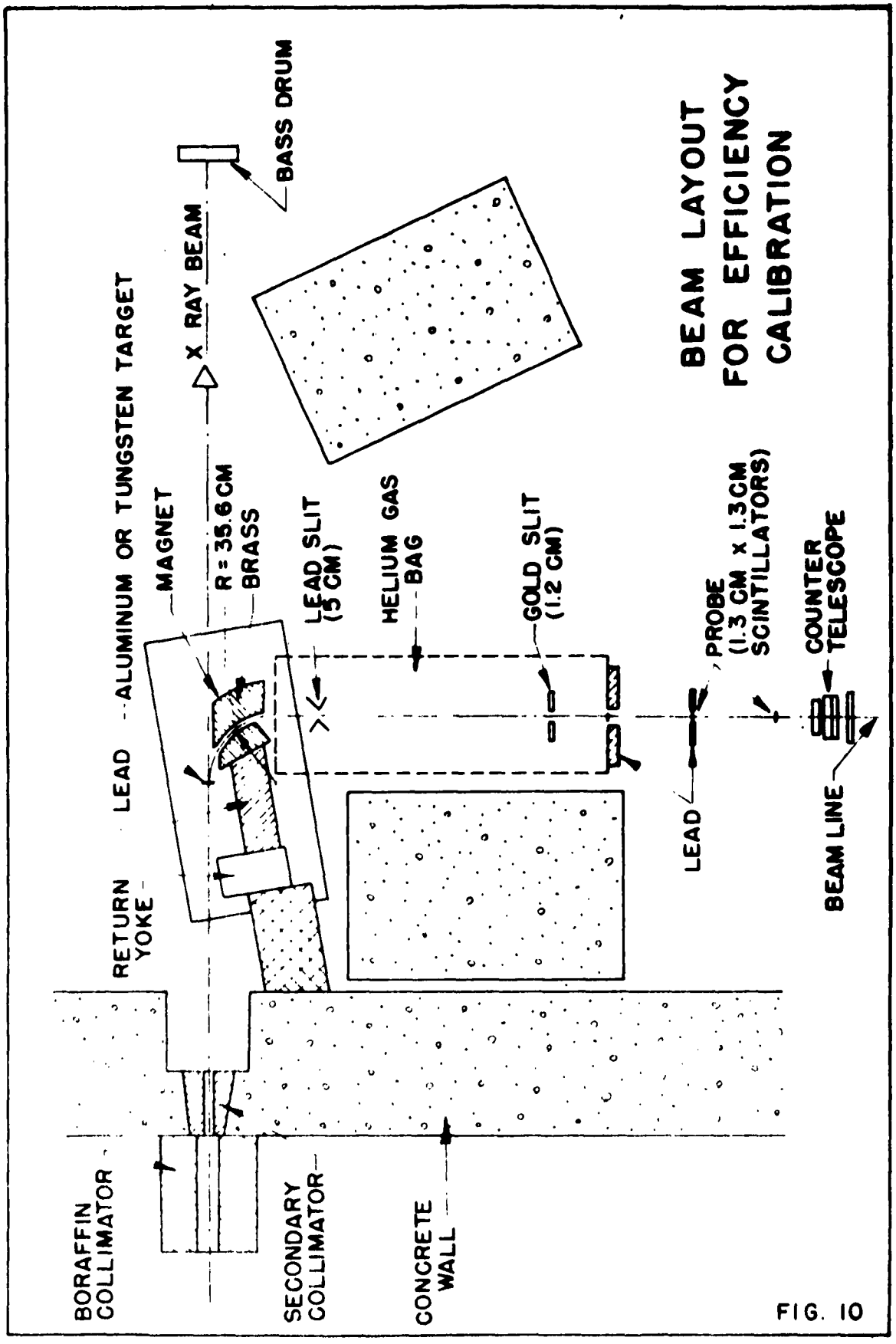
BEAM LAYOUT
FOR EFFICIENCY
CALIBRATION
BASS DRUM
X RAY BEAM
MAGNET
R = 35.6CM
BRASS
LEAD SLIT
(5 CM)
HELIUM GAS
BAG
GOLD SLIT
(1.2 CM)
PROBE
(1.3 CM x 1.3CM
SCINTILLATORS)
COUNTER
TELESCOPE
LEAD
BEAM LINE
RETURN
YOKE
LEAD
ALUMINUM OR TUNGSTEN TARGET
BORAFFIN
COLLIMATOR
SECONDARY
COLLIMATOR
CONCRETE
WALL

FIG. 10

for the beam-probe, counter-telescope system is given in Fig. 11.

III-E. Experimental Method For the Counter Efficiency Calibration Using a Positron Beam

The beam-probe electronics system was aligned following the same procedures used for the main counter telescope. It was unnecessary for the beam-probe to be perfectly efficient. Instead the primary requirement was that no accidentals occur. Because of this the counters could be aligned quite easily by keeping the double-coincidence discriminator high and raising the high voltage on the photomultipliers until the average particle through a counter caused it to just limit.

The beam-probe was positioned relative to the beam to maximize the efficiency and minimize the change of efficiency with angle. To find this position the first counter was set at a definite angle to the magnet exit and the angle of the second counter was varied relative to the line from the magnet exit to the first counter. The number of beam-probe counts and the efficiency was determined as a function of the angle of the second counter. Then the first counter was moved to a different angle and the test repeated. In general the efficiency was quite sensitive to the angle while the counting rate dropped more slowly. The angle through which the second counter could be moved agreed approximately with multiple scattering predictions based on the thickness of the first counter.

When a tungsten rod 1/8-inch in diameter was used as a vertical target it was found that the rod could be positioned

BLOCK DIAGRAM OF ELECTRONICS USED IN THE EFFICIENCY CALIBRATION WITH THE POSITRON BEAM

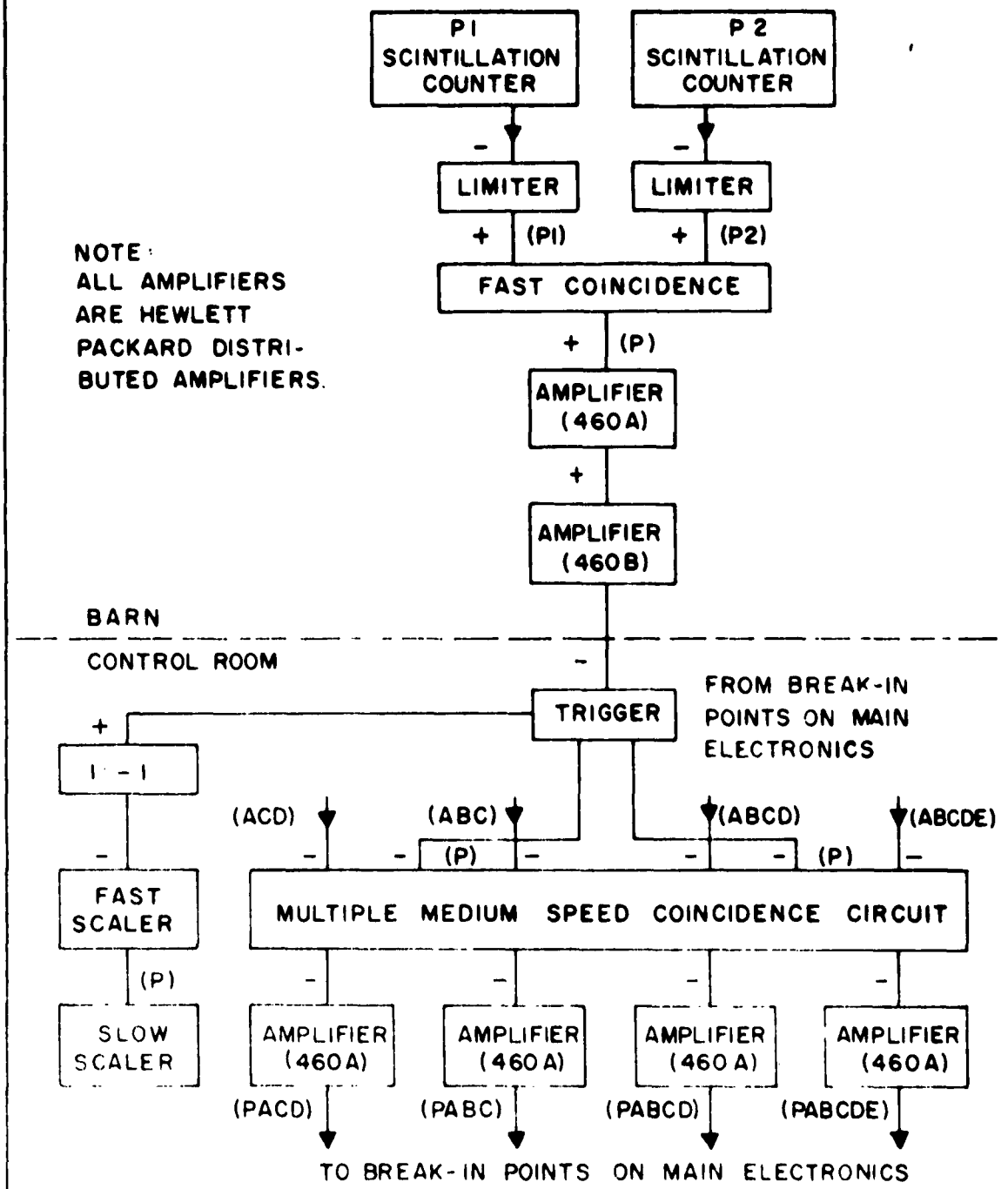

FIG. 11

in the x ray beam to within 1/8 inch. The counting rate dropped to half the peak value when the rod was moved 3/16 inch to either side. (The x ray beam was approximately one inch in diameter at the target.) The target in-target out ratio ranged from 25 to 75 depending on the nature of the target. This ratio was roughly the one expected if the air column before the target was considered.

Collimating slits were installed to diminish beam contamination. They could be positioned to better than 1/8 inch. When the second slit was opened the beam-probe count rate increased and the efficiency dropped. This probably indicated that in collimating the beam the lead slit acted as a source of low energy particles.

Putting nitrogen in the gas bag rather than helium lowered the counting rate slightly. The decreased counting rate was probably due to increased multiple scattering.

Tests were made for accidentals by delaying A and by increasing the yield. The PACD accidental rate was roughly .3% of the net counting rate so that accidentals were not an important factor.

In order to test the previous electronic alignment of the counter telescope the photomultipliers on the counter telescope were all lowered 100 volts. The largest change of efficiency under this severe test was 3%. Varying all the trigger discriminators by eight divisions had even less effect.

On several occasions the magnet current was reversed in

order to see if the efficiency for electrons differed from that of positrons. Positrons of about 60 Mev were indistinguishable from electrons. At 30 Mev electrons seemed to be slightly less efficient for ABC and more efficient for the thicker counters. However the difference was very slight. (No counts were registered when the magnet was turned off.)

Before the counter telescope was moved from its position for the main part of the experiment mercury pulser and radium checks were run on the equipment. Then the equipment was moved and the checks were rerun. The slight change in the magnetic environment produced no effect. These checks were continued throughout the efficiency runs.

In a normal run the counter telescope was located in the desired position relative to the positron beam. Four runs were made, lowering the magnet current along a standard hysteresis loop each time. At the lowest energy the tungsten target was usually replaced with a thicker aluminum target in order to increase the counting rate. After the lowest energy point the counter telescope was positioned for the next point and the procedure was repeated.

The magnet field was measured before and after the run on slightly different hysteresis curves by several other groups[45,46]. They used a proton-resonance apparatus and a Hall-effect probe to calibrate the magnet. It was felt that their calibrations could be extrapolated to the hysteresis curve used in this experiment with sufficient accuracy for the purpose at hand.

IV. DATA ANALYSIS AND EXPERIMENTAL RESULTS

IV-A. Data Reduction

The average yields for a two sma monitor obtained for the carbon absorber runs are tabulated in Tables III and IV, and in Figures 12, 13, 14,and 15. AD + BC has been omitted because it is very close to ABCD. The uncertainty assigned to each activation point is the standard deviation on the average value based on the deviation among the individual runs at the particular energy. Several corrections have been made on the raw experimental activities to obtain the data in the tables. The number of standard monitors, q_o, was obtained from the experimental monitor q using the formula:

$$q_o = q \frac{1013}{p} \quad \frac{(273.2 + T_c)}{293.2} \qquad \text{(IV-1)}$$

where p is the pressure in millibars and T_c is the temperature in degrees centigrade. The individual pressures had previously been lowered slightly, ($\sim$.3%) to account for barometer temperature changes. The normalized yields were obtained by dividing the number of counts by q_o. For normal runs this factor was between 1.01 and 1.06. No drift corrections were made on the monitor since the maximum drift observed represented a correction of less than 01%. Similarly no corrections were made for recombination in the bass drum since experimental evidence indicated that it was less than .1% (see monitor appendix). The background due to cosmic rays for a particular coincidence, Δ , was subtracted from the individual normalized activities using the formula:

TABLE III. FILLED TARGET ACTIVATION DATA FOR CARBON ABSORBER RUNS

Betatron Nominal Energy E_o	No. of Runs	Average activity for a two sma run ABC	ACD	ABCD	ABCDE
180	11	6149±59	4972±49(10)	2000±20	1194±15(8)
178	8	5694±73	4547±50	1799±27	1071±23(5)
176	8	5290±100	4130±42	1637±15	986.8±24(7)
174	8	4737±100	3616±35	1436±18	872.6±17(6)
172	6	4263±56	3223±13	1273±11	765.9±16(4)
170	9	3893±58	2782±20	1109±17	669.8±16(6)
168	8	3519±50	2427±26	958.1±15	565.6±7 (6)
166	8	3075±60	2064±46	778.8±17	490.4±9 (6)
164	9	2746±56(8)	1728±16	652.1±4	393.1±6 (7)
162	8	2501±73(7)	1433±16	531.2±9	335.1±10(6)
160	10	2313±31(9)	1124±16	406 2±6	255.3±7 (7)
158	12	2102±46(11)	899.1±13	315.2±6	199.0±3 (10)
156	8	1887±56	704.3±26	246.7±4	157.2±2 (6)
154	10	1811±46	600.1±17(9)	192.4±5	129.8±6 (8)
152	10	1811±45	591.7±11	187.7±5	120.6±5 (8)
150	9	1842±47	573.4±13	181.5±5	116.9±4 (6)
148	2	1866±22	558.7±16	184.9±1	113.7±11(1)
146	1	1822±43	674.0±26	224.9±15	138.9±12
144	1	1968±44	513.8±23	152.0±12	116.4±11
140	5	1981±68	566.2±28	179.1±12	111.7±7 (3)
135	1	2041±45	654.4±26	195.2±14	---
130	1	2047±45	560.0±24	200.1±14	---

NOTE: Numbers in parentheses specify the number of runs for a particular coincidence when it differed from the number given in the second column.

In the cases where only one run was made the uncertainty assigned to the run was based solely on counting statistics.

TABLE IV. EMPTY TARGET DATA FOR CARBON ABSORBER RUNS

Betatron Nominal Energy E_o	No. of Runs	Average Activity for a Two sma Run			
		ABC	ACD	ABCD	ABCDE
180	10	1403±32	413±11	137±5	79±3
178	1	1418±38	400±20	136±12	81±9
170	13	1446±36	364±9	110±3	64±2
168	1	1494±39	319±18	96±10	53±7
160	14	1445±37	307±12	97±4	54±2
158	1	1412±38	342±18	95±10	45±7
150	14	1527±31	290±10	83±2	47±2
140	10	1648±31	300±10	84±3	47±1
130	1	1728±42	296±17	84±9	49±7

In the cases where only one run was made the uncertainty assigned to the run was based solely on counting statistics.

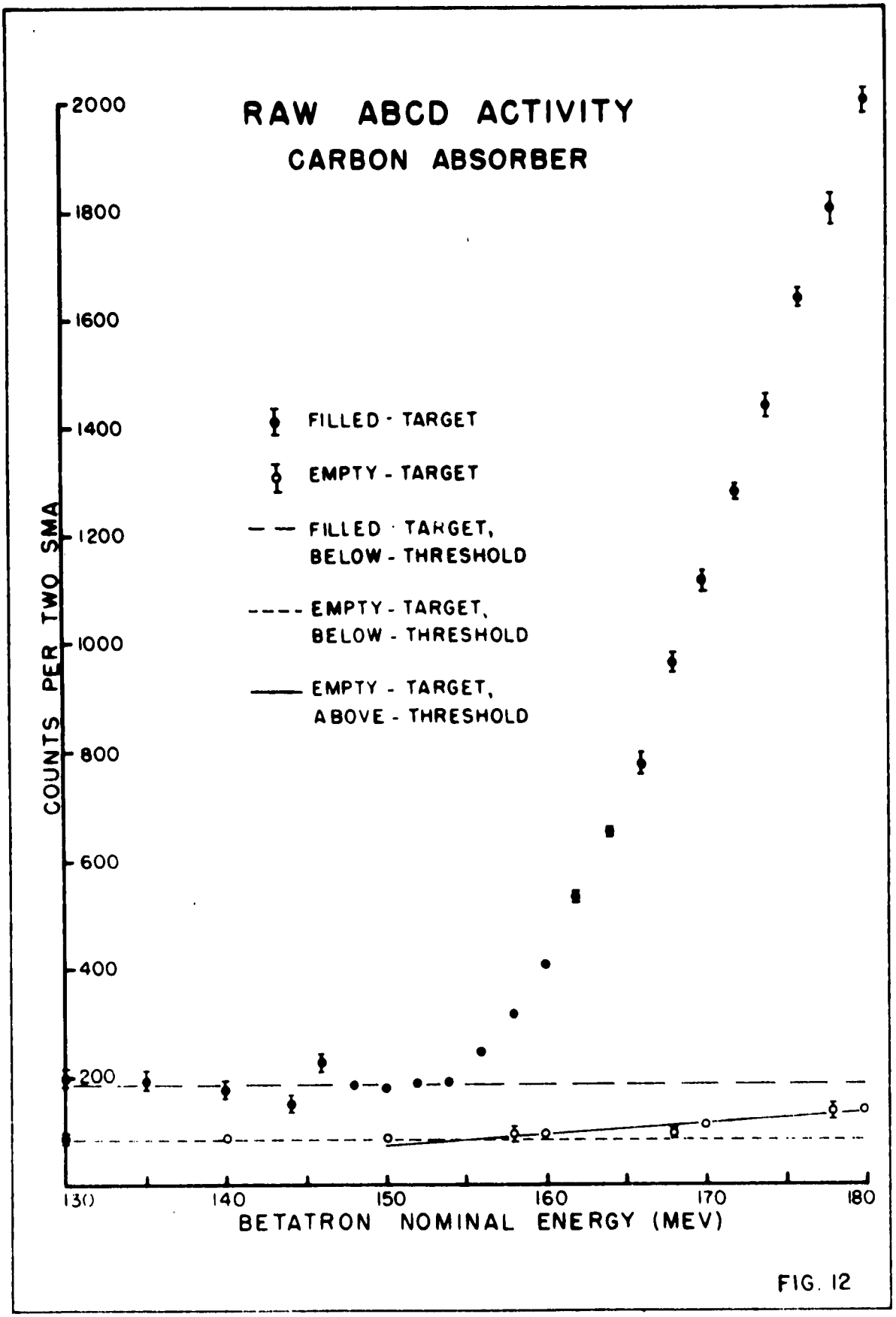
RAW ABCD ACTIVITY
CARBON ABSORBER
FILLED - TARGET
EMPTY - TARGET
FILLED - TARGET, BELOW - THRESHOLD
EMPTY - TARGET, BELOW - THRESHOLD
EMPTY - TARGET, ABOVE - THRESHOLD
COUNTS PER TWO SMA
2000
1800
1600
1400
1200
1000
800
600
400
200
130
140
150
160
170
180
BETATRON NOMINAL ENERGY (MEV)

FIG. 12

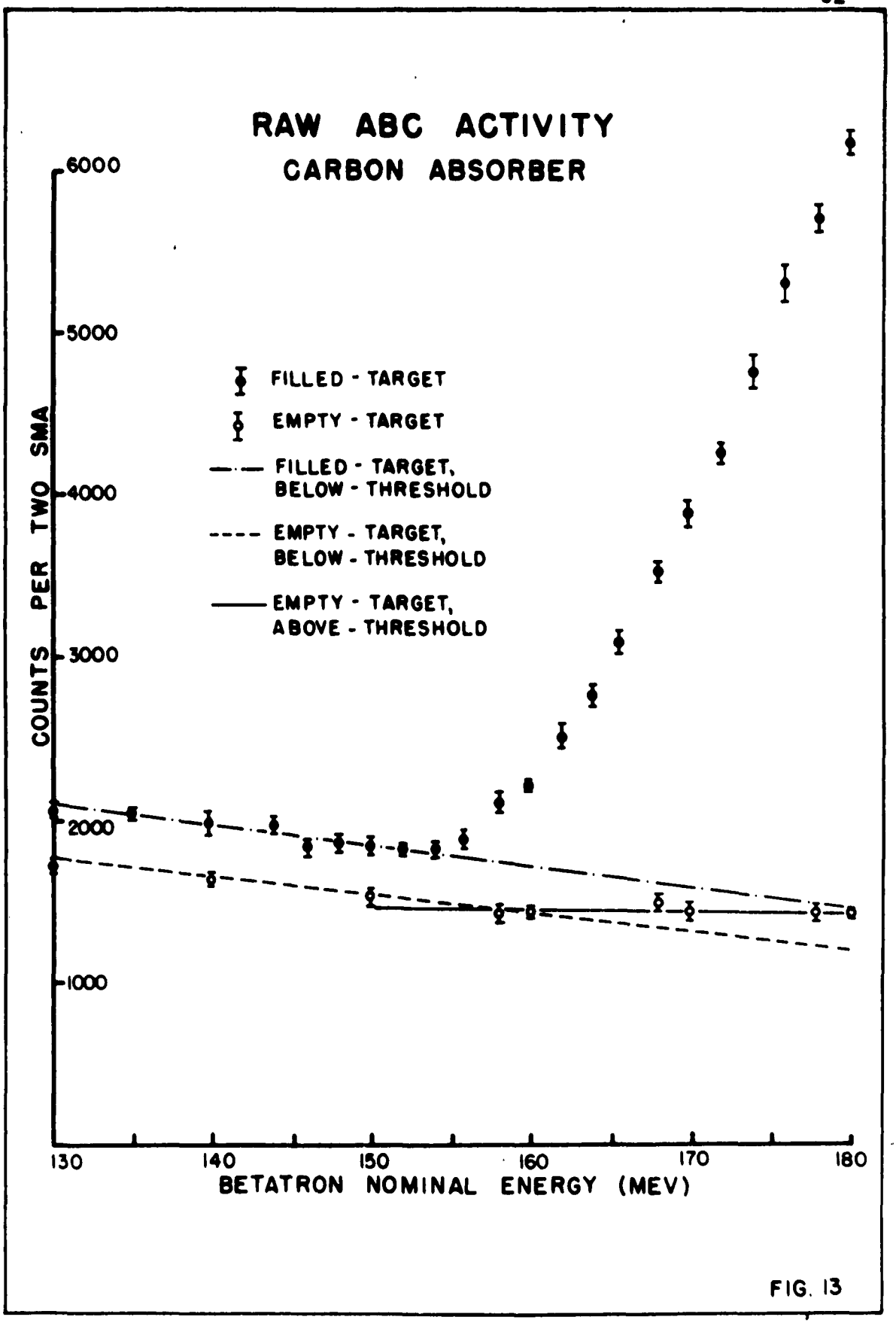
RAW ABC ACTIVITY
CARBON ABSORBER
6000
5000
4000
3000
2000
1000
COUNTS PER TWO SMA
FILLED - TARGET
EMPTY - TARGET
FILLED - TARGET, BELOW - THRESHOLD
EMPTY - TARGET, BELOW - THRESHOLD
EMPTY - TARGET, ABOVE - THRESHOLD
130
140
150
160
170
180
BETATRON NOMINAL ENERGY (MEV)

FIG. 13

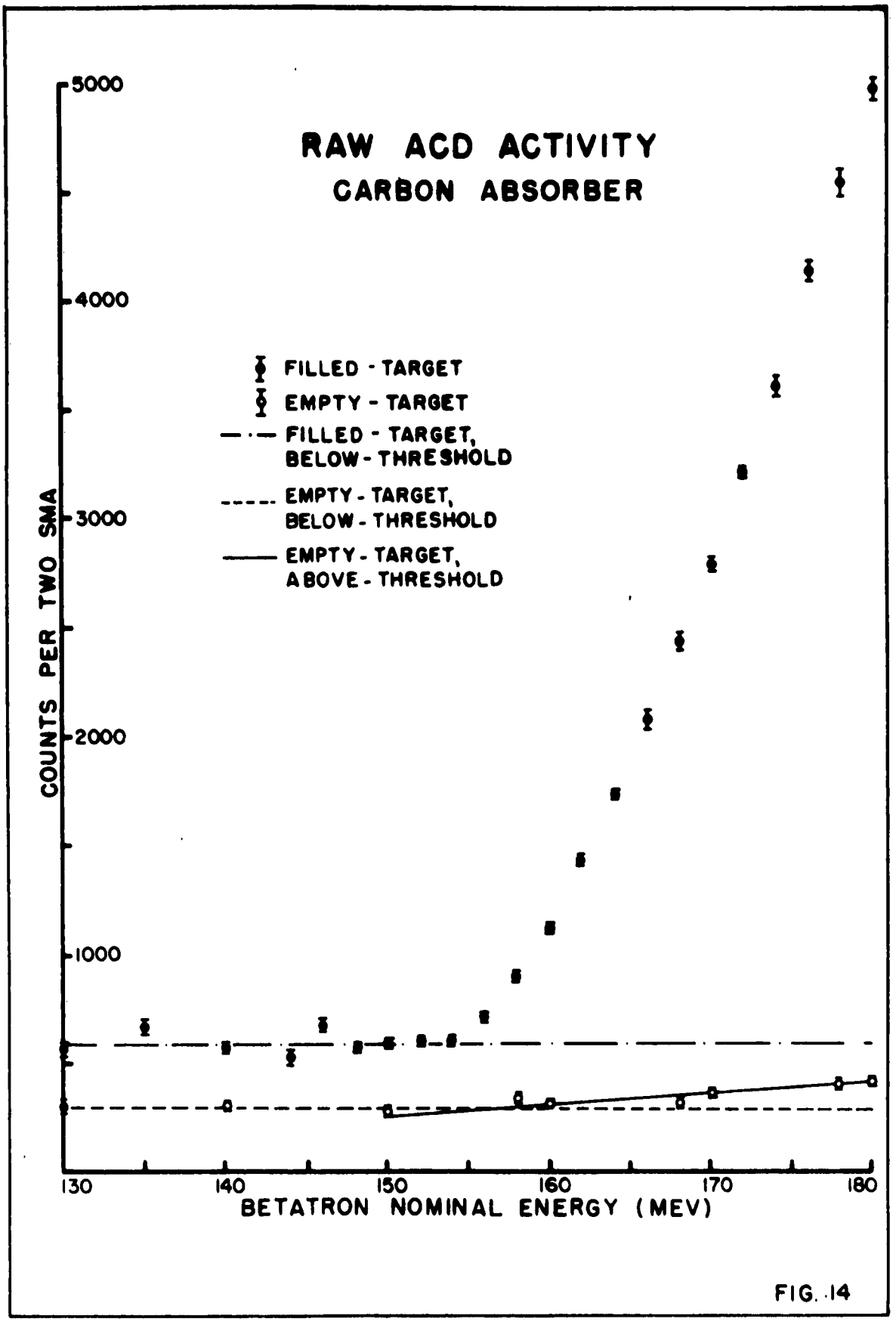
RAW ACD ACTIVITY
CARBON ABSORBER
FILLED - TARGET
EMPTY - TARGET
FILLED - TARGET, BELOW - THRESHOLD
EMPTY - TARGET, BELOW - THRESHOLD
EMPTY - TARGET, ABOVE - THRESHOLD
COUNTS PER TWO SMA
5000
4000
3000
2000
1000
130
140
150
160
170
180
BETATRON NOMINAL ENERGY (MEV)

FIG. 14

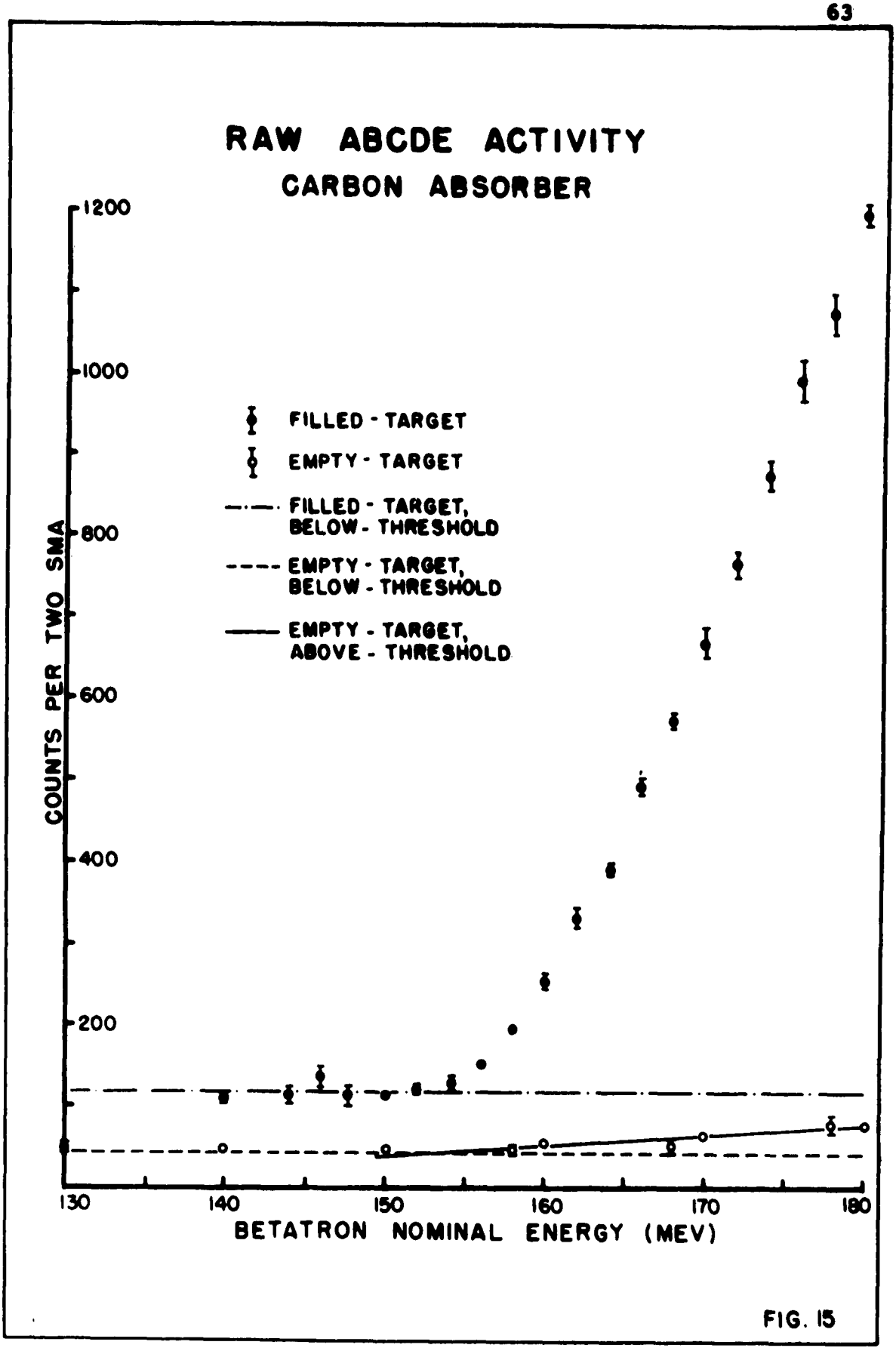
RAW ABCDE ACTIVITY
CARBON ABSORBER
COUNTS PER TWO SMA
1200
1000
800
600
400
200
FILLED - TARGET
EMPTY - TARGET
FILLED - TARGET, BELOW - THRESHOLD
EMPTY - TARGET, BELOW - THRESHOLD
EMPTY - TARGET, ABOVE - THRESHOLD
130
140
150
160
170
180
BETATRON NOMINAL ENERGY (MEV)

FIG. 15

$$\Delta^i = C^i T \qquad \text{(IV-2)}$$

where C^i is the average number of cosmic ray counts per minute for the coincidence times the betatron duty cycle, and T is the length of the run in minutes. The values of C^i used for the coincidences were:

Coincidence	C^i
ABC	.384
ACD	.402
ABCD	.198
ABCDE	.098

At 180 Mev this correction amounted to less than .7% in all cases. However at energies near and below threshold it was much larger. The method of background subtraction used in the experiment tends to cancel the correction so that the main effect of the correction is to compensate variations in running time at a particular energy. A correction was also made for accidentals in three of the channels; ABCD, AD + BC, and ABC. The form of the correction and its experimental basis is discussed in Appendix D. It consisted of one part which was constant with energy and therefore tended to cancel after the background was subtracted, and a second part with nearly the same energy dependence as the yield. Thus the effect of the second part was to linearly multiply the yield and the cross section by a factor slightly less than 1. For ABCD the correction ranged from 1 to 2 1/2%.

The background subtraction was handled in the following way. Weighted, least-squares fits were made to the below-threshold,

filled-target counting rates using polynomials in E. The degree of each polynomial was chosen to minimize the root mean square error for the particular fit. (P. Cziffra and M. J. Moravscik[47] have reviewed several useful goodness-of-fit criteria for fitting curves by the least-squares method.) In every case except ABC the best fit was obtained with a constant coefficient. In the case of ABC it was necessary to use a linear fit with a negative energy dependence. The below-threshold counting rate for ABC was also relatively larger than those of the other coincidences. In addition the deviations on the runs at each energy were on the order of twice those of ACD although the counting rates were nearly the same at higher energies. The extra deviations were due in part to a poor scaler. Because of these difficulties the information obtained for ABC was rejected except in the efficiency analysis section.

Similar fits were made to the empty-target yields below threshold and the empty-target yields above threshold. The coefficients of the actual fitting curves are tabulated in Table V. In the filled-target, below-threshold cases a deviation is quoted based on the standard deviation among all the below-threshold runs. The below-threshold fits for the empty-target and the filled-target runs are quite consistent with each other.

The background for each coincidence was subtracted as follows. The extrapolated fit for the filled-target, below-threshold counting rate was subtracted from the filled-target yields above threshold to give the total meson yields. Similarly the empty-target, below-threshold fit was subtracted from the empty-target, above-threshold

TABLE V. LEAST-SQUARES FITS TO THE BACKGROUND AND BELOW-THRESHOLD COUNTING RATES.

$$\frac{\text{COUNTS}}{\text{TWO SMA}} = A + BE \text{ (MEV, NOMINAL)}$$

	COINCIDENCE	A	B
Filled-target, below-threshold	ABC	3752	-12.7
	ACD	580±8.7	
	ABCD	184±3.5	
	ABCDE	118±2.7	
Empty-target, below-threshold	ABC	3236	-11.4
	ACD	294	
	ABCD	84	
	ABCDE	47	
Empty-target, above-threshold	ABC	1739	- 1.80
	ACD	-511	5.13
	ABCD	-207	1.89
	ABCDE	-151	1.27

fit. This latter subtraction gave the activities due to mesons photoproduced in the carbon absorber and the target end windows. In turn these activities were subtracted from the total meson activities to give the activities due to the mesons from hydrogen.

Each activity was multiplied by the monitor response in sma/erg, $\overline{W}(E')$, for the nominal energy of the activity. (The monitor response is given in Appendix B) The activities were also multiplied by $A(E_{\gamma m})$, the bremsstrahlung energy per electron in Mev/electron for a Schiff integrated-over-angles spectrum from Table T3 of the Penfold-Leiss tables[48]. In addition each activity was multiplied by a factor to convert ergs to Mev and divided by $C_2/C_1 = 1.9817$, the ratio of the capacitor used to monitor the yield to the one used to define the sma. (This ratio was averaged over the 1956 and 1958 measurements listed in the monitor appendix.) Thus the counts/electrons, Y(E), was:

$$Y(E) = 1.602 \times 10^{-6} \quad \frac{A(E)\overline{W}(E')\alpha_c(E')}{C_2/C_1} \qquad \text{(IV-3)}$$

where $\alpha_c(E')$ is the yield per monitor after the appropriate corrections and the background subtraction.

At this stage in the analysis the energy was determined. The two-thirds power of each ABCD yield point was found in the nominal energy region from 156 to 170 Mev. These points, appropriately weighted, were fitted with a line using a least-squares fit. The nominal energy at which the yield was zero was found and compared to a theoretical calculation of the same quantity. Then the difference between the two values, 1.5 Mev , was subtracted from all of

the nominal energies. This procedure is discussed in some detail in Appendix C along with its relationship to other methods of determining the energy.

The Y(E) for various coincidences have been tabulated in Table VI. The uncertainties assigned to the yield points are based on the square root of the sum of the squares of the standard deviations for the below-threshold activity and the activity at the particular energy. The yield curves are also plotted in Figures 16, 17, and 18.

IV.-B. Cross Section Analysis

Effect of the Bremsstrahlung Spectrum: The choice of a bremsstrahlung spectrum affects the values obtained for the cross section because the integrand of the yield integral is linear in both the bremsstrahlung spectrum and the cross section. For that reason it is necessary to devote some attention to the problem of bremsstrahlung spectra before discussing the determination of the cross section from the activation curve.

Very little experimental information on bremsstrahlung is available, particularly in the energy region above 100 Mev. One experiment has been performed at 200 Mev by Leiss, Yamagata, and Hanson[18] using a pair spectrometer. However the 2.3% resolution of the apparatus and uncertainties connected with the efficiency make it difficult to draw conclusions from the experimental results concerning the high energy tip of the spectrum.

Although the basic physical processes are considered to be well understood, all the theoretical bremsstrahlung spectra in

TABLE VI. ACTIVITIES FOR THE CARBON ABSORBER RUNS IN COUNTS/ ELECTRON X 10^{12}.

$E_{\gamma m}$(Mev)	ACD	ABCD	ABCDE
178.5	5394±63	2230±25	1319±19
176.5	4832±64	1965±34	1157±29
174.5	4286±53	1752±19	1046±30
172.5	3630+44	1494±22	900±21
170.5	3132+19	1287±15	765±20
168.5	2584±27	1082±21	645±19
166.5	2147±33	896±18	518±8
164.5	1709±55	680±21	426±12
162.5	1309±22	529±6	311±7
160.5	965±21	387±11	243±12
158.5	610±21	243±8	152±9
156.5	359±18	141±8	89±5
154.5	141±31	66±6	44±4
152.5	23±21	9±7	13±7

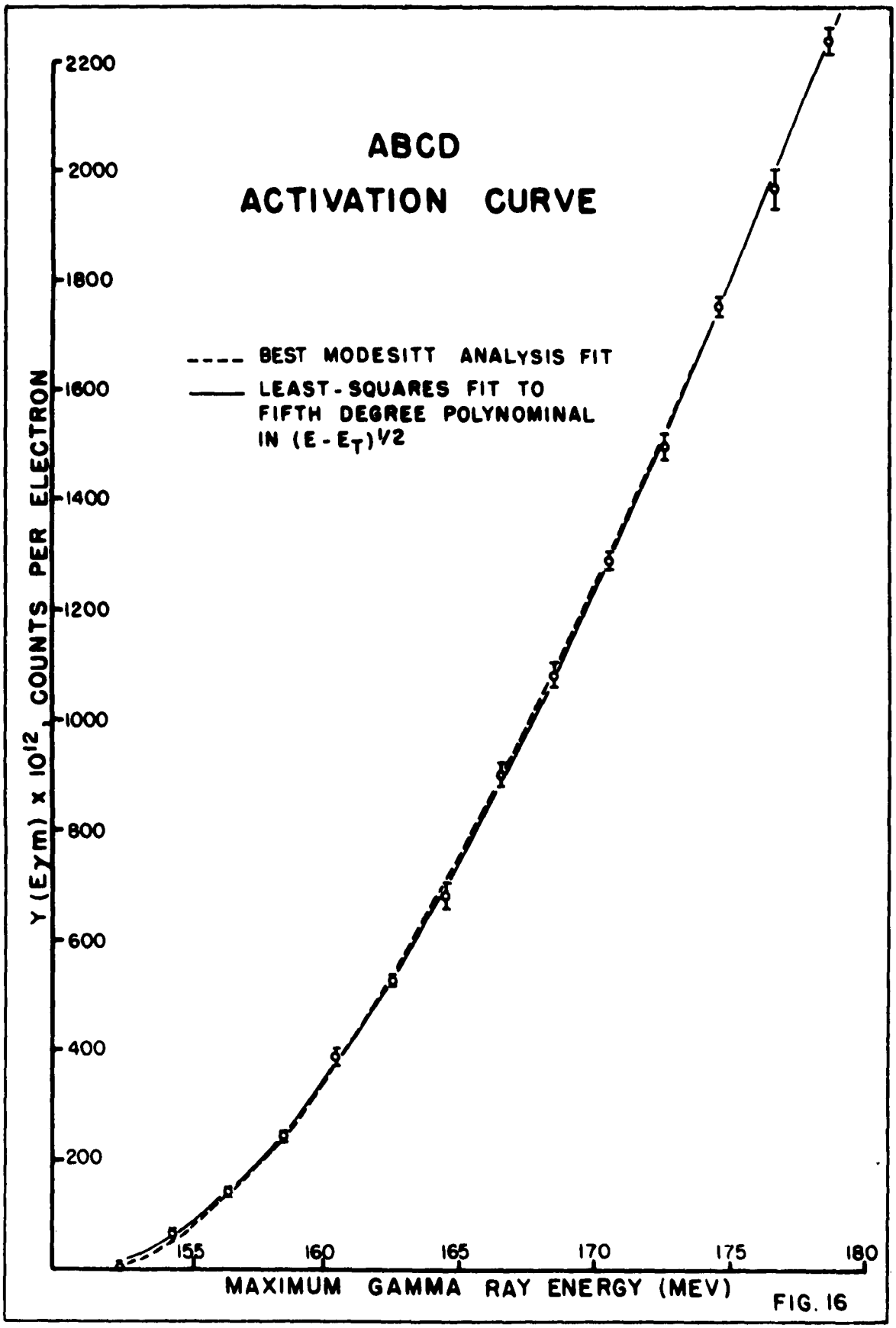
ABCD
ACTIVATION CURVE
---- BEST MODESITT ANALYSIS FIT
—— LEAST-SQUARES FIT TO FIFTH DEGREE POLYNOMINAL IN $(E-E_T)^{1/2}$
Y (Eγm) x 10^{12} COUNTS PER ELECTRON
2200
2000
1800
1600
1400
1200
1000
800
600
400
200
155
160
165
170
175
180
MAXIMUM GAMMA RAY ENERGY (MEV)

FIG. 16

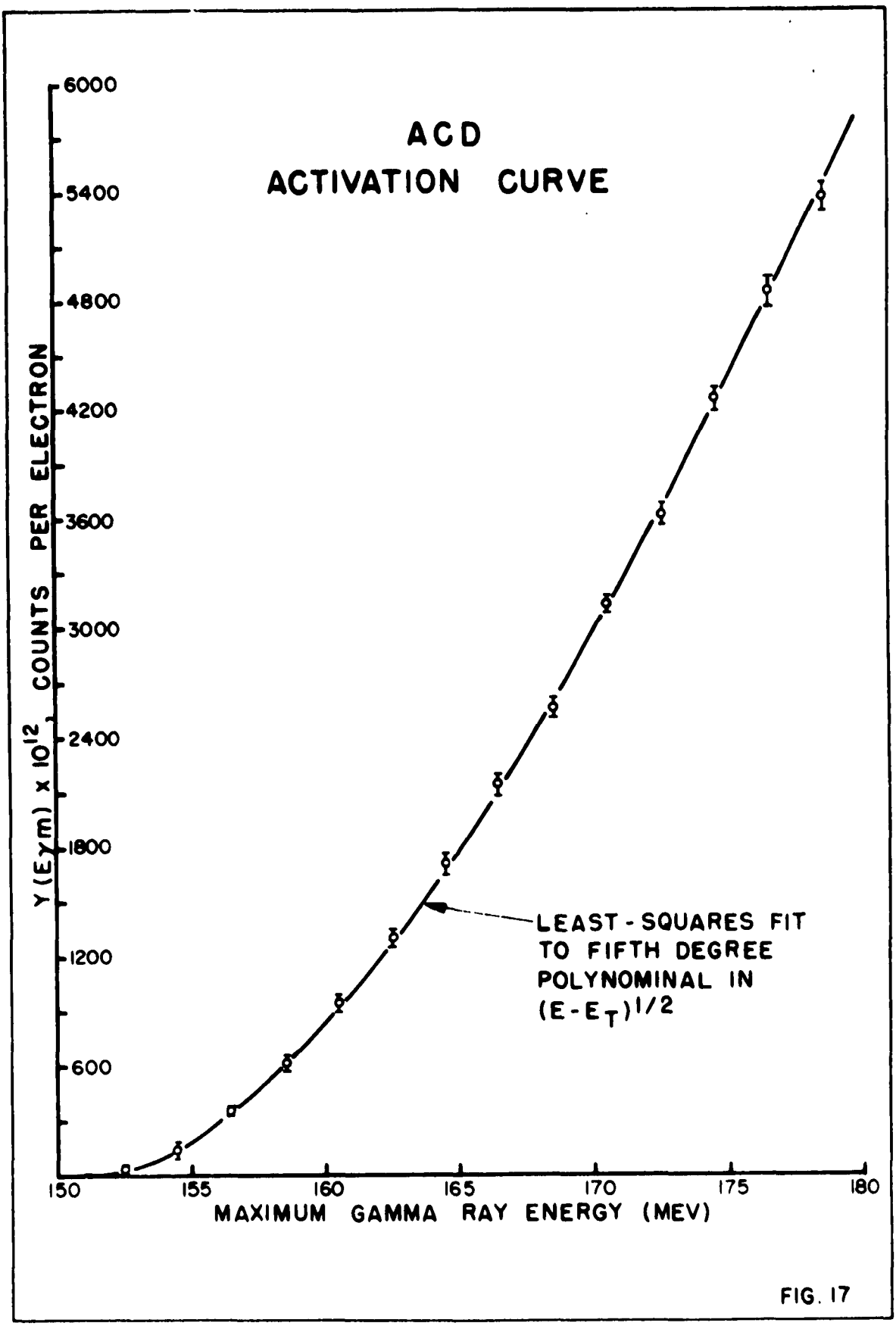
ACD
ACTIVATION CURVE
6000
5400
4800
4200
3600
3000
2400
1800
1200
600
Y(Eγm) x 10^12 COUNTS PER ELECTRON
150
155
160
165
170
175
180
MAXIMUM GAMMA RAY ENERGY (MEV)
LEAST-SQUARES FIT
TO FIFTH DEGREE
POLYNOMINAL IN
(E-E_T)^1/2

FIG. 17

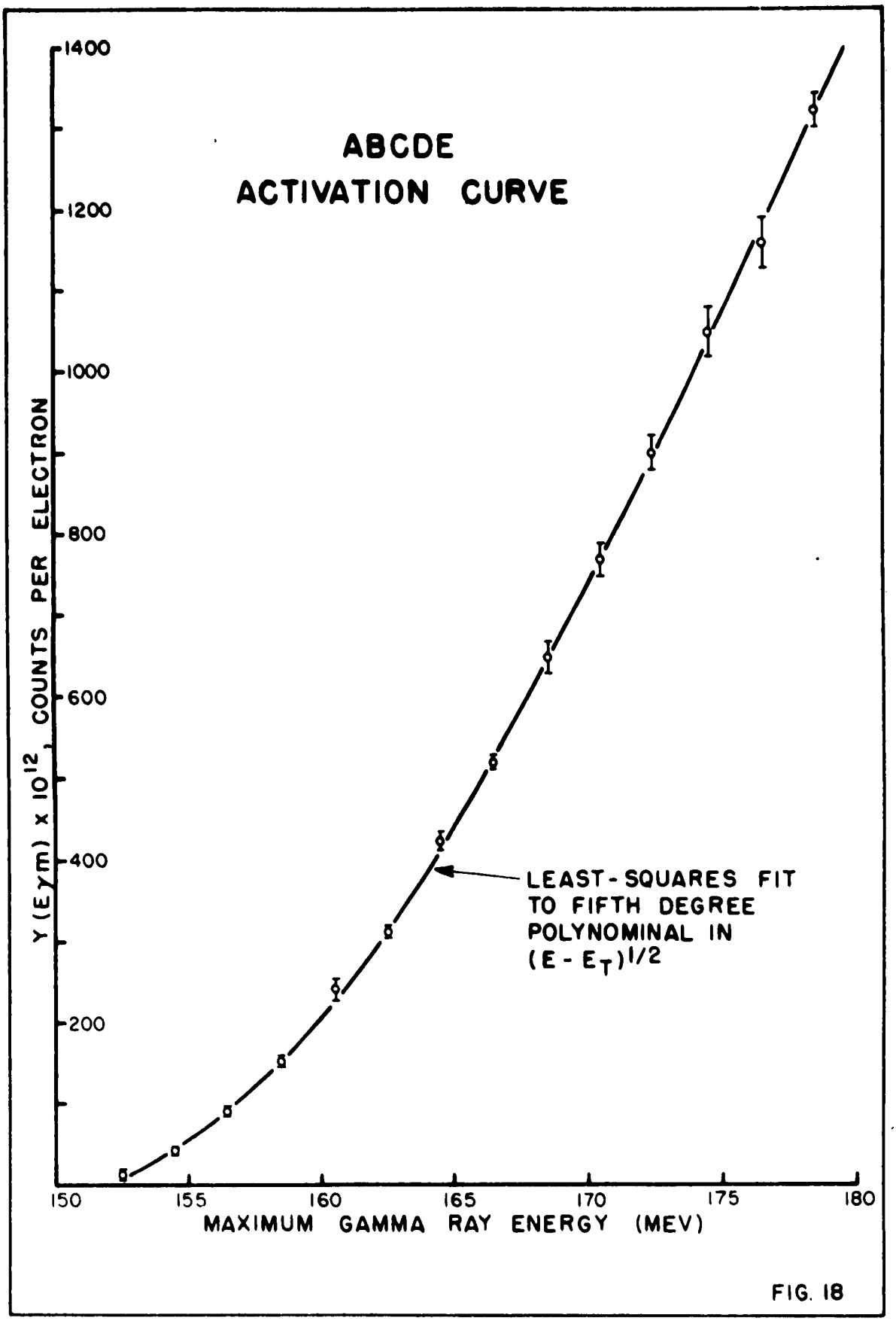
ABCDE
ACTIVATION CURVE
Y (E,m) x 10^12, COUNTS PER ELECTRON
1400
1200
1000
800
600
400
200
150
155
160
165
170
175
180
MAXIMUM GAMMA RAY ENERGY (MEV)
LEAST-SQUARES FIT
TO FIFTH DEGREE
POLYNOMINAL IN
(E - E_T)^1/2

FIG. 18

common use represent some form of approximation. Typically these approximations concern such things as the degree of screening, the possibility of making extreme relativistic approximations, and the angular distribution of the spectrum. Koch and Motz[49] have assembled a detailed tabulation of many bremsstrahlung spectra along with a discussion of the approximations involved in each one.

In any situation it is necessary to choose some spectrum in which the approximations are compatible with the requirements of the experiment. In this experiment enough multiple scattering occurred in the target so that an integrated-over-angles spectrum should be a good approximation. In the 150 Mev energy range the extreme relativistic approximation is good over most of the spectrum. However near the high energy tip, which is most important from the activation analysis standpoint, the approximation breaks down.

Three integrated-over-angles spectra are in common use for representing the x ray spectrum from a high-energy accelerator. All of them involve the extreme relativistic approximation. The Schiff spectrum (3BSe in the Koch and Motz article) assumes an approximate screening potential. It has the desirable property that at the high energy tip it has a finite value on the same order of magnitude as the experimental cross section. In addition it has a simple mathematical form. The Schiff spectrum is used as the bremsstrahlung spectrum in the Penfold-Leiss tables[48].

The original Bethe-Heitler spectrum (3BS, 3BN) is also used frequently. Graphs are necessary to incorporate the effect of the screening functions. The nonscreened case is available in an

analytical form in which the extreme relativistic approximation is not made. However the formula is very difficult to evaluate. The Bethe-Heitler formulas are now deemed most reliable for representing the region near the tip of the bremsstrahlung spectrum.

The Davies, Bethe, and Maximon formulas (3CS, 3CN) were used by Leiss and Penner[7] for the reanalysis of their original π^+ threshold data. These formulas include coulomb corrections on the wave functions (which are most important with high Z targets such as the platinum target used in the betatron) by adding an additional term to the Bethe-Heitler formulas. One of the triumphs of the Davies, Bethe, and Maximon formulation was that it removed a 10% discrepancy between theory and experiment for absolute pair production cross sections. At the present time there is some feeling that the Davies, Bethe, and Maximon spectrum is less accurate than the Bethe-Heitler spectrum near the high energy tip. However it probably gives a better value for the total bremsstrahlung radiation cross section.

These three integrated-over-angles intensity spectra have been plotted in Fig. 19 for a peak gamma ray energy of 150 Mev (Z = 78). The Bethe-Heitler and Davies, Bethe, and Maximon spectra have been normalized to the same area as the Schiff intensity spectrum (using the factor A listed by the spectrum). The high energy region has also been magnified on the graph by a factor of ten to illustrate the rather large differences that exist between the spectra in that region.

The bremsstrahlung cross section should be modified somewhat

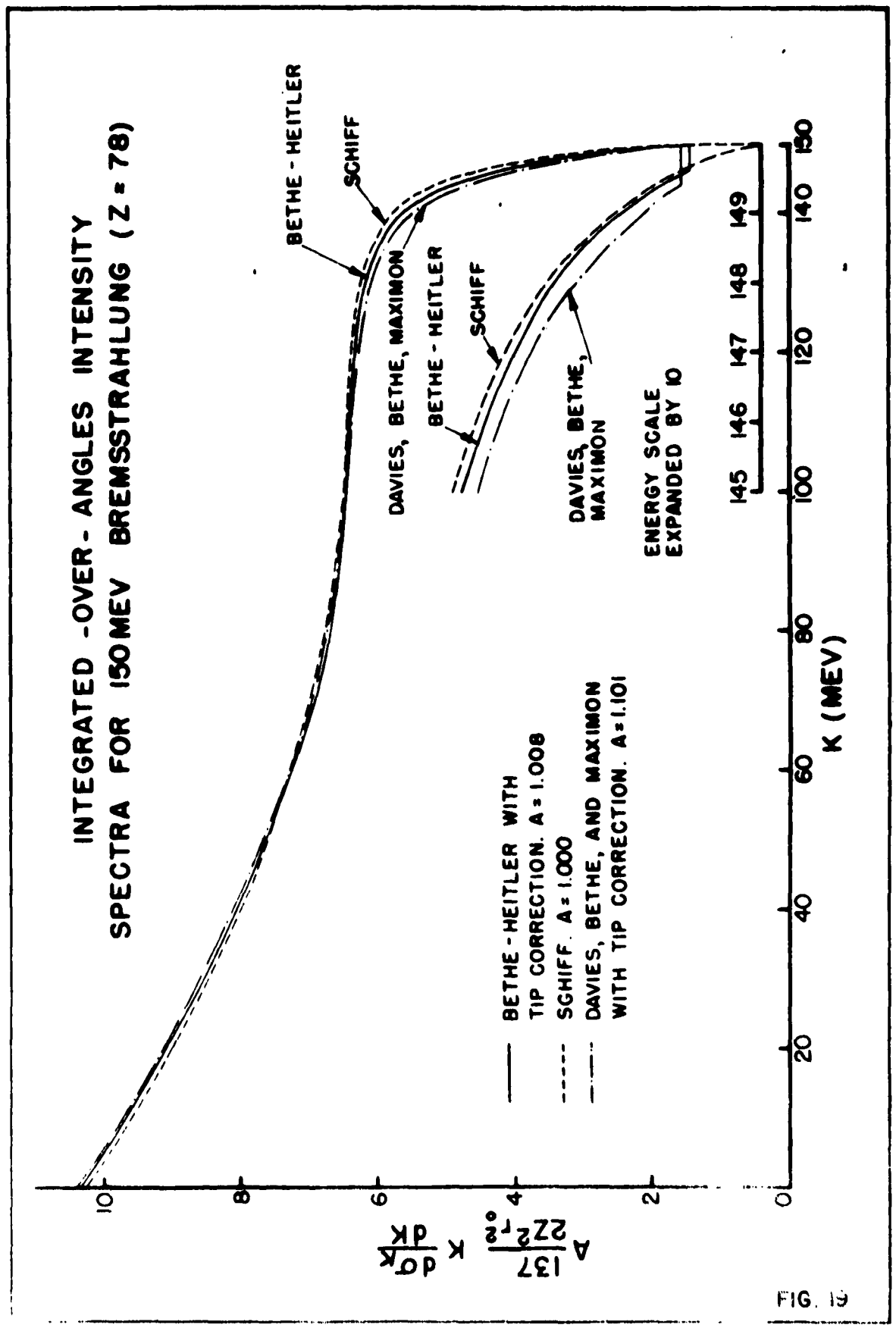
INTEGRATED -OVER- ANGLES INTENSITY
SPECTRA FOR 150 MEV BREMSSTRAHLUNG (Z = 78)
BETHE - HEITLER
SCHIFF
DAVIES, BETHE, MAXIMON
BETHE - HEITLER
SCHIFF
DAVIES, BETHE, MAXIMON
ENERGY SCALE EXPANDED BY 10
BETHE-HEITLER WITH TIP CORRECTION. A = 1.008
SCHIFF. A = 1.000
DAVIES, BETHE, AND MAXIMON WITH TIP CORRECTION. A = 1.101
$A\frac{137}{22Z^2r_e^2}\ K\frac{d\sigma_K}{dK}$
K (MEV)
0
2
4
6
8
10
20
40
60
80
100
120
140
145
146
147
148
149
150

FIG. 19

right at the high energy limit because electron bound states must be considered. Fano derived a cross section formula for this effect based on an approximation by Sauter. Later Fano et al.[50] proposed a modification which made use of the inverse of the bremsstrahlung process at the tip--the photoelectric effect. The effect has been demonstrated experimentally at 15 Mev by Fuller et al.[51] and Hall and Hanson[52] and agrees quite well with the modified Sauter-Fano correction. The effect only seems to influence the spectrum in a region of less than .4 Mev at the tip so that it is relatively unimportant even in the type of activation analysis employed in this experiment. However it has been incorporated into the Bethe-Heitler and Davies, Bethe, and Maximon spectra shown in Fig. 19 by assuming that the intensity spectrum was constant back from the tip to the point at which the normal spectrum exceeded the constant portion. The constant value chosen was the experimental value for tungsten. This procedure avoids a computational difficulty associated with the fact that the two cross sections can have negative values at the tip (a region in which they are not valid, of course).

In the analysis of this experiment no attempt has been made to apply thick-target corrections. Hisdal corrections[49] are not effective at the tip and apply to a case where the detector (the hydrogen target in this experiment) subtends a small angle on the electron beam-target axis. Thus such corrections are not important in this experiment. The Penfold method[49] considers the effects of electron energy loss in the target. However the correction is difficult to calculate. Graphs in the review

article by Koch and Motz[49] indicate that the Penfold corrections tend to lower the bremsstrahlung cross section near the tip.

Leiss[53] suggests that bremsstrahlung spectra other than the Schiff integrated-over-angles spectrum can be incorporated into the present Penfold-Leiss analysis in the following way. A theoretical activation curve is formed using the desired bremsstrahlung spectrum and some theoretical cross section. The activation curve is analyzed using the present Penfold-Leiss tables. Then the cross section correction factor is just the theoretical cross section divided by the cross section obtained using the Penfold-Leiss analysis. For this experiment factors were obtained to convert the Penfold-Leiss analysis to both Bethe-Heitler and Davies, Bethe, and Maximon spectra (with Sauter-Fano correction). Two different theoretical cross sections were used in both cases. One was a close approximation to CGLN while the other had an energy dependence consisting of only the phase space and wave function normalization factors. The corrections were found to be quite independent of the change in cross section.

For both of the spectra the correction has the effect of increasing the cross section. For the Bethe-Heitler case the correction goes from 1 at 170 Mev to 3.5 at 154 Mev. For the Davies, Bethe, and Maximon case it goes from 1.5 at 180 Mev to 13 at 154 Mev.

Penfold-Leiss Analysis: Perhaps the most straightforward method of activation curve analysis is that of Penfold and Leiss. Their procedure along with the necessary tables for its application have been presented in a Physics Research Laboratory Report[48].

(A condensed version of the report has appeared in the Physical Review[54].)

In a particular situation the validity of their approximations can be tested by applying their method to a theoretical yield curve and noting the extent to which the solution reproduces the original cross section. When this is done for the CGLN π^+ photoproduction cross section near threshold the Penfold-Leiss solution is found to agree with the original cross section to within 1% in the region from 156 to 180 Mev. Larger fluctuations occur below 156 Mev because assumptions concerning the nature of the weighting functions employed by Penfold and Leiss become more important. Reasonable changes in the form of the theoretical cross section are also adequately reproduced.(In practice the fluctuations near threshold were independent of the shape of the cross section so that the ratio, L(E), of the theoretical cross section to the Penfold-Leiss solution could be used as a correction factor on the final Penfold-Leiss solution.) Thus the Penfold-Leiss method is capable of rendering useful solutions to exact π^+ yield curves near threshold.

Unfortunately experimental yield curves are subject to statistical fluctuations. Hence some procedure must be established for discriminating between the purely random fluctuations and those due to the physical process under study. Penfold and Leiss suggest that the raw activation points be used for the cross section analysis. They reason that smoothing tends to wash out the important higher derivatives. They suggest that if smoothing is necessary it can be performed on the raw cross section values.

There are several, related objections to this technique. In the first place, weighting of the data is difficult. Second, analysis for a particular energy uses only information below that energy although the yield points above the energy do contain some further information on the cross section. Third, the possibility of negative cross sections exists in the intermediate analysis. Modesitt[55] has examined this situation in some detail. He points out that the use of the raw data is unwarranted to a certain extent since it introduces high frequency noise into the cross section. He has developed a method of cross section analysis in which the weighting and smoothing can be incorporated from the start. This method will be discussed in more detail in a later section.

For the π^+ cross section near threshold the energy dependence is closely approximated by $(E-E_T)^{1/2}$. Additional terms may exist that go as ηv^2 or $(E-E_T)^{3/2}$ so that terms can be expected in the yield curve up to the fifth power of $(E-E_T)^{1/2}$. In this experiment weighted, least-squares fits were made to the yield curves with polynomials in powers of $(E-E_T)^{1/2}$. Originally standard statistical tests (χ^2 and F tests--see for instance Cziffra and Moravscik[47]) were used to truncate the polynomial. These tests indicated that polynomials with n=4 or 5 provided reasonable fits to the activation curves. In the final analysis quintic fits were used in all cases in order to allow for the possibility of terms in the cross section of the form ηv^2. The weights were taken as $W(E) = \frac{1}{\sigma^2(E)}$ where $\sigma(E)$ is the uncertainty listed in Table VI at a particular energy. This uncertainty includes the effect of the below-threshold subtraction but not the much smaller, empty-

target background subtraction. The polynomials were used to obtain the yield at 153.5 Mev, 155.5 Mev..., 179.5 Mev in order that the values near threshold be on bin edges, as suggested by Penfold and Leiss. A standard Penfold-Leiss analysis was used to obtain the reduced cross section. The cross sections were calculated using the fitted efficiencies from the Monte Carlo calculation (Appendix E) and a target thickness of 4.845×10^{23} nuclei/cm^2. (The average target thickness over the area of the beam was 11.45 cm. A hydrogen density of .0708[56] was assumed.) The cross sections were then multiplied by correction factors to convert the Penfold-Leiss analysis to Bethe-Heitler and Davies, Bethe, and Maximon bremsstrahlung spectra. In addition they were multiplied by the ratio, L(E), of a theoretical cross section divided by the Penfold-Leiss solution for the theoretical cross section in order to compensate the effect of the Penfold-Leiss weighting functions near threshold. The values for ACD were multiplied by 1.16 = 1/f to compensate the fact that the solid angle of A was poorly specified. (The need for this correction is discussed in the section dealing with changes in the counter-target efficiency and also in the efficiency analysis appendix.) The final corrected values of the cross sections obtained with polynomial fits are tabulated in Table VII for ACD, ABCD, and ABCDE. Values for the square of the matrix element, $\sigma/4\pi W'$, have been obtained by dividing the cross section by $4\pi W' = \frac{4\pi\eta\omega}{(1+\frac{\omega}{E_n})(1+\frac{k}{E_p})}$, the phase space factor. These values

TABLE VII. TOTAL CROSS SECTION OBTAINED USING THE PENFOLD-LEISS ANALYSIS. Cross Section is in Units of 10^{-29} cm^2.

Bremsstrahlung Spectrum			Bethe-Heitler			Davies, Bethe, and Maximon
Coincidence	ABCD	ACD	ABCDE	ABCD	ACD	ABCDE
Energy (Mev)						
178.35	9.28	9.04	8.39	9.39	9.14	8.49
176.35	9.15	9.17	8.53	9.27	9.30	8.65
174.35	8.83	9.03	8.43	8.87	9.08	8.47
172.35	8.59	8.89	8.33	8.68	8.99	8.42
170.35	8.21	8.52	8.03	8.40	8.72	8.22
168.35	7.73	7.97	7.56	7.91	8.16	7.73
166.35	7.32	7.44	7.10	7.48	7.60	7.25
164.35	6.77	6.74	6.46	6.94	6.92	6.63
162.35	6.22	6.06	5.81	6.35	6.19	5.94
160.35	5.58	5.33	5.09	5.97	5.44	5.20
158.35	4.79	4.66	4.27	4.97	4.84	4.43
156.35	3.87	4.01	3.57	4.06	4.20	3.73
154.35	2.24	3.98	2.18	2.45	4.35	2.37
152.35	2.61	1.45	2.65	2.92	1.62	2.97

along with $4\pi\mathcal{W}'$ (nuclear constants from UCRL 8030-rev[56]) are tabulated in Table VIII. The values of the stripped matrix element squared have been found by dividing the cross section by $4\pi\chi' = 4\pi\mathcal{W}'/k\omega$. They are tabulated in Table IX along with $4\pi\chi'$. The stripped matrix element squared, $\sigma/4\pi\chi'$, has been plotted in Figures 20, 21, and 22 for both Bethe-Heitler and Davies, Bethe, and Maximon spectra. It should be stressed again that the experiment was planned to obtain a cross section using the coincidence ABCD. Thus neither ACD nor ABCDE were designed to yield as reliable results as those obtained from ABCD. With that reservation the agreement between the solutions for the three coincidences is quite good, indicating that the efficiency functions are consistent throughout the energy range covered in the experiment.

Possible objections to the fitting procedure can be studied with the same technique used to examine the adequacy of the Penfold-Leiss solutions. Quartic and quintic polynomials in $(E-E_T)^{1/2}$ were fitted to several theoretical yield curves (assuming an ABCD efficiency). Penfold-Leiss analyses were then made on both the original and fitted theoretical curves. Quintic fits distorted the cross section values by less than the inherent distortion of the Penfold-Leiss analysis. Quartic fits gave correct cross section values except in the region above 174 Mev. (By 178 Mev the cross section using the fitted curve was 6% lower than the original theoretical cross section. This 6% change was also observed in analyzing the experimental yield curves and prompted

TABLE VIII. VALUES FOR $\sigma_T/4\pi W'$ OBTAINED WITH THE PENFOLD-LEISS ANALYSIS. $\sigma_T/4\pi W'$ is in Units of 10^{-30} cm^2.

Bremsstrahlung Spectrum		Bethe-Heitler			Davies, Bethe and Maximon		
Coincidence		ABCD	ACD	ABCDE	ABCD	ACD	ABCDE
Energy	$4\pi W'$						
178.35	5.863	15.8	15.4	14.3	16.0	15.6	14.5
176.35	5.594	16.4	16.4	15.2	16.6	16.6	15.5
174.35	5.320	16.6	17.0	15.8	16.7	17.1	15.9
172.35	5.038	17.0	17.6	16.5	17.2	17.8	16.7
170.35	4.749	17.3	17.9	16.9	17.7	18.4	17.3
168.35	4.469	17.3	17.8	16.9	17.7	18.2	17.3
166.35	4.143	17.7	18.0	17.1	18.1	18.4	17.5
164.35	3.820	17.7	17.6	16.9	18.2	18.1	17.4
162.35	3.478	17.9	17.4	16.7	18.3	17.8	17.1
160.35	3.114	17.9	17.1	16.3	18.3	17.5	16.7
158.35	2.716	17.6	17.2	15.7	18.3	17.8	16.3
156.35	2.266	17.1	17.7	15.8	17.9	18.5	16.5
154.35	1.724	13.0	23.1	12.5	14.2	25.2	13.8
152.35	.946	27.6	15.3	28.0	30.8	17.1	31.3

TABLE IX. VALUES FOR $\sigma_T/4\pi\chi'$ OBTAINED WITH THE PENFOLD-LEISS ANALYSIS. $\sigma_T/4\pi\chi'$ is in Units of 10^{-30} cm^2.

Bremsstrahlung Spectrum		Bethe-Heitler			Davies, Bethe, and Maximon		
Coincidence		ABCD	ACD	ABCDE	ABCD	ACD	ABCDE
Energy	$4\pi\chi'$						
178.35	4.72	19.7	19.2	17.8	19.9	19.4	18.0
176.35	4.59	20.0	20.0	18.6	20.2	20.3	18.8
174.35	4.44	19.9	20.3	19.0	20.0	20.4	19.1
172.35	4.29	20.0	20.7	19.4	20.2	20.9	19.6
170.35	4.13	19.9	20.6	19.4	20.4	21.1	19.9
168.35	3.95	19.6	20.2	19.2	20.0	20.7	19.6
166.35	3.75	19.5	19.9	18.9	20.0	20.3	19.4
164.35	3.52	19.2	19.1	18.3	19.7	19.6	18.8
162.35	3.28	19.0	18.5	17.7	19.4	18.9	18.1
160.35	3.00	18.6	17.8	17.0	19.0	18.2	17.4
158.35	2.67	17.9	17.5	16.0	18.6	18.1	16.6
156.35	2.28	17.0	17.6	15.7	17.8	18.4	16.4
154.35	1.77	12.7	22.5	12.3	13.8	24.6	13.4
152.35	0.99	26.3	14.6	26.7	29.4	16.3	29.8

TOTAL CROSS SECTION DIVIDED BY $4\pi\chi'$ (FOR THE ACD COINCIDENCE)

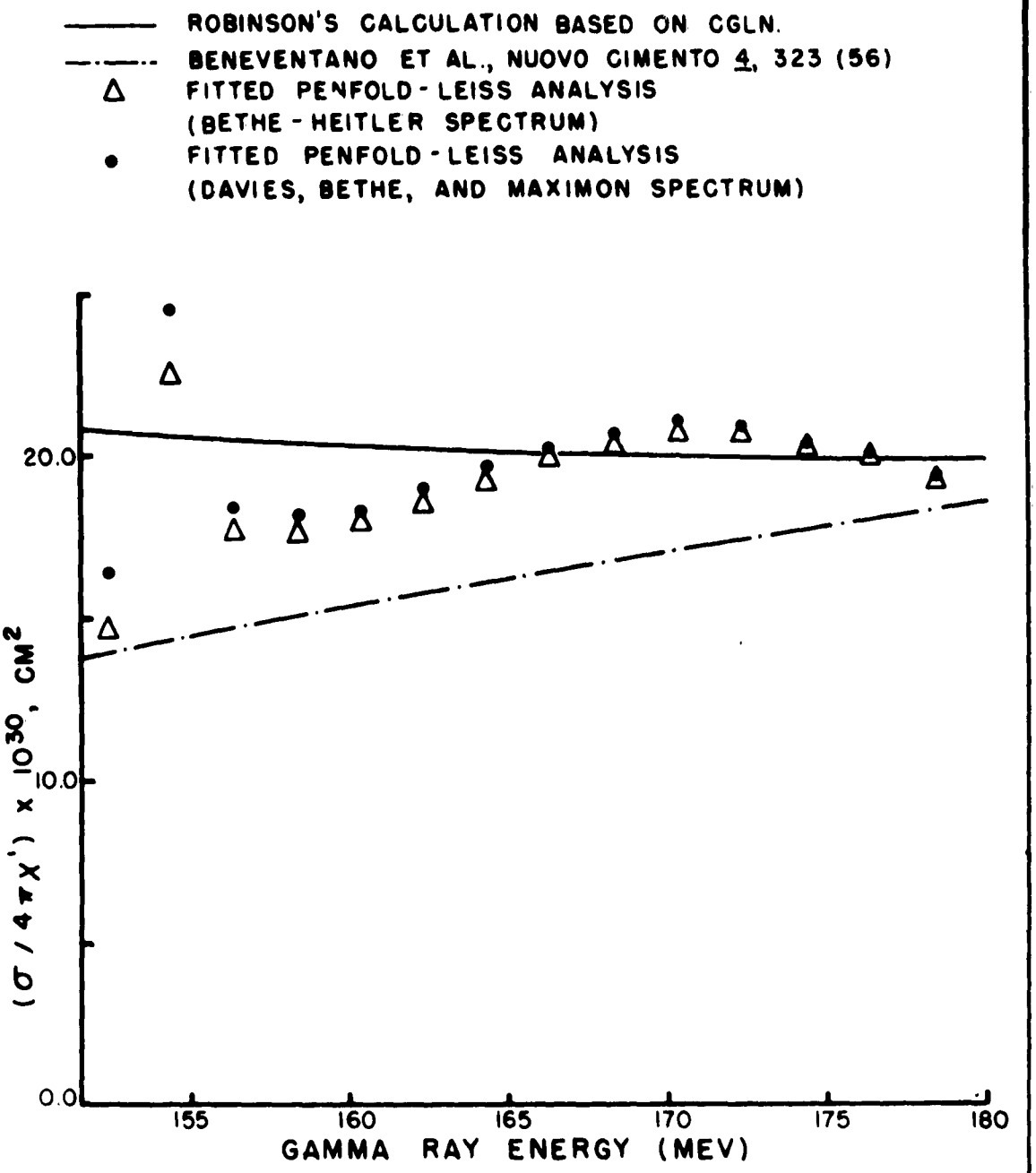

FIG. 20

TOTAL CROSS SECTION DIVIDED BY $4\pi\chi'$

(FOR THE ABCDE COINCIDENCE)

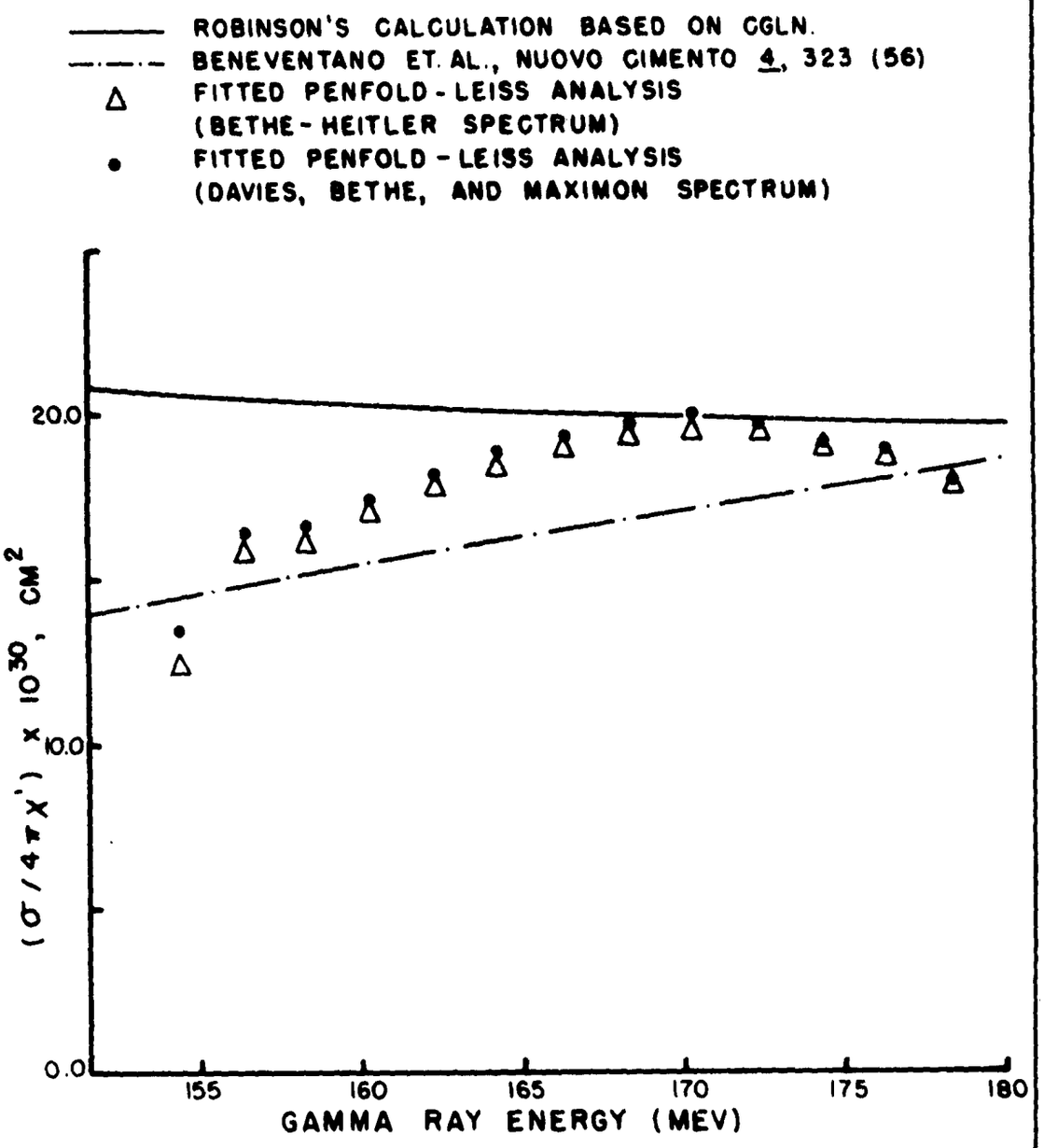

FIG. 21

the decision to always use quintic fits.)

A second test of the validity of the fitting procedure was made by dropping in turn two sets of three points from the upper end of the yield curve before it was fitted and noting the effect on the cross section. In general the cross section was relatively unchanged by this procedure except for the upper two or three points.

These tests guarantee that enough high-frequency terms have been retained in the fitting procedure. Effectively the yield curves have been fitted with a fifth-degree polynomial in the meson center of mass velocity. (Momentum $\propto$ velocity over most of the energy range.) Present theories indicate that the v^3 and v^5 terms are the important terms in the yield curves. The other coefficients serve, in part, to compensate for the fact that the efficiency is not constant, etc. There is some danger, however, that some unnecessary terms have been retained in the polynomial. Thus if a different fitting procedure is found which involves fewer coefficients but gives as good a fit, then it should be used. The next section discusses such a fit.

Modesitt Analysis: The Modesitt (least squares) method of cross section analysis[55] works in the following way. The reduced cross section $(N_1 F(E) \frac{\sigma(E')}{E'}$, where N_1 = number of nuclei per cm^2 in the target) is approximated by a linear combination of arbitrary functions $\bar{\sigma}(E) = \sum_{j=1}^{m} a_j g_j(E)$. The approximate reduced cross section defines an approximate activation curve:

$$\bar{Y}(E) = \sum_{j=1}^{m} a_j \int_{E_T}^{E} I(E,E')\, g_j(E')\, dE' \qquad \text{(IV-4)}$$

Standard least-squares techniques can be employed to determine the coefficients which give the best fit of $\bar{Y}(E)$ to $Y(E_i)$, the experimental yield points.

Modesitt suggested that the functions $g_j(E)$ be chosen to give as rapid convergence as possible. For general analysis he suggested that a convenient set might be $g_j(E) = (E-E_T)^{j-1}$. For the π^+ threshold cross section this is nearly equivalent to expanding the cross section in powers of v^2.

A more specialized approach was used in the analysis of this experiment. Since the efficiency function was known it was possible to expand the cross section itself rather than the reduced cross section. It has already been pointed out in the chapter dealing with theory that certain phase space and matrix element normalization terms can be stripped out of the cross section on quite plausible grounds. In addition the square of the stripped matrix element near threshold appears to consist mainly of an expression of the form $b_o + b_1 v^2$, where b_o and b_1 may contain the slowly-varying, dynamical variables ω and k. Under these circumstances the functions $g_j(E)$ were chosen to consist of $v^{2(j-1)}$ times the phase space and normalization factors. Specifically a matrix, H, was constructed with a set of elements:

$$H_j(E_i) = \int_{E_T}^{E_i} \frac{I(E_i,E')\ F(E')}{E'} \frac{4\pi\eta}{k(1+\omega/E_n)(1+k/E_f)}\ v^{2(j-1)}dE' \qquad \text{(IV-5)}$$

where E_i = 152.5, 154.5, ···, 178.5 Mev (the energies of the experimental yield points) and j = 1,2,3. The smoothed efficiency for ABCD was used for F(E'). One of the three bremsstrahlung distributions illustrated in Fig. 19 (divided by $2Z^2\ r_0^2/137$) was used for $I(E_i,E')$. Then the fitted yield curve is:

$$Y^s(E) = \sum_{j=1}^{n} a_j\ H_j(E) = \sum_{j=1}^{n} \frac{\alpha_j\ N_1\ A}{16}\ H_j(E) \qquad \text{(IV-6)}$$

or in matrix notation:

$$Y^s = Ha.$$

(The superscript s refers to the fact that the experimental yield points were normalized to counts/electron using a Schiff spectrum. A is a yield renormalization factor to convert to different spectra. The scaling factor 16 compensates the scaling diviser in the Penfold-Leiss tables for bremsstrahlung energy per electron in Mev/electron.) The fitted cross section is:

$$\sigma(E) = \sum_{j=1}^{n} \alpha_j\ \frac{4\pi\eta}{k(1+\omega/E_n)(1+k/E_f)}\ v^{2(j-1)} \qquad \text{(IV-7)}$$

The coefficients were obtained by the least-squares fitting procedure outlined by Modesitt, that is:

$$a = (H^T\ WH)^{-1}\ H^T\ W\ Y^s \qquad \text{(IV-8)}$$

where Y^s consists of the experimental yield points with a Schiff spectrum normalization, and W consists of the weights discussed in the section dealing with the Penfold-Leiss analysis. The errors in the coefficients were found by multiplying the square roots of the diagonal elements of $(H^T W H)^{-1}$ by $E'_{rms} = \sqrt{\sum_i d_i^2/N-n}$ where $d_i = Y_i^s - \bar{Y}_i$.

In the first application of this method three fits were made to the experimental yield points by successively increasing n from 1 to 3. This was done for each of the three bremsstrahlung distributions illustrated in Fig. 19. The best fit was obtained for n = 2. (The coefficient a_2 could be accepted at about a 99% confidence level.) The coefficients obtained for the n = 2 case were:

Spectrum	α_1	α_2/α_1
Schiff	$(16.5 \pm .26) \times 10^{-30} cm^2$	$1.003 \pm .164$
Bethe-Heitler	$(16.9 \pm .24) \times 10^{-30} cm^2$	$.960 \pm .149$
Davies, Bethe, and Maximon	$(18.3 \pm .29) \times 10^{-30} cm^2$	$.522 \pm .161$

(The uncertainties assigned to α_2/α_1 are based on the uncertainty in α_2 alone.)

The coefficients for the Bethe-Heitler and Davies, Bethe, and Maximon spectra have been used to plot the energy dependence of the stripped matrix element squared in Fig. 22. The corresponding Penfold-Leiss values have also been plotted along with the CGLN prediction and the original Beneventano et al.[2] extrapolation. The coefficients have also been used to plot the total cross

TOTAL CROSS SECTION DIVIDED BY $4\pi\chi'$
(FOR THE ABCD COINCIDENCE)

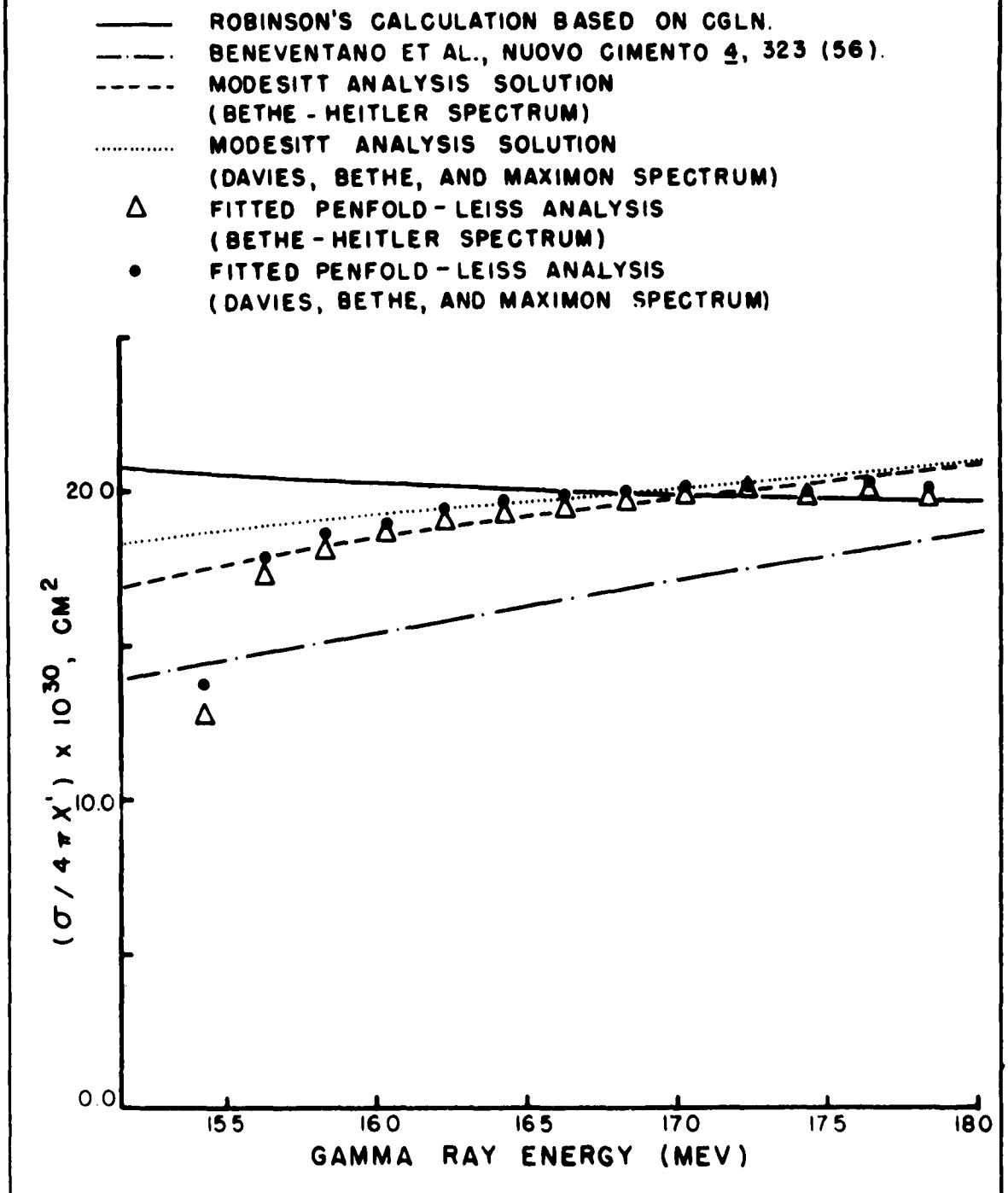

FIG. 22

section as a function of energy in Fig. 23. The fitted yield curve is shown in Fig. 16. It was actually identical to within the precision of the drawing for all three spectra.

The Modesitt analysis curves in Fig. 22 and the theoretical CGLN curve are very nearly straight lines. This is because v^2 is roughly proportional to energy near threshold. Thus if n is set equal to 2 the experimental yield curve must be determined by placing a sloping straight line on Fig. 22. The effect of improperly estimating the energy is illustrated in Appendix C. It tends to cause some local curvature near threshold on Fig. 22 and also, in turn, on the yield curve. Since the line on Fig. 22 must be straight it can only accommodate the error slightly. The three lowest points on the experimental yield curve were indeed higher than the fitted curve. Since the difference was small (roughly that expected from a .2 Mev shift) this particular systematic difference was discounted. The fact that the differences over the rest of the yield curve seem to be randomly distributed in sign indicates that other systematic departures from the assumed shape are not detectable with this set of experimental yield points. The question can be further investigated by fitting only a portion of the yield points and checking to see if the same values of the coefficients are obtained. This was done for the upper eight points (of the fourteen) since it was felt that they suffered less from many of the systematic experimental errors. In addition they had a relatively small effect on the original fits because of their low weights. When a fit was made to the upper eight points

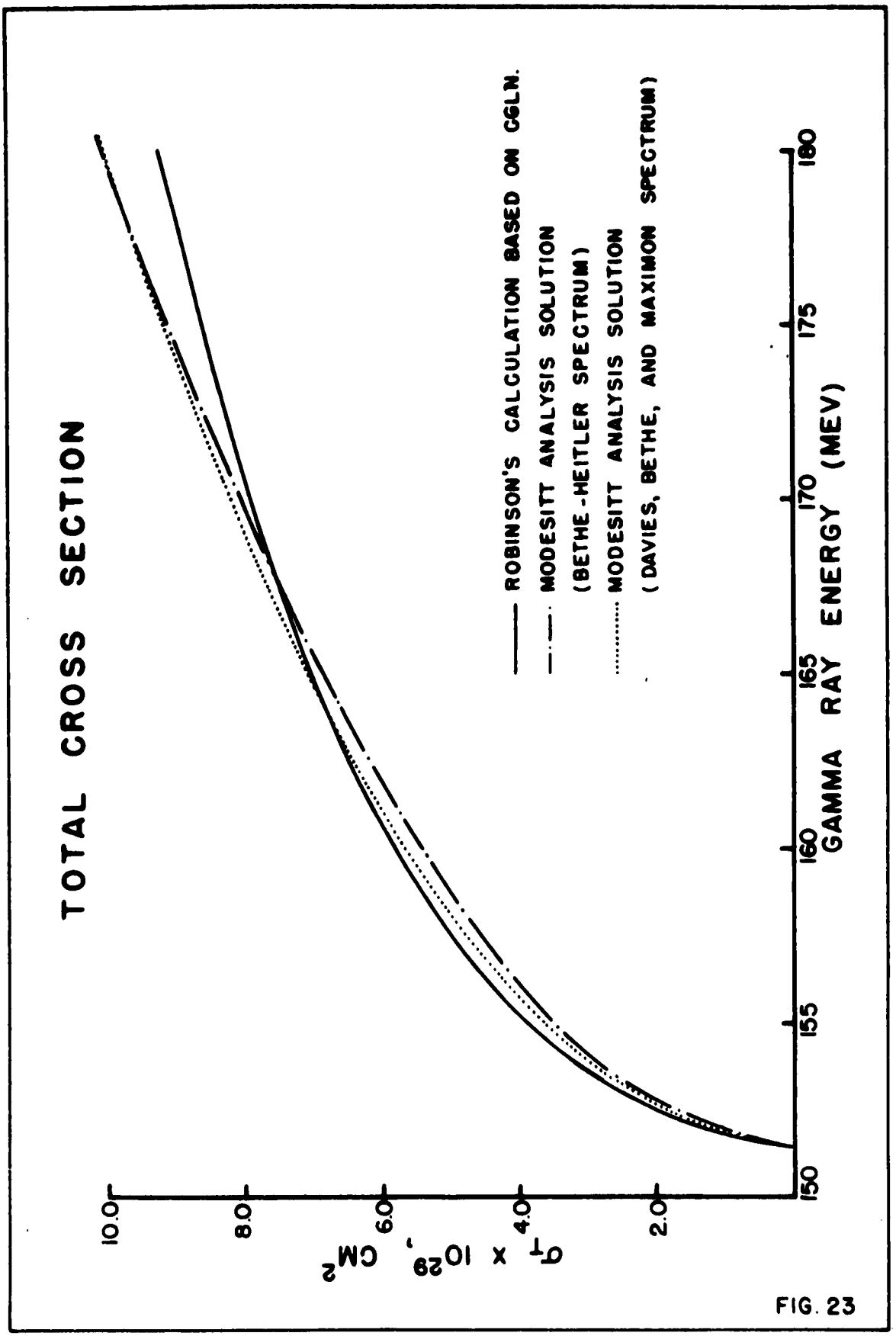
TOTAL CROSS SECTION
ROBINSON'S CALCULATION BASED ON CGLN.
MODESITT ANALYSIS SOLUTION
(BETHE-HEITLER SPECTRUM)
MODESITT ANALYSIS SOLUTION
(DAVIES, BETHE, AND MAXIMON SPECTRUM)
$\sigma_T \times 10^{29}$, CM^2
10.0
8.0
6.0
4.0
2.0
150
155
160
165
170
175
180
GAMMA RAY ENERGY (MEV)

FIG. 23

the same coefficients were obtained to within the limit of the errors on the coefficients. This is quite important information since it also indicates, when considered with the original fits, that the lower 6 points would lie on the same straight line.

The statistical errors assigned to the coefficients are quite small, particularly when viewed in the light of the errors that would have been assigned on the basis of the Penfold-Leiss technique. In the Penfold-Leiss technique the cross section is essentially a difference between yield points. This produces a set of independent cross section values at the expense of a decrease in the precision of each one. In the Modesitt analysis, however, a particular choice of the form of the cross section is made so that all cross section values are interdependent. In turn all of the experimental yield points act in concert to establish the size of the coefficients.

E'_{rms} gives some indication of the relative goodness-of-fit between the various fitting functions (that is, different spectra and type of polynomial). Cziffra and Moravscik[47] point out that E'_{rms} should be approximately one when a reasonable fit is obtained (for the weights used in this experiment). Presumably the best fit is the one with the smallest E'_{rms}. For the Modesitt analysis n=2 cases and the ABCD, fifth-degree polynomial in $(E-E_T)^{1/2}$ there were the following values for E'_{rms}:

Fit	E'_{rms}
Schiff	.92
Bethe-Heitler	.84
Davies, Bethe, and Maximon	.92
Fifth-degree Polynomial in $(E-E_T)^{1/2}$	.66

These values are gratifyingly close to one. In addition there is relatively little to choose between them. (The Modesitt n=1 cases had $E'_{rms} \simeq 2$. Thus successive fittings produced much larger changes than the differences among the above values.) The fit in $(E-E_T)^{1/2}$ probably has a lower E'_{rms} because it is better able to fit the entire curve. The lower value for the Bethe-Heitler spectrum offers some very slight supporting evidence for its use.

The Modesitt values for the cross section seem to be preferable to the fitted Penfold-Leiss values for several reasons. In the first place the same goodness-of-fit is achieved with fewer arbitrary parameters. This indicates that some of the energy dependence predicted by the fitted Penfold-Leiss method is really unjustified by the precision of the data. In the second place the Modesitt analysis offers more consistent results when the yield curve is broken into smaller segments for fitting. The Penfold-Leiss solutions have one virtue. If some undetected, systematic, experimental error exists that is not linear with energy then the Penfold-Leiss method will be more able to accommodate such an error. However it has already been pointed out that the random signs of the individual deviations in the Modesitt analysis

preclude the possibility of detecting such errors with the yield curve of this experiment.

IV-C. Changes in the Target-Counter Efficiency; Copper Absorber Runs

The proper evaluation of the target-counter efficiency is very important for a measurement of the absolute cross section. In the experiment various multifold coincidences were used to provide different solid angles and absorber depths which resulted in different efficiencies. The copper absorber runs effectively provided an additional set of absorber depths. The cross section values obtained should be independent of the particular target-counter system if the efficiencies for the various target-counter arrangements were properly evaluated. Conversely, some idea of the systematic errors involved in the efficiency analysis can be gained if the results are not independent of the target-counter system.

In all of the cases, measurement of the cross section involved an activation curve. The cross section measurements were subject to larger errors than the yield points because they were essentially yield point differences. For this reason it is more practical to use the yield points to analyze the effect of changing the efficiency. For a particular target-counter system the yield is:

$$Y_i(E) = \eta \int_{E_T}^{E} N(k)\sigma(k)\, F_i(k)\, dk \qquad (IV-9)$$

where $F_i(k)$ is the particular efficiency. The efficiency can be removed from the integral if the efficiency is independent of energy. Even if the efficiency is not independent of energy a factor, $F_i(t)$, which is dependent on the solid angle or absorber thickness, can be removed from the integral provided all of the target-counter systems have the same energy dependence, $F(k)$ (so that $F_i(k) = F_i(t)\ F(k)$). For all of the cases where the energy dependence was found this was approximately true. In fact the efficiency was relatively constant down to 160 Mev and then increased toward threshold. For yields near 180 Mev the increase near threshold has only a small effect because the cross section is relatively smaller there. Based on these approximations a ratio can be formed;

$$R_i = \frac{Y_i(E_o)}{F_i(E_o)} = \eta \int_{E_T}^{E_o} N(k)\sigma(k)\ F(k)\ dk \qquad \text{(IV-10)}$$

If the efficiencies have been evaluated properly and if the approximations listed above are correct this ratio should be independent of the target-counter system. Notice that it is only necessary to determine the yield and evaluate the efficiency at one energy to obtain the ratio.

The ratios for the various multifold coincidences were obtained for carbon by dividing the yield at 178.5 Mev (in counts per monitor) by the smoothed efficiency at 178 Mev. (This slight shift facilitated a simplification of the computer program for the copper efficiency.)

The values of the ratio and the efficiencies used were:

Coincidence	F	R
ACD	$.3812 \times 10^{-2}$	$(1.121 \pm .024) \times 10^{6}$
ABC	$.3613 \times 10^{-2}$	$(1.236 \pm .028)$ "
AD + BC	$.1357 \times 10^{-2}$	$(1.290 \pm .047)$ "
ABCD	$.1357 \times 10^{-2}$	$(1.302 \pm .047)$ "
ABCDE	$.0838 \times 10^{-2}$	$(1.246 \pm .057)$ "

The errors assigned here are based solely on the fractional deviations for the efficiency calculation at 178 Mev with no allowance for the increase in precision due to smoothing. The effect of counting statistics is small and has been neglected.

Only ACD differs significantly. The difference is due to the fact that the computer program overestimates the solid angle of A. (This has been discussed in the efficiency analysis appendix.) In order to normalize ACD to ABCD the efficiency function must be multiplied by

$$f = \frac{R_{ACD}}{R_{ABCD}} = .862.$$

Ratios for the copper absorber runs were formed in much the same manner. Background subtraction presented more of a problem since relatively fewer copper empty-target and below-threshold runs were made. In every case except ABC the below-threshold counting rate was constant with energy and consequently was subtracted directly from the yield at 178.5 Mev. The energy dependence of the below-threshold counting rate for ABC was poorly determined. As a result it was impossible to make a useful ratio for the ABC copper run. The effect of the empty-target energy dependence was accounted for by forming the difference (Δ), of the

empty-target counting rates at 180 Mev and 150 Mev (nominal) and subtracting it from the yield at 178.5 Mev.

The raw counting rates (N_r), yields (Y), etc. for copper are tabulated in Table X. The errors assigned to the counting rates are based on counting statistics. The erros assigned to R are based on the fractional deviations for the efficiency functions. On the average these ratios are slightly lower than the carbon ratios. However the difference is not statistically significant.

The primary difference, outside of solid angle, among the various target-coincidence systems is the absorber depth. The ratio, R_1, has been plotted in Fig. 24 as a function of absorber depth. The equivalent thickness is based on the equivalent carbon thickness of the counter telescope to the front face of the last counter in the coincidence plus $\sqrt{2}$ times the equivalent thickness of the target absorber. The copper absorber added roughly 7.0 g/cm^2 carbon equivalent to the carbon coincidences. ACD for copper has been included in Fig. 24 by renormalizing the efficiency by the factor f determined from the carbon runs. ABCD and AD+BC have been combined as ABCD.

The range of absorber thickness and efficiency (illustrated in Fig. 24) is substantial. The absorber depth changes by more than two while the efficiency changes by a factor of ten. The insensitivity of R_1 to these changes indicates that the approach to the efficiency analysis used in the experiment was basically sound.

TABLE X. COPPER ABSORBER COUNTING RATES AND EFFICIENCY RATIOS

Coincidence	ACD	AD + BC	ABCD	ABCDE
N_r	2640±18	1028±11	1019±11	594±14
B.T.	666±15	212±8	212±8	115±6
Δ	97±21	44±12	47±12	29±9
Y	1877±31	772±18	760±18	450±18
$F \times 10^2$	.1838	.0658	.0658	.0380
$R \times 10^{-6}$	1.021±.040	1.173±.076	1.155±.076	1.184±.100

SYMBOLS:

N_r = total counts per two sma.

B.T. = below threshold counts per two sma.

Δ = difference between 180 Mev and 150 Mev empty target counting rate.

$Y = N_r$ - B.T. - Δ = meson counts per two sma at 180 Mev (nominal).

F = counter-target efficiency.

YIELD DIVIDED BY EFFICIENCY AS A FUNCTION OF ABSORBER DEPTH

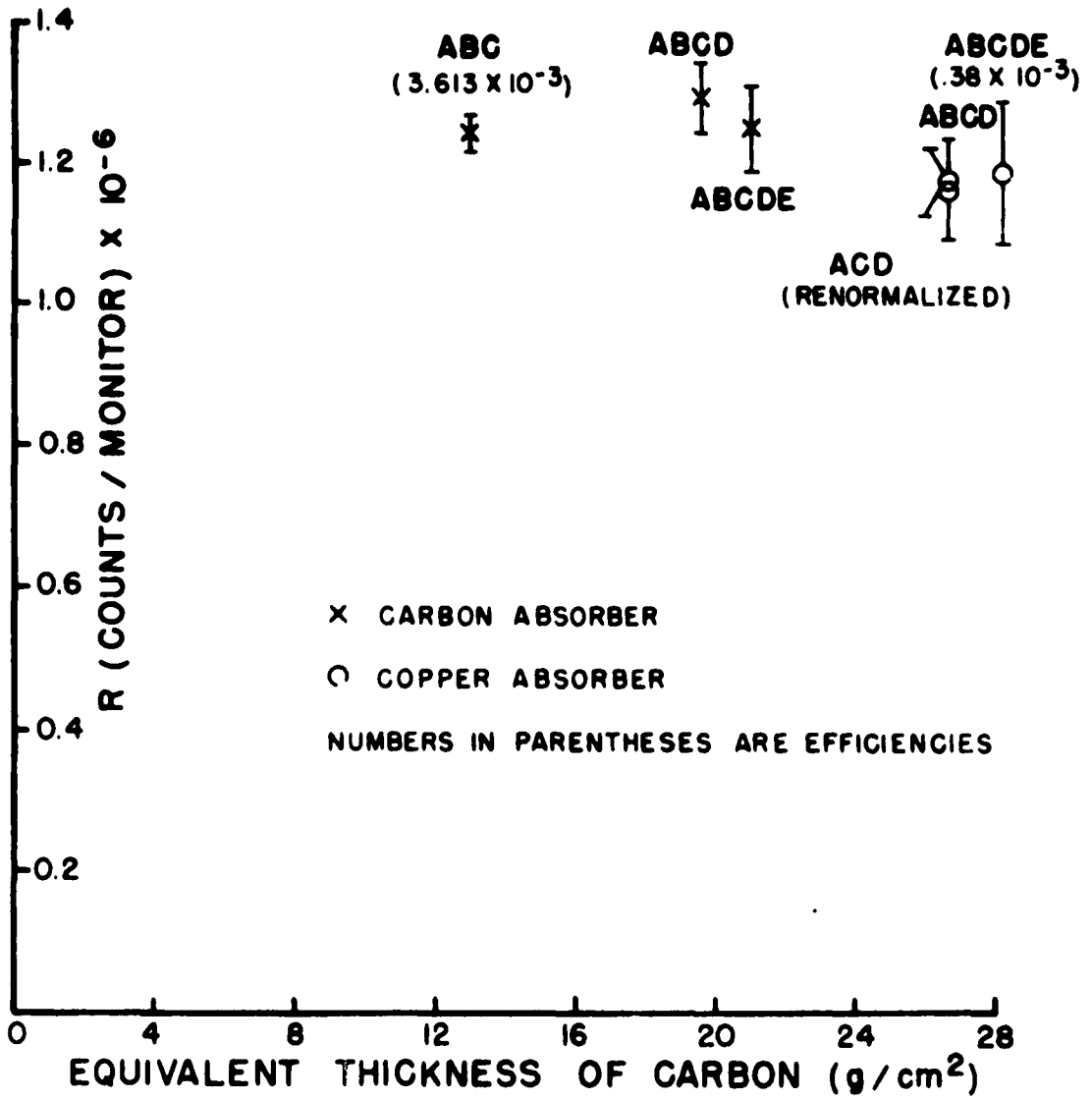

FIG. 24

IV-D. Analysis of the Counter Efficiency Calibration with a Positron Beam

The efficiency of a counter telescope coincidence for a particular positron energy and beam position should have been the number of coincidence counts divided by the number of positron counts. Over most of the surface of the counter the measured efficiency was independent of the beam position on the face of the counter. Although some fluctuations did occur they appear to have been due to changes in the background (to be discussed later). Near the edges the efficiency dropped off in the way that was expected from consideration of the position resolution of the beam and multiple scattering. When the beam was cocked at a 9° angle , the counter no detectable efficiency change occurred. (None was predicted by the efficiency calculation.) The efficiency for ACD and ABCD was the same to better than 1% with no accidentals correction. (On the average ACD might have been slightly more efficient.) Based on these facts five runs near the center of the telescope were averaged to minimize the effect of background fluctuations. The average, raw, experimental efficiencies in the central area of the telescope, E_r, were:

Coincidence	ABC	ABCD	ABCDE
t(g/cm^2, carbon equivalent)	8.3	14.9	16.6
Energy (Mev)			
61.9	.908	.841	.802
50.8	.850	.747	.693
39.6	.739	.570	.458
28.0	.508	.068	.020

The values tabulated for t are based on the carbon equivalent thickness of a coincidence plus the two probe counters. No estimate on the deviation has been given for these numbers. Counting statistics alone would have given deviations of one to two percent. The actual mean deviations were slightly larger because of the background fluctuations. By far the largest uncertainty in comparing theory and experiment is introduced by the statistical nature of the Monte Carlo calculation.

These values of E_r have been plotted against coincidence thickness in Fig. 25. The theoretical values from Appendix E are also shown along with their statistical uncertainties. Displaying the results in this fashion should produce a figure corresponding quite closely to the Leiss et al. positron range-straggling curves. The theoretical curves do have such a shape. However the experimental curves do not.

One possible explanation is that the experimental efficiencies were indeed lower than the Monte Carlo prediction. A second possibility is that the positron energy calibration was incorrect. One characteristic of the data seems to preclude both of these possibilities. A visual extrapolation of the raw efficiency at a particular energy shows that at zero thickness it always appears to have an efficiency less than one. For linear distortions of range-straggling curves this does not occur. A more plausible explanation is that some background produced counts in the beam telescope probe which did not count in the counter telescope. Such a background might have been due to positrons which scattered off

COUNTER TELESCOPE EFFICIENCY

△ 61.9 MEV
□ 50.8 MEV
○ 39.6 MEV
◇ 28.0 MEV

OPEN POINTS ARE RAW EXPERIMENTAL EFFICIENCIES.
CLOSED POINTS ARE RENORMALIZED EXPERIMENTAL EFFICIENCIES.
POINTS WITH FLAGS ARE THEORETICAL EFFICIENCIES.

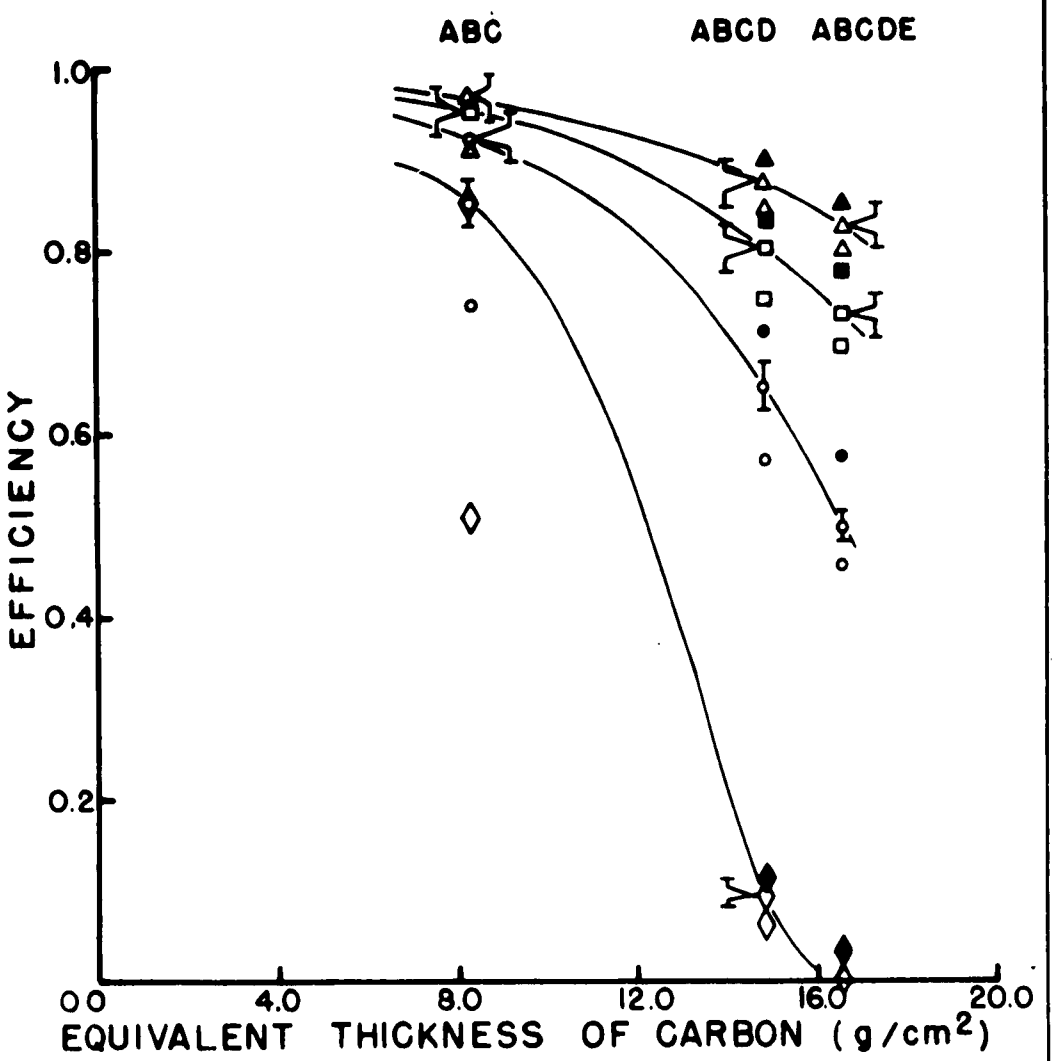

FIG. 25

of the slits. When the second slit was opened the efficiency did decrease indicating that the first slit might have served to produce such a background. During the run some precautions, such as careful adjustment of the slits, were taken to guard against the possibility of a background. Rough checks indicated agreement between the experimental efficiency and theory at some points. The apparent agreement was taken to mean that the background in the beam probe had been reduced sufficiently. The exact theoretical efficiencies and magnet calibration were not available at the time so that accurate comparisons were not made.

If a background of this type existed it rules out the possibility of using the data from the positron run for an absolute calibration of the counter telescope efficiency. However it is still possible to determine the variation of efficiency with coincidence thickness by the following procedure. Assume all of the false counts in the beam probe, P_f, are so low in energy that they cannot make a coincidence in the counter telescope. Then $E_{ri} = P_i/(P_t+P_f)$ where P_i is the number of counts in the coincidence channel and P_t is the number of true probe counts. The "true" efficiency is $E_{ti} = P_i/P_t = gE_{ri}$ where $g = (P_t+P_f)/P_t$. For this set of assumptions g is independent of depth. If g is obtained at one depth using the theoretical efficiency it can be used to give the "true" efficiency at the other depths. The most severe test of this procedure is to normalize ABC since it should be most sensitive to any low energy counts. The "true" efficiencies for ABCD and ABCDE and the values of g are:

Energy (Mev)	g	ABCD	ABCDE
61.9	1.060	.891	.850
50.8	1.119	.836	.775
39.6	1.245	.710	.570
28.0	1.673	.114	.033

These values have also been plotted in Fig. 25. They are just about as much above the theoretical points as the raw points were below. This indicates that some of the background had sufficient energy to count in ABC. Certainly neither set of experimental points agrees with the theoretical prediction. However the fact that a reasonable correction overcompensates the initial discrepancy offers some evidence that the major difficulty was not with the efficiency calculation but with the experimental arrangement.

V. INTERPRETATION OF RESULTS

In the last chapter values of the total cross section as a function of energy were obtained for positive pion photoproduction near threshold. Several methods of analysis and different bremsstrahlung spectra were employed. Reasons were given for preferring the cross section values obtained with the Modesitt analysis. (The Penfold-Leiss values actually only departed slightly from the Modesitt analysis values except very near threshold.) In addition the Bethe-Heitler spectrum was thought to provide the best representation of the high energy region of the x ray spectrum. The total cross section using the Modesitt analysis and a Bethe-Heitler bremsstrahlung spectrum was:

$$\sigma = 4\pi \chi' \times 16.9 \times 10^{-30} \left\{(1 \pm .014) + (.960 \pm .149)\, v^2\right\} \quad \text{(V-1)}$$

The uncertainties given for the coefficients are based solely on counting statistics. Several other things make contributions to the uncertainty of the cross section that are almost independent of energy. The monitor calibration was accurate to 3%. The statistical errors on the Monte Carlo calculation were about 3 1/2% for the individual points before smoothing. Statistical uncertainties in the below-threshold counting rate were already included implicitly in the uncertainties assigned to the coefficients. The uncertainty in the Michel parameter also contributed to the uncertainty in the cross section. Penner[19] calculated that a 7% change in the Michel parameter caused less than a 2% uncertainty in this type of experiment. Measurements of the Michel parameter

are now accurate to 3 1/2% (Dudziak et al.[38], Plano[57]) so that this introduces less than 1% uncertainty in the cross section.

The cross section including the overall uncertainty due to all of the effects listed above is:

$$\sigma = 4\pi \lambda\!\!\!^{-2} \times 16.9 \times 10^{-30} \left\{(1 \pm .049) + (.960 \pm .149)\, v^2\right\} \qquad (V\text{-}2)$$

Several other systematic uncertainties affect the measurement of the cross section. A plausible change in the shape of the bremsstrahlung (going to the Davies, Bethe, and Maximon spectrum) causes about a 7% change in the threshold value of the cross section. In addition the change in the spectrum causes a 50% change in the coefficient of v^2. An uncertainty in the method of defining the solid angle of B(discussed in Appendix E) could increase the cross section by as much as 2%. The energy analysis appendix showed that energy errors on the order of 1 Mev near threshold resulted in large errors in the evaluation of the matrix element. However the systematic deviation of the Modesitt fits near threshold indicated that the energy setting errors were appreciably less than 1 Mev. Uncertainties in the efficiency calculation due to energy loss parameters also cause systematic errors. For instance a change in the positron ionization loss of 4% is equivalent to a change in absorber thickness of 4%. The difference in thickness between ABCD and ABCDE is about 11% (for the counter telescope) and results in a change of 25 to 30% in efficiency. Thus a 4% change in the ionization loss could result in roughly 10% uncertainty in the cross section. The agreement among the various target-counter arrangements rules out the possibility

that such effects could be very large. Systematic errors may have occurred in the extrapolation of the below-threshold counting rates. However they were minimized by the choice of counter telescope thickness.

With these limitations in mind it is possible to compare the cross section obtained with this experiment to theoretical predictions for the cross section. At threshold the cross section for photoproduction should be:

$$\sigma_\tau = 4\pi \chi' 2e^2 f^2 \left(\frac{\hbar}{\mu c}\right)^2 \left[1-R(\omega=1)\right] = 4\pi \chi' \alpha_1 \qquad \text{(V-3)}$$

where $R(\omega)$ is some recoil term. The coupling constant is then:

$$f^2 = \frac{\alpha_1}{2e^2 \left(\frac{\hbar}{\mu c}\right)^2 \left[1-R(\omega=1)\right]} \qquad \text{(V-4)}$$

If $R(\omega) = \frac{g_p + g_n}{M} \omega$ (See Cini et al.[3] for instance) then at threshold $R = .130$ and the value of the expression inside the brackets is .870. This gives a value for the coupling constant of $f^2 = .067 \pm .003$. (Use of a Davies, Bethe, and Maximon spectrum gives $f^2 = .072$.) Such a values is appreciably below the values obtained from other sources. (For instance a recent analysis by Noyes and Edward[58] of many scattering experiments below 220 Mev indicated that $f^2 = .086 \pm .019$.)

Major contributions to the coefficient of v^2 come from several sources. The effects of the direct interaction term tend to make the coefficient negative. If k were equal to one and the angular distribution of the direct interaction term was isotropic the net effect of the direct interaction would be to make $\alpha_2 = -1/2\ \alpha_1$. Actually the angular distribution reduces the

effects of the term on the total cross section by about 1/3. In addition the effect of the p wave terms tends to make the coefficient of v^2 positive. (They have 1/3 to 1/2 of the effect of the direct interaction.) Thus α_2 is expected to be negative and about 1/6 of α_1. This experiment gives a positive value of α_2 that is nearly equal to α_1.

Increasing the magnitude of the recoil effect tends to diminish the coupling constant discrepancy. Doubling the size of the recoil term would make $f^2 = .0785$. Increasing the size of the recoil term would also lead to an increase in the π^-/π^+ ratio.

Reversal of the sign of the direct interaction term for some unknown reason (and also contrary to the experimental evidence, see Malmberg[39] for instance) would result in agreement between the experimental and theoretical values for α_2. However the lack of agreement for the coupling constant would be unchanged. Increasing the p wave contribution would have a similar effect, that is it would tend to make the coefficient of v^2 positive but would not reconcile the coupling constant difference.

Several alterations on the theoretical cross section near threshold have been proposed. Hamilton and Woolcock[35] have illustrated the effect of a small electric dipole moment amplitude on the cross section. They find that a negative value would decrease the cross section but not alter the energy dependence appreciably. Ball[59] has calculated the effect of a π-π resonance on the threshold cross section in terms of a second coupling constant, Λ. (Similar calculations have also been made

by De Tollis et al.[60] and Gourdin et al.[61]) Negative values lower the cross section in a manner quite similar to that of an electric dipole moment amplitude so that it would be difficult to distinguish between the two effects. Either one of these could diminish the coupling constant difference but not change the coefficient of α_2. Baldin[36] has proposed that the effect of the unphysical region can be minimized by considering only differential cross sections at the angles corresponding to the momentum transfer at threshold. Recently Walker[62] applied Baldin's proposal to positive pion photoproduction and detected evidence of a resonance at 210 Mev which he attributed to a π-π interaction. The effect was to increase the cross section above that of CGLN. A π-π resonance acting this close to threshold might serve to increase α_2.

None of the alternatives proposed above offers a clear path away from the inconsistencies. In order to remove both of them a theory must provide some mechanism for decreasing the theoretical cross section at threshold and making the matrix element increase with v^2 near threshold.

It is worthwhile to point out that nearly every group of experimental measurements of the cross section near threshold shows a trend of increasing faster than CGLN. In the published correction for the Leiss, Penner, and Robinson experiments[7] the agreement with CGLN was reported to be good. However the correction was made with a Davies, Bethe, and Maximon bremsstrahlung spectrum. If a Bethe-Heitler spectrum was used instead their corrected values for the matrix element would presumably increase

with v^2 also.

APPENDIX A. CIRCUIT DIAGRAMS

Diagrams of the fast electronic circuits employed in this experiment are shown in the following seven figures. Detailed discussions of this type of circuitry have been given by Leiss[18] and Jones[42].

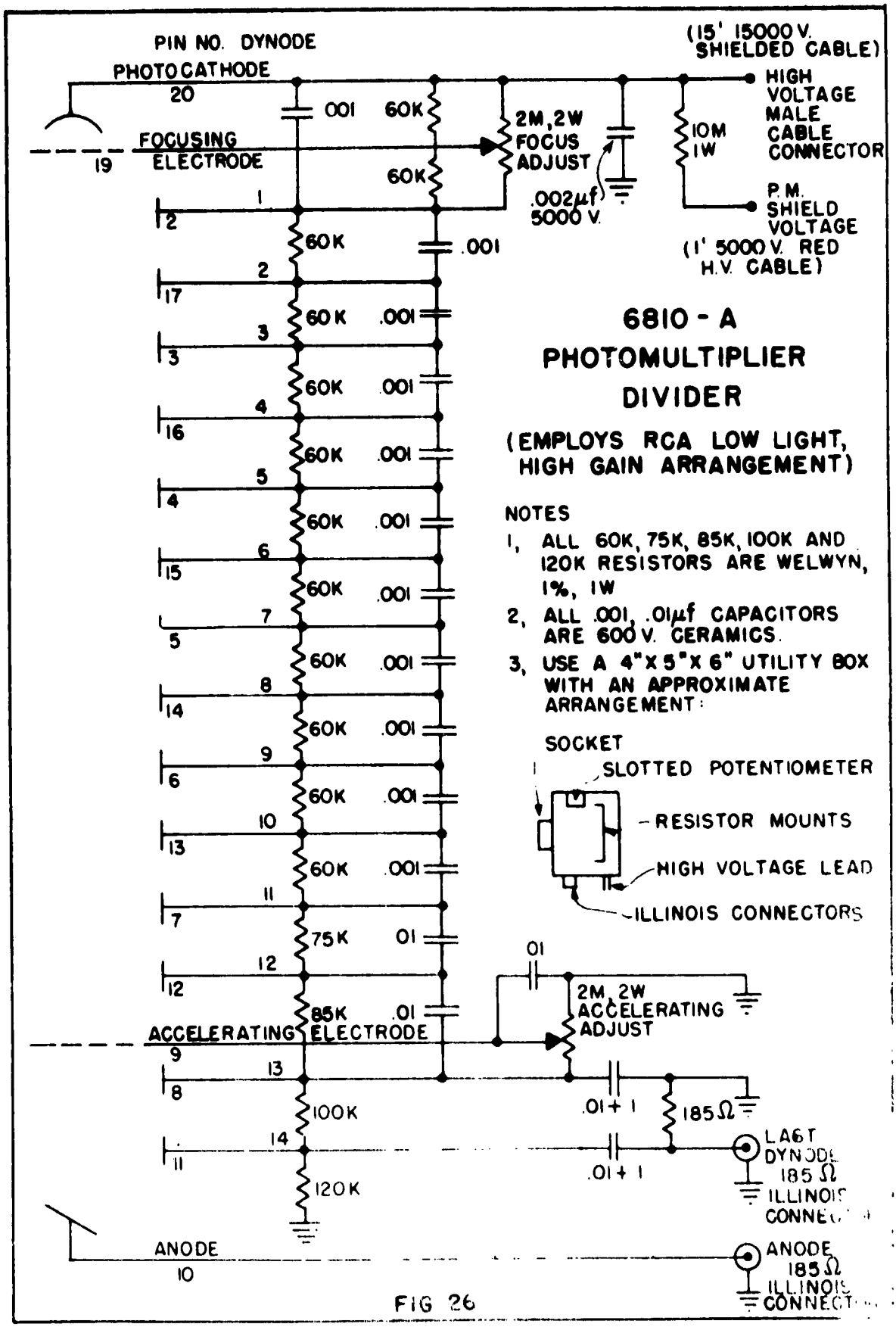
PIN NO. DYNODE
PHOTOCATHODE
20
FOCUSING
ELECTRODE
19
(15' 15000 V. SHIELDED CABLE)
HIGH VOLTAGE MALE CABLE CONNECTOR
P.M. SHIELD VOLTAGE
(1' 5000 V. RED H.V. CABLE)
.001
60K
2M, 2W FOCUS ADJUST
.002μf 5000 V.
10M 1W
6810 - A
PHOTOMULTIPLIER
DIVIDER
(EMPLOYS RCA LOW LIGHT, HIGH GAIN ARRANGEMENT)
NOTES
1, ALL 60K, 75K, 85K, 100K AND 120K RESISTORS ARE WELWYN, 1%, 1W
2, ALL .001, .01μf CAPACITORS ARE 600 V. CERAMICS.
3, USE A 4"X 5"X 6" UTILITY BOX WITH AN APPROXIMATE ARRANGEMENT:
SOCKET
SLOTTED POTENTIOMETER
RESISTOR MOUNTS
HIGH VOLTAGE LEAD
ILLINOIS CONNECTORS
75K
.01
85K
ACCELERATING ELECTRODE
2M, 2W ACCELERATING ADJUST
100K
120K
.01+1
185Ω
LAST DYNODE 185 Ω ILLINOIS CONNECTOR
ANODE
10
ANODE 185 Ω ILLINOIS CONNECTOR

FIG 26

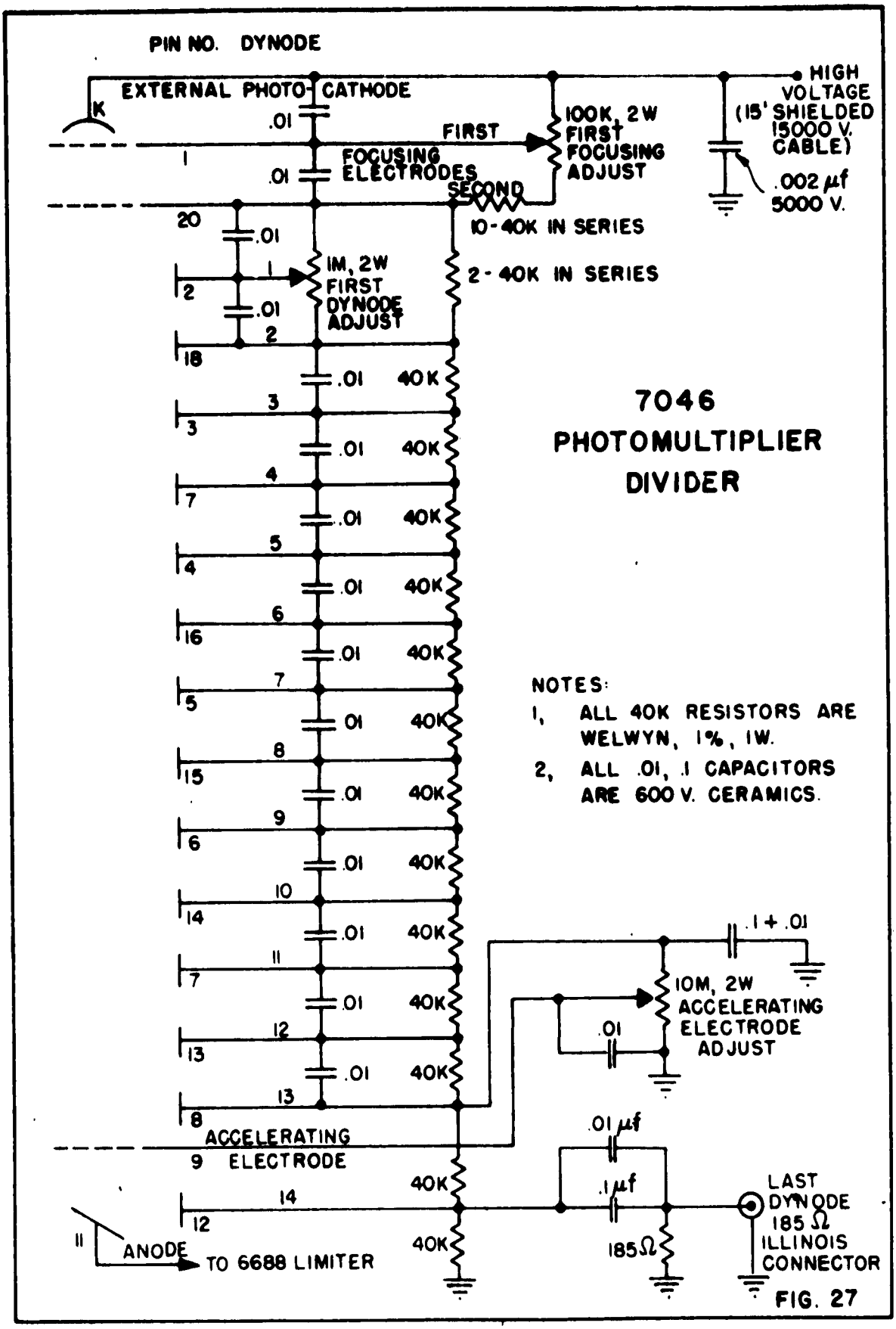
PIN NO. DYNODE
EXTERNAL PHOTO-CATHODE
K
.01
FIRST
FOCUSING ELECTRODES
.01
100K, 2W FIRST FOCUSING ADJUST
HIGH VOLTAGE (15' SHIELDED 15000 V. CABLE)
.002 μf 5000 V.
SECOND
10-40K IN SERIES
2-40K IN SERIES
1M, 2W FIRST DYNODE ADJUST
.01
40K
7046
PHOTOMULTIPLIER
DIVIDER
NOTES:
1, ALL 40K RESISTORS ARE WELWYN, 1%, 1W.
2, ALL .01, .1 CAPACITORS ARE 600 V. CERAMICS.
.1 + .01
10M, 2W ACCELERATING ELECTRODE ADJUST
ACCELERATING ELECTRODE
.01 μf
.1 μf
185Ω
LAST DYNODE 185 Ω ILLINOIS CONNECTOR
ANODE
TO 6688 LIMITER

FIG. 27

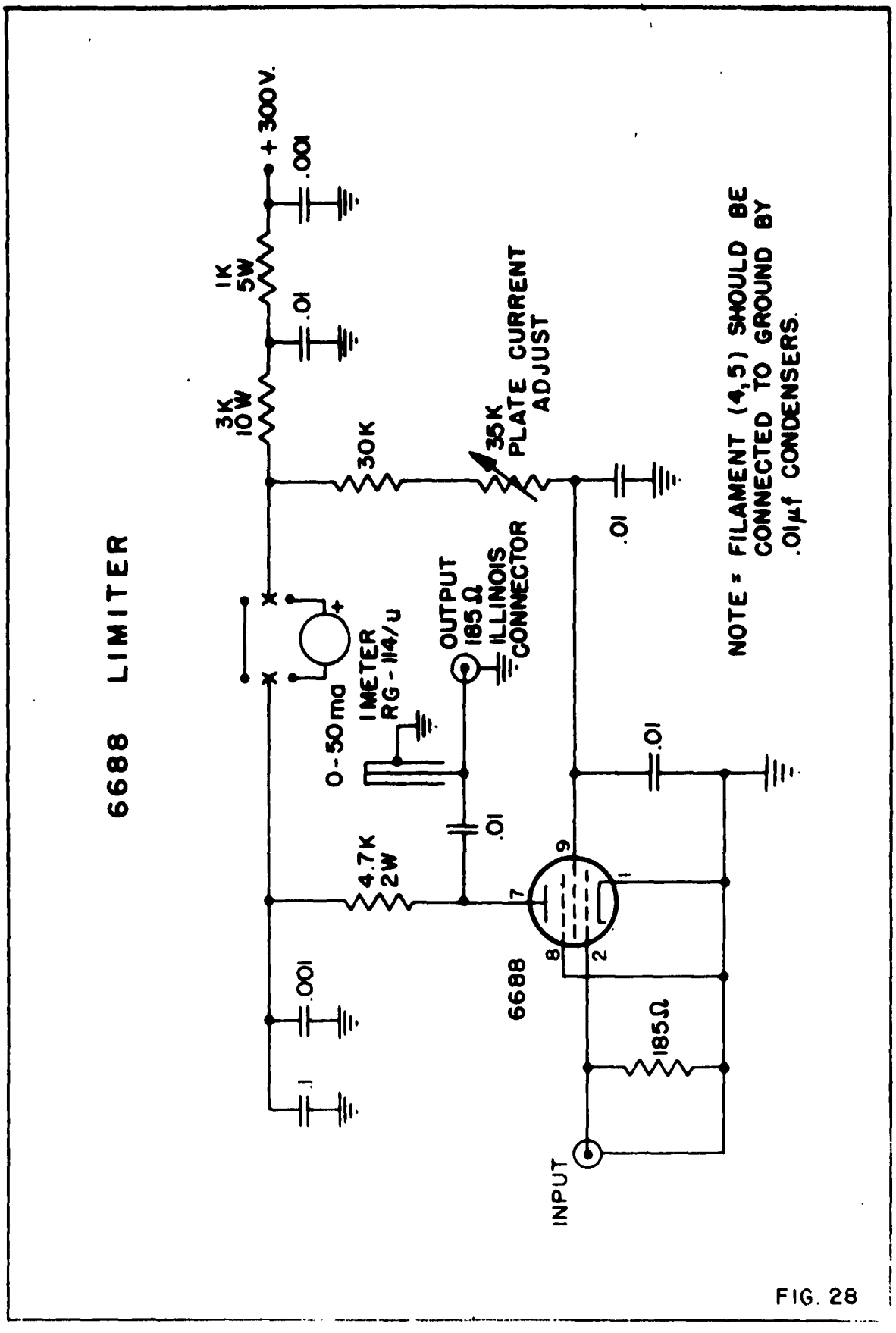
6688 LIMITER
+300V
.001
1K 5W
.01
3K 10W
30K
35K PLATE CURRENT ADJUST
.01
OUTPUT 185Ω ILLINOIS CONNECTOR
0-50 ma
IMETER RG-114/U
.01
4.7K 2W
.001
.1
6688
185Ω
INPUT
NOTE = FILAMENT (4,5) SHOULD BE CONNECTED TO GROUND BY .01μf CONDENSERS.

FIG. 28

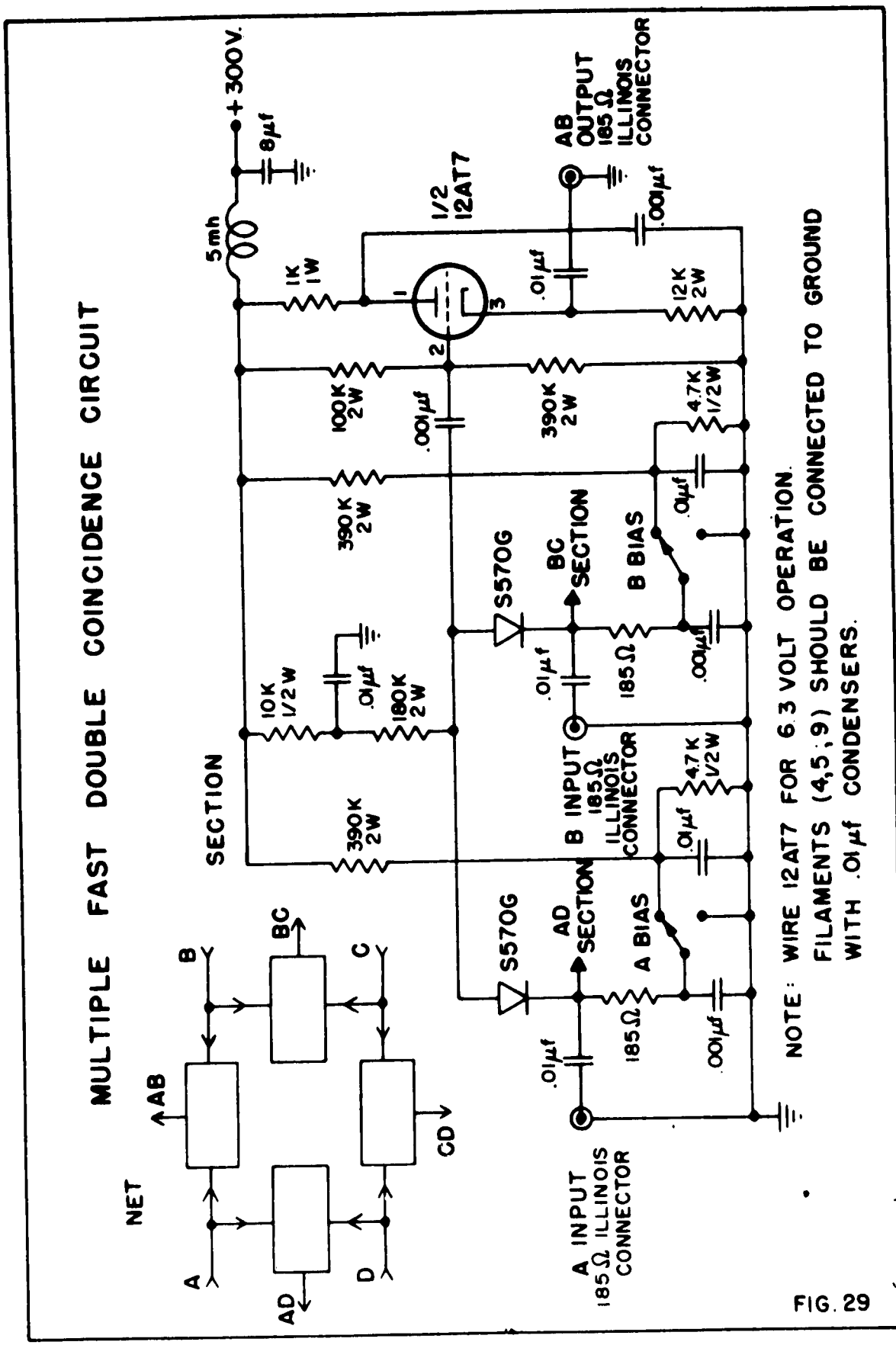
MULTIPLE FAST DOUBLE COINCIDENCE CIRCUIT
+300V.
8μf
5mh
1K 1W
1/2 12AT7
AB OUTPUT 185Ω ILLINOIS CONNECTOR
.001μf
.01μf
12K 2W
100K 2W
.001μf
390K 2W
4.7K 1/2W
390K 2W
.01μf
B BIAS
.001μf
S570G
BC SECTION
10K 1/2W
.01μf
180K 2W
185Ω
B INPUT 185Ω ILLINOIS CONNECTOR
4.7K 1/2W
390K 2W
SECTION
.01μf
S570G
AD SECTION
A BIAS
185Ω
.001μf
.01μf
A INPUT 185Ω ILLINOIS CONNECTOR
NET
A
B
C
D
AB
BC
CD
AD
NOTE: WIRE 12AT7 FOR 6.3 VOLT OPERATION.
FILAMENTS (4,5;9) SHOULD BE CONNECTED TO GROUND
WITH .01μf CONDENSERS.

FIG. 29

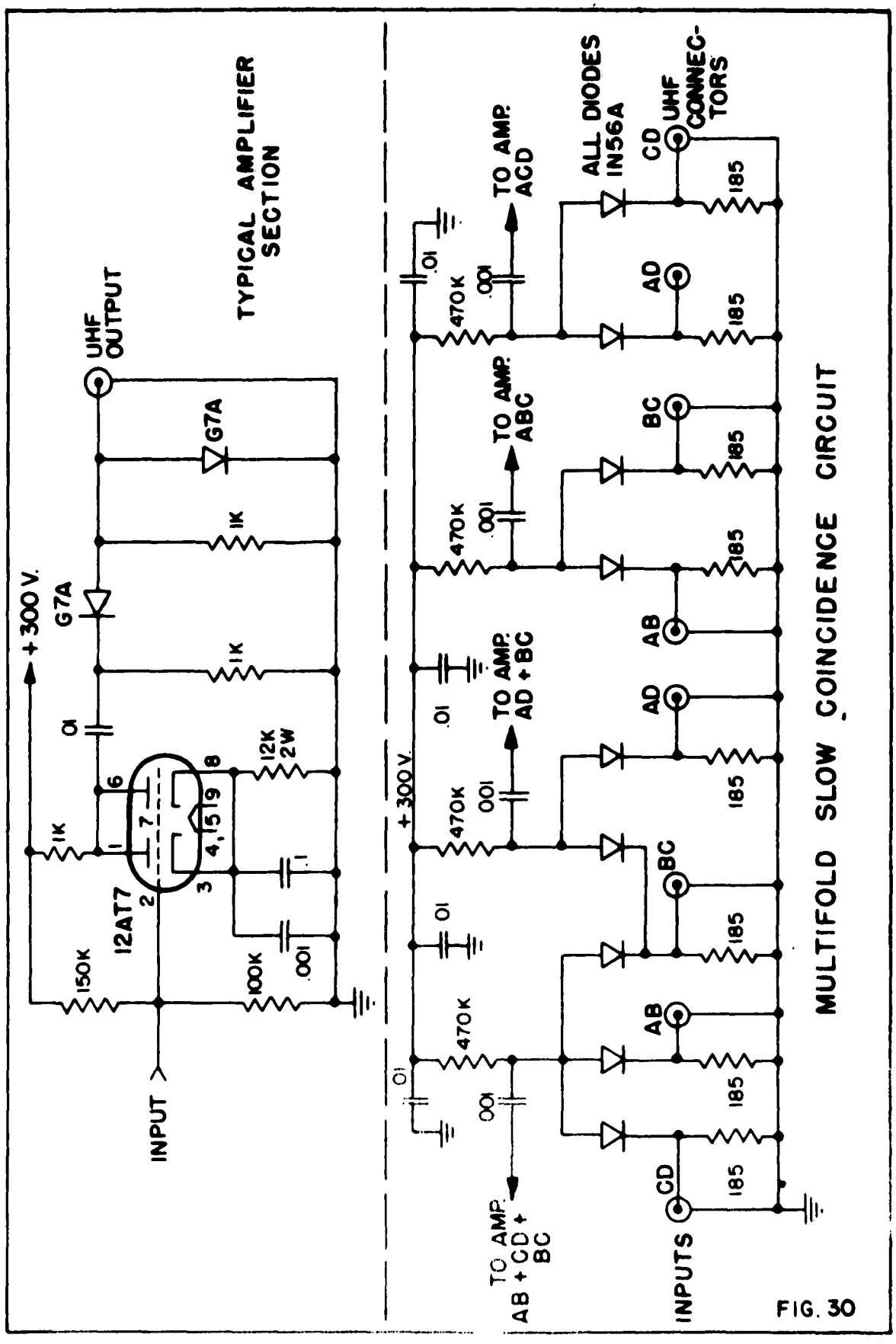
TYPICAL AMPLIFIER SECTION
UHF OUTPUT
+300 V.
G7A
1K
1K
.01
12K 2W
1K
12AT7
4,1519
150K
100K
.001
.1
INPUT
MULTIFOLD SLOW COINCIDENCE CIRCUIT
ALL DIODES IN56A
UHF CONNEC-TORS
TO AMP. ACD
TO AMP. ABC
TO AMP. AD + BC
TO AMP. AB + CD + BC
470K
185
AD
BC
AB
CD
INPUTS

FIG. 30

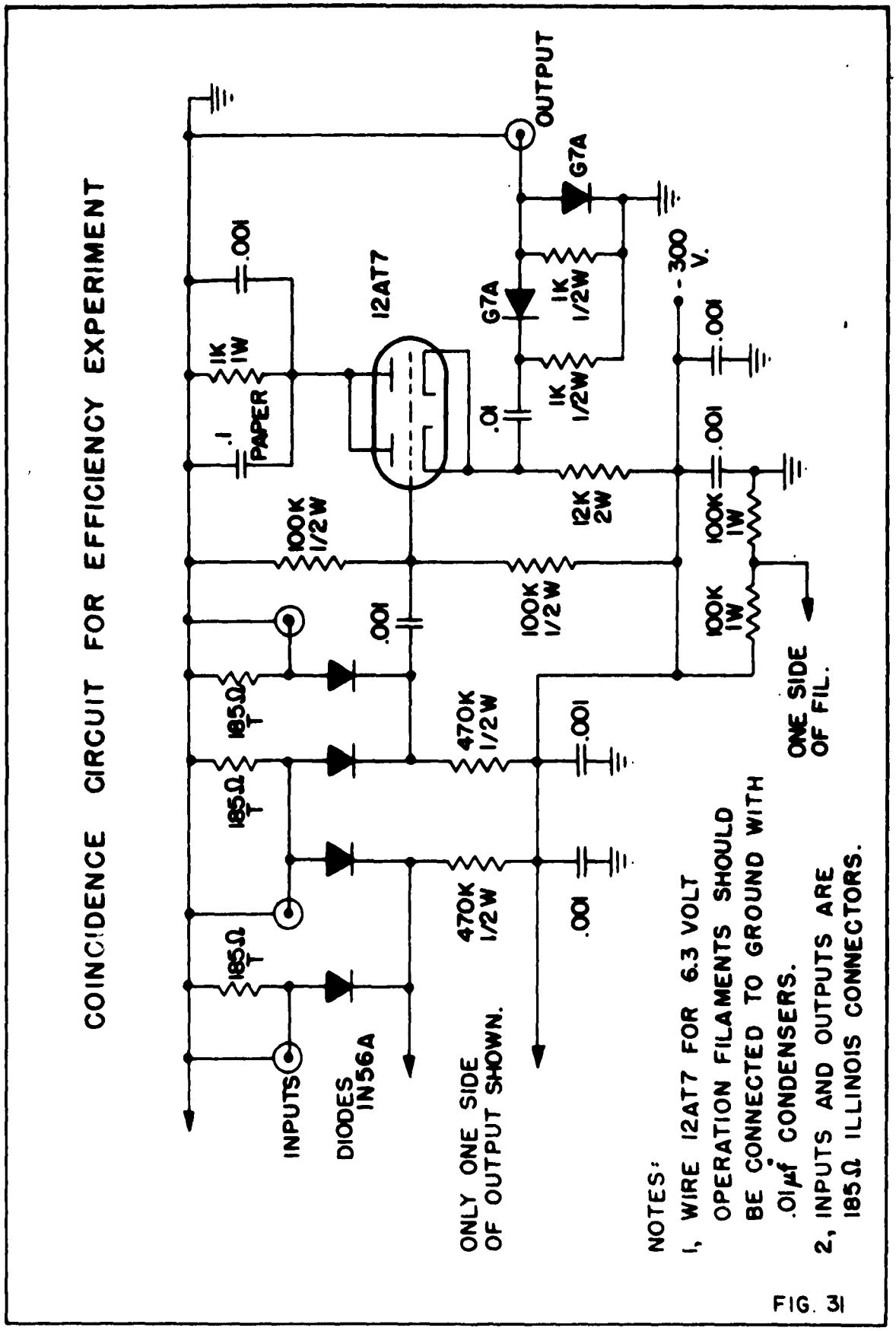
COINCIDENCE CIRCUIT FOR EFFICIENCY EXPERIMENT
OUTPUT
G7A
12AT7
.001
1K 1W
.1 PAPER
G7A
1K 1/2W
1K 1/2W
-300 V.
.001
.01
.001
12K 2W
100K 1/2W
100K 1W
100K 1/2W
100K 1W
.001
185Ω T
185Ω T
185Ω T
470K 1/2W
470K 1/2W
.001
.001
ONE SIDE OF FIL.
INPUTS
DIODES IN56A
ONLY ONE SIDE OF OUTPUT SHOWN.
NOTES:
1, WIRE 12AT7 FOR 6.3 VOLT OPERATION FILAMENTS SHOULD BE CONNECTED TO GROUND WITH .01μf CONDENSERS.
2, INPUTS AND OUTPUTS ARE 185Ω ILLINOIS CONNECTORS.

FIG. 31

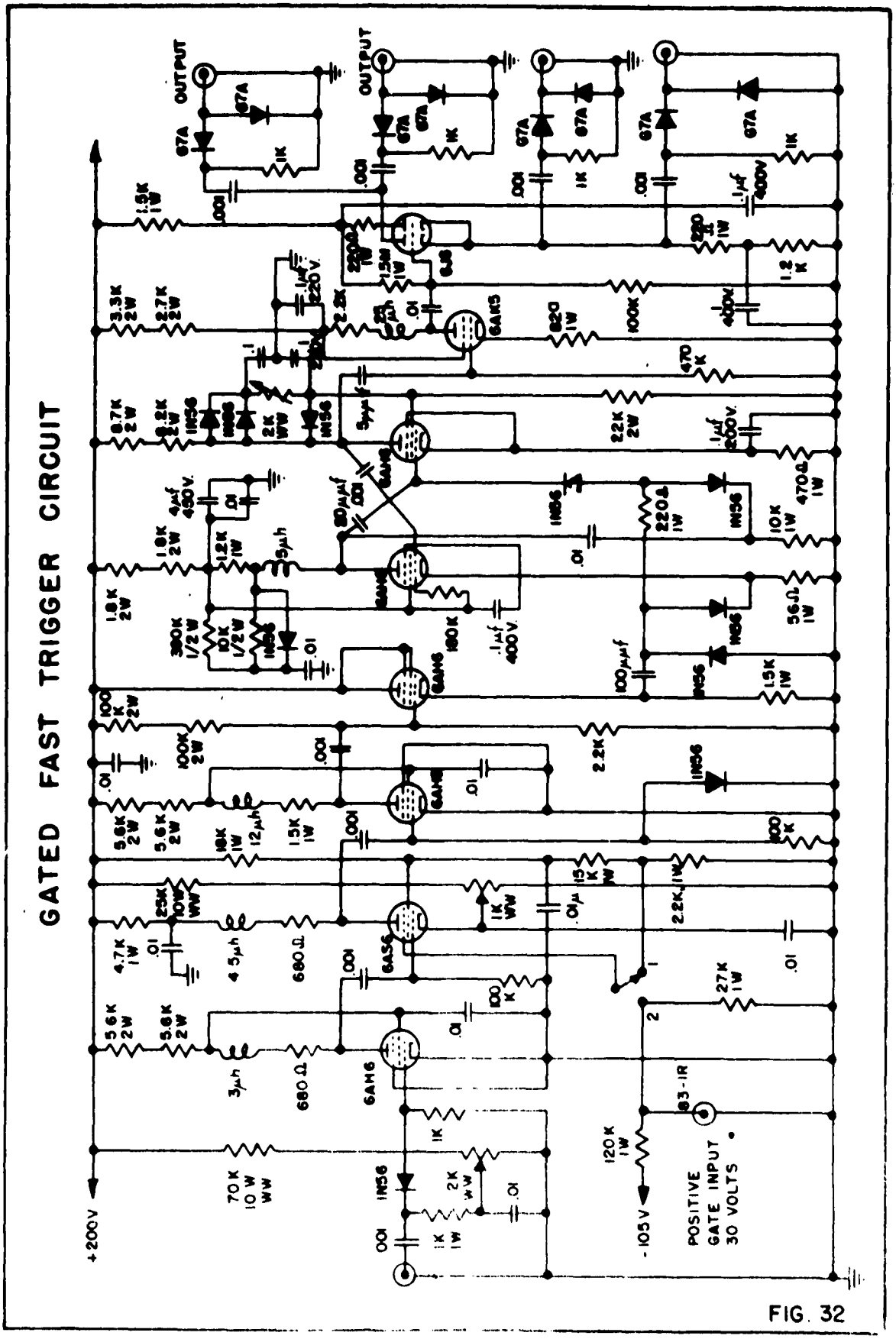
GATED FAST TRIGGER CIRCUIT
OUTPUT
OUTPUT
6AH6
6AM6
6AS6
6AN5
1N56
+200V
-105V
POSITIVE
GATE INPUT
30 VOLTS
83-1R

FIG. 32

APPENDIX B. MONITOR CALIBRATION

Introduction: When an absolute photoproduction cross section is measured it is necessary to know the total beam energy irradiating the sample. A variety of methods have been used to find this. For instance Edwards and Kerst[63] used a lead calorimeter with the amount of energy indicated by the temperature rise of the lead while Leiss, Pruitt, and Schrack[64] used a sodium iodide crystal to record essentially all the gamma rays as counts of various pulse heights and then integrated counts times pulse height to give the energy.

Neither of these methods provide a direct, convenient reading. To avoid this difficulty they are treated as primary standards and a more convenient device such as an ionization chamber is calibrated against them and becomes the secondary standard.

Two such secondary standards are in use at the 300 Mev betatron. They are a replica of the four-inch copper chamber first used by Edwards and Kerst and a replica of the National Bureau of Standards dural chamber[65] (P2-11). A third chamber, the bass drum, is used for nearly all monitoring on the 300 Mev betatron. It has been calibrated against both the Edwards and Kerst chamber and the replica of the N. B. S. dural chamber. It is the purpose of this appendix to present a summary of some of the calibrations.

Before the calibrations are discussed some information on the various ionization chambers will be summarized.

Ionization Chambers: Table XI contains a list of some of the important parameters for three of the ionization chambers in

TABLE XI. PARAMETERS FOR IONIZATION CHAMBERS

	Parameter	Edwards and Kerst	Bass Drum	N. B. S.
1.	Material	Copper	Copper and brass	Dural Aluminum (2024)
2.	Thickness of material to start of air gap	.25"	Brass=.125" Copper=.336"	3.700"
3.	Thickness of material to start of air gap in radiation lengths	.44	.80	1.10
4.	Total length of air gap	.104"	.072"	2.000"
5.	Number of segments in air gap	2	2	12
6.	Thickness of intermediate foils (all aluminum)	.016"	.100"	.0313"
7.	Intended aperture	4"	9"	10"
8.	Total diameter	6"	13 1/2"	13 1/2"
9.	Type of mechanical spacing	Polystyrene	Polystyrene	Stainless steel
10.	Type of electrical connectors	Victoreen	83-1R Female UHF for H.V 82-805 Female Series HN for collector	82-805 Female Series H.N.
11.	Typical capacitance	220 μμf	900 μμf (b)	1700 μμf (b)
12.	Electrical insulation	Collecting electrode at high voltage	High voltage separated from collecting electrode only by polystyrene	Collecting electrode separated from ground guard electrode by Kel-F(a)

TABLE XI. (CONTINUED)

13. Normal high voltage	390 v	275 v	1200 v
14. Typical leakage current	3×10^{-13} amps	3×10^{-14} amps	3×10^{-15} amps
15. Recombination factor (Δ_o)	.55%	.62 %	3.6 %
16. Characteristic Collection time t	14μs	10μs	46μs
17. Normal atmospheric conditions for calibration (all require dry air)	20°C, 1013mbar	20°C, 1013mbar	22°C, 760mm of mercury

(a) Illinois replica (P 2-11) may not have Kel-F.

(b) High voltage terminal grounded to case.

common use at the 300 Mev betatron. Most of the items are self explanatory. The capacities given are rough experimental values. Capacities computed on the basis of A/d tend to be 10% lower than these. The typical leakage rates are intended only to indicate an order of magnitude. In practice they vary appreciably with the cleanliness of the chamber and connectors. The recombination factors given are the percent inefficiencies predicted by the Langevin formula[66]. The Langevin formula for cases where the inefficiency is small is:

$$\Delta_o = 50 \frac{\alpha_o n_o}{(k_+ + k_-)} \quad d\ (d/V) \qquad \text{(B-1)}$$

where Δ_o = percent inefficiency = percent of ions lost to recombination

n_o = ion pairs/burst -cm^3

d = separation between plates in cm

V = voltage across plates

k = ion drift velocity/unit voltage gradient in cm/sec/volts/cm

α_o = recombination coefficient = 1.6×10^{-6} cm^3/sec (for air).

This formula assumes that all the ionization occurs instantaneously. Rossi and Staub[67] give a different formula for the steady-state case where the ionization occurs over a time long compared to a characteristic collection time for the chamber. If the collection time is defined as the time for an ion pair to drift apart a distance equal to the thickness of the chamber then:

$$t = \frac{d}{(k_+ + k_-)}\ (d/V) \qquad \text{(B-2)}$$

where

t = collection time.

The Rossi and Staub formula can then be rewritten:

$$\Delta_1 = \frac{(k_+ + k_-)^2}{3k_+ k_-} \Delta_o \frac{t}{T} = 1.36\ t/T \quad \Delta_o \text{ (for air)} \qquad \text{(B-3)}$$

where

Δ_1 = steady-state recombination percent inefficiency

T = length of betatron pulse.

This form is valid when $T \gg t$. In computing the recombination factors it was assumed that all of the chambers were placed 8.2 meters from the betatron (the present position of the bass drum), a 1/4-inch collimator was used, the yield rate was one standard milliamp per 8 minutes, the energy of the betatron was 180 Mev, and the voltage gradient for all chambers was 3000 volts/cm. ("One standard milliamp" is the charge on a particular condenser with one volt across it. The capacity of the condenser is about 1.020μf.) For long-pulse operation the recombination factor given in Table XI should be used as Δ_o in the formula based on Rossi and Staub.

The "normal" atmospheric conditions are based on Pruitt and Domen[65], and C. S. Robinson[68].

The configurations of the three chambers are given in Fig. 33.

The Edwards and Kerst chamber was designed specifically for the high x ray flux of the betatron. Thus the spacing between plates is small to overcome recombination, while the total ionization yield is proportionately smaller than the N.B.S. chamber.

Later the bass drum was designed along the same lines but with a larger aperture and provisions for use with a more convenient

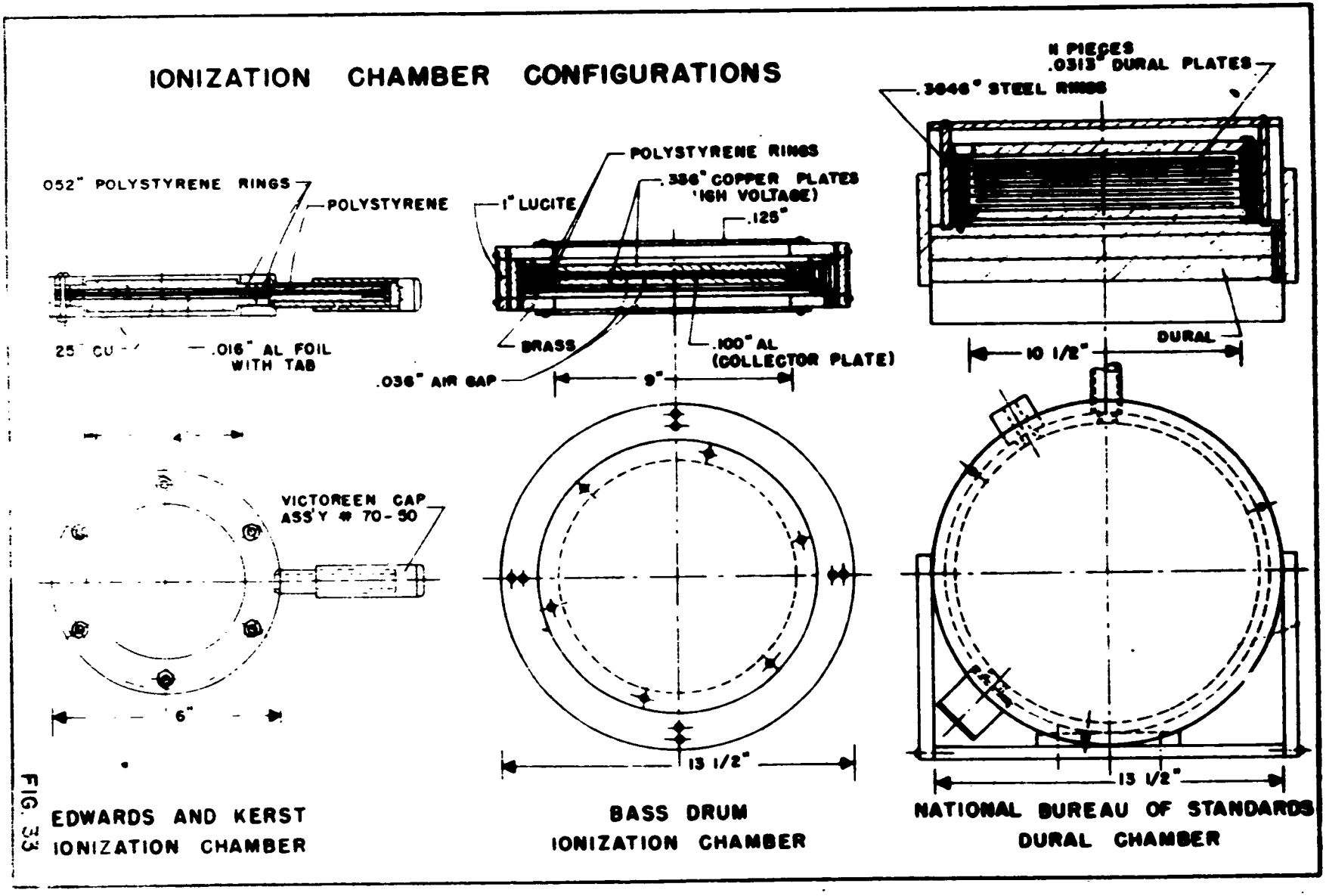
IONIZATION CHAMBER CONFIGURATIONS
.052" POLYSTYRENE RINGS
POLYSTYRENE
25" CU
.016" AL FOIL WITH TAB
POLYSTYRENE RINGS
1" LUCITE
.386" COPPER PLATES (HIGH VOLTAGE)
.125"
BRASS
.036" AIR GAP
.100" AL (COLLECTOR PLATE)
9"
N PIECES .0313" DURAL PLATES
.3046" STEEL RINGS
DURAL
10 1/2"
4"
VICTOREEN CAP ASS'Y # 70-50
6"
13 1/2"
13 1/2"
EDWARDS AND KERST IONIZATION CHAMBER
BASS DRUM IONIZATION CHAMBER
NATIONAL BUREAU OF STANDARDS DURAL CHAMBER

FIG. 33

reading system incorporating an A. P. C. vibrating reed. Both the bass drum and the Edwards and Kerst chamber employ organic material for spacing the plates. When the plates on the Edwards and Kerst chamber are tightened capacity changes on the order of one percent occur indicating changes of the air gap on the same order. Since the screws controlling the gap length move 30 mils per turn, an excess tightening of 1/30 of a turn is sufficient to throw the calibration off by one percent.

The N. B. S. chamber employs steel spacers to overcome this difficulty. In addition it is more sensitive and is designed to have less leakage. The decrease in leakage was accomplished by separating the collector from the high-voltage electrode by a grounded guard electrode and increasing the distance between plates. Such an arrangement makes the chamber more sensitive to recombination. In addition the front plate was made thicker with the idea of flattening the response of the chamber as a function of energy.

Two other ionization chambers have recently been put into use as monitors at the 300 Mev betatron. One is a thin-walled chamber designed as a transmission monitor. It contains argon at one atmosphere pressure and has a total air gap of two inches. The other is a low-leakage, sensitive chamber, containing roughly five atmospheres of an argon-carbon dioxide mixture, for use with low yields employed for the bubble chamber.

History of Monitor Calibrations

Most methods employed in past, absolute, x ray monitor calibrations fall into three categories:

1) Calorimetric, of which the Edwards and Kerst experiment is an example;

2) Methods depending on accurate knowledge of the ionization produced by x ray-induced showers such as that of Blocker, Kenney, and Panofsky[69] and the quantameter developed by Wilson[15] at Cornell;

3) X ray spectral methods such as the NaI(Tl) crystal spectrometer of Leiss, Pruitt, and Schrack and the pair spectrometer calibration of DeWire[70].

In addition to these absolute methods there are several methods which determine the relative monitor response with energy such as the copper activation method employed by Leiss, Yamagata, and Hanson[18]. Recently a calibration of the Cornell thick-walled ionization chamber was made by Loeffler, Palfrey, and Tautfest[71] from 60 to 300 Mev using all of these methods. Since then the calibration of that chamber from 100 to 1100 Mev has been summarized in a note by J. W. DeWire[70].

The calorimetric method involves the dissipation of most of the x ray energy as heat by some suitable converter such as the lead cylinder employed by Edwards and Kerst (4.5 cm in diameter and 8 cm long). The temperature rise of the block is then measured and presumed to be proportional to the energy brought in by the beam. In the Edwards and Kerst calorimeter the temperature rose typically .05°C in a five-minute run. Such a small temperature rise makes this method practical only on machines with high rates of energy output. Some of the energy does leak out of the calorimeter via photo neutrons ($\sim .4\%$) and x rays

($\sim$9%). These numbers can be reduced by increasing the size of the block but this in turn reduces the temperature rise after a certain point. The overall error on the Edwards and Kerst run was estimated to be three percent. Edwards and Kerst used their calorimeter to measure the response of the Edwards and Kerst ionization chamber at approximately 150, 200, 250 and 300 Mev. These measurements have been extended down to 18 Mev by Pruitt and Domen who estimate their latest calorimetric method to be accurate to one percent. When both sets of data are considered along with the crystal spectrometer points it appears that the Edwards and Kerst value for coulombs/Mev-cm at 150 Mev is about 4% low.

A typical method involving ionization is that of the Wilson quantameter, now used as the monitor at Cornell. The instrument consists of twelve air gaps in a deep block of copper converter placed in such a way that the ionization produced by the shower at various depths is automatically integrated. Since all the x ray energy is absorbed in the chamber, the response of the chamber should not change as a function of energy. The constant of calibration is computed theoretically on the basis of the number of ion pairs created, the relative stopping power of the filling gas and the copper converter, and consideration of the track length distribution. Wilson estimates that the theoretical constant should be accurate to 2%. He notes that the theoretical constant differs by 6% from an experimental calibration involving a pair spectrometer. The quantameter has also been investigated by Komar and Kruglov[72]. A method somewhat similar to this in

principle but measuring the ionization as a function of depth experimentally has been employed by Blocker, Kenney, and Panofsky[69] and McMillan, Blocker, and Kenney[73]. In their experiments elements of different Z were used to eliminate consideration of divergences due to the Compton effect. The energy brought in by the beam was calculated by using a theoretical estimate of pair production and extrapolating to an ion chamber of zero air-gap thickness to eliminate multiple scattering and zero converter thickness to eliminate shower effects.

A NaI(Tl) crystal has been employed at the National Bureau of Standards by Leiss, Pruitt, and Schrack in an x ray spectrometer calibration of monitor response. A 100% -absorbing crystal 9 inches long was placed after an ion chamber and the counts in the crystal were monitored by a 100-channel analyzer. Then the product of the number of counts in a channel times the energy of a particular channel was formed and summed over all channels to give the energy brought in. In practice a carbon beam hardener of between 200 and 600 g/cm^2 was placed before the NaI(Tl) crystal in order to attenuate the low energy photons. The crystal efficiency was actually 98 percent. The estimated accuracy of the Leiss et al. experiment was $\sim$3 percent. The method was used to calibrate both the Edwards and Kerst and the N. B. S. dural chambers at energies from 18 to 170 Mev. A similar approach can be made using a pair spectrometer. However the converter will no longer be 100% efficient since the electrons must leave it with no energy loss and one is faced with the problem of determining just how efficient it is.

Only the calorimetric method gives a direct answer for the energy brought in without using information about the bremsstrahlung spectrum, stopping power, or absorption coefficients.

Koester and Dyal[74] have made a relative calibration of the bass drum by using the reaction Cu^{63} $(\gamma,n)Cu^{62}$ as an isochromat. This reaction can be treated as a monoenergetic line at 17.3 Mev. Then the amount of activity excited per erg of radiation is proportional to the number of photons in the bremsstrahlung spectrum at that energy. The response as a function of energy was obtained by dividing the number of standard milliamps (the normal units of bass drum response) by the counts observed from the copper and then multiplying this number by the number of bremsstrahlung photons at 17.3 Mev for the particular betatron energy. The copper activity was measured at six points from 50 Mev to 275 Mev. Some further consideration was also given to the possibility of $(\gamma,3n)$. Absolute values were then found by normalizing to an absolute value near 200 Mev.

In addition Koester made a theoretical calculation of the expected energy dependence of the response of the Edwards and Kerst chamber based on Wilson's shower curves[75]. The agreement between this calculation and the experimental calibrations is excellent above 150 Mev although Wilson's curves are for lead while the chamber is copper.

Bass Drum Calibrations

The bass drum has been used as the monitor on the 300 Mev betatron since 1954. Since its installation it has been compared to Edwards and Kerst chambers at least six times. On nearly

every occasion runs were made with both the chambers in the beam at the same time (with the Edwards and Kerst chamber about 1.75m closer to the betatron) in order to determine quantities called the "sacred ratios". These quantities consist of the response of the Edwards and Kerst chamber with an assumed capacity divided by the response of the bass drum. Any change in the "sacred ratios" implies some change in the ion chambers or their reading systems. Some of the values were previously summarized in a report prepared in February, 1957[76]. Table XII gives a listing of the "sacred ratios" including the more recent measurements. In the latest r-thimble run a considerable lowering of the "sacred ratio" occurred (about 4% possibly because the Edwards and Kerst chamber was closer to the bass drum than the 1.75m specified. Other small changes in the past seem to have been due to changes in the calibration of the M-70 Victoreen charger used to read the Edwards and Kerst chamber. That is, the deflection of the Edwards and Kerst chamber should actually be divided by the number of volts to deflect the M-70 full scale. This change has amounted to 2% in six years. The voltage to deflect the M-70 100 divisions = E has also been tabulated in Table XII. No attempt has been made in Table XII to correct the slight shifting of energies found by integrator recalibrations.

It is not possible to obtain an absolute calibration of the bass drum by placing both it and the standard in the beam at the same time since this type of ionization chamber absorbs an appreciable fraction of the energy in the beam. Instead they

TABLE XII: SACRED RATIOS FOR RECENT 300 MEV BETATRON MONITOR CALIBRATION RUNS USING THE EDWARDS AND KERST CHAMBER AND THE BASS DRUM.

	June 1954	Oct. 1954	May 1955	May 1958	July 1960
Edwards and Kerst Chamber Number	3	3	3	6	6
E	253.9v			251.0v	247.8v
E/X					
150	214.7	213.2	220.6	209.9	203.1
200	195.9			192.7	182.2
225					177.5
250	180.6	179.3	186.6	179.8	
300	173.4			170.8(290 Mev)	

are placed in the beam one at a time and compared by using some device which indicates relative yield and is only a small fraction of a radiation length thick. Prior to 1959 the comparison was performed by using the radioactivity induced in thin copper foils. This procedure was cumbersome because of the counting time involved. In 1959 the foil counting was supplanted by a vacuum transmission chamber which gave a direct reading. In the runs of July, 1960 the relative yield was measured by placing a thin brass foil just after the secondary collimator and using the radiation from it to discharge an r-thimble slightly off the beam. The runs of October, 1960 utilized the thin-walled, argon ion chamber as an intercomparison monitor. Table XIII contains a summary of some recent absolute calibrations of the response of the bass drum.

Before 1959 various Edwards and Kerst chambers were used as standards. The energy calibration employed was that of Edwards and Kerst with the gamma ray energy scale lowered by 2 1/2 percent. (That is to say, the additional calibrations of the Edwards and Kerst chamber performed at the National Bureau of Standards were not considered.) Two such runs, June, 1954 (using the No. 3 Edwards and Kerst chamber) and May, 1958 (using the No. 6 Edwards and Kerst chamber) are tabulated in Table XIII.

In November, 1959 a bass drum calibration was performed using a replica of the N. B. S. dural chamber (designated P2-11). A striking 5 to 10% difference in the bass drum response was noted when the two calibrations were compared. At the time several

TABLE XIII: BASS DRUM MONITOR RESPONSE IN sma/erg x 10^8 FOR RECENT 300 MEV BETATRON MONITOR CALIBRATION RUNS.

Secondary Standards E_γ	Edwards and Kerst				N. B. S.		
	June 1954	May 1958	July 1960	Oct.* 1960	Nov. 1959	July 1960	Oct. 1960
125				2.128			2.132
130					2.150		
150	1.707	1.800	1.789	2.028	2.061	2.049	2.035
170					2.003	1.991	
200	1.670	1.775	1.788	1.873			
225							
250	1.582	1.624		1.699			
282.7				1.622			
300	1.354	1.481(290Mev)					

*Based on an assumed thickness of No. 6 of .1096 inches.

possibilities were suggested as the cause of the discrepancy. One possibility was that the original calibration of one of the standards was in error. A second possibility was that one of the standard ion chambers was defective. Finally the actual intercomparison runs might have been faulty.

The July, 1960 runs were undertaken as a quick check on the last possibility. This was done by using a different intercomparison system to check the May, 1958 and November, 1959 calibrations. The runs reproduced the original data to within the accuracy of the r-thimble readings, leading to the conclusion that the discrepancy was not the result of a poor intercomparison method.

In September, 1960 the Edwards and Kerst No. 6 chamber and the N. B. S. dural replica were taken to the National Bureau of Standards and compared to similar chambers there. The response of the N. B. S. replica dural chamber (P2-11) was very close to the N. B. S. standard. However the Edwards and Kerst chamber No. 6 gave 1% more yield than an N. B. S. chamber known to have a 3 to 4% larger air gap then the original Edwards and Kerst chamber. At the same time careful measurements of the thicknesses and densities of the two chambers were made. The measurements for the N. B. S. replica were within 1% of the N. B. S. specifications. The air gap of the Edwards and Kerst chamber No. 6 appeared to be 5 to 6% too large. (The measurements were based on an indirect measurement of the overall thickness. The spacers for the air gap were only 2% too thick. Previous tests with an indicator gauge had shown that the front and back plates were slightly bowed.)

In October, 1960 the intercalibration was checked once more at the betatron. At that time the bass drum was calibrated against two N. B. S. chambers (the betatron replica P2-11 and an N. B. S. standard P2-3) and two Edwards and Kerst chambers (No. 6 and the N. B. S. improved version with steel spacers). A great deal of attention was paid to the proper calibration of the vibrating reeds and standard capacitors, recombination effects, and leakage corrections. Both of the Edwards and Kerst chambers were adapted so that they employed vibrating reeds rather than Victoreen readers as charge collection devices.

The charge output of P2-11 (the betatron replica) was .993 of the charge output of P2-3, demonstrating that the replica was not defective. The charge output of the No. 6 Edwards and Kerst chamber was 1.02 times the charge output of the N. B. S. version (with a 107.3 mil air gap). The conclusion was drawn from this and the earlier information that the effective air gap of the No. 6 was 5 to 6% larger than specified.

At that time a calibration for the Edwards and Kerst chamber was adopted based on the combined N. B. S. and Edwards and Kerst points. The main effect was to neglect the Edwards and Kerst point at 150 Mev. Such a procedure removes 4% of the discrepancy in the 150 Mev region.

In summary the recent discrepancy was due to the combined effects of a defective Edwards and Kerst chamber (No. 6), which had an air gap 5 to 6% too large, and the use of the Edwards and Kerst calibration point at 150 Mev, which appears to deviate

In October, 1960 the intercalibration was checked once more at the betatron. At that time the bass drum was calibrated against two N. B. S. chambers (the betatron replica P2-11 and an N. B. S. standard P2-3) and two Edwards and Kerst chambers (No. 6 and the N. B. S. improved version with steel spacers). A great deal of attention was paid to the proper calibration of the vibrating reeds and standard capacitors, recombination effects, and leakage corrections. Both of the Edwards and Kerst chambers were adapted so that they employed vibrating reeds rather than Victoreen readers as charge collection devices.

The charge output of P2-11 (the betatron replica) was .993 of the charge output of P2-3, demonstrating that the replica was not defective. The charge output of the No. 6 Edwards and Kerst chamber was .02 times the charge output of the N. B. S. version (with a 107.3 mil air gap). The conclusion was drawn from this and the earlier information that the effective air gap of the No. 6 was 5 to 6% larger than specified.

At that time a calibration for the Edwards and Kerst chamber was adopted based on the combined N. B. S. and Edwards and Kerst points. The main effect was to neglect the Edwards and Kerst point at 150 Mev. Such a procedure removes 4% of the discrepancy in the 150 Mev region.

In summary the recent discrepancy was due to the combined effects of a defective Edwards and Kerst chamber (No. 6), which had an air gap 5 to 6% too large, and the use of the Edwards and Kerst calibration point at 150 Mev, which appears to deviate

by 4% from a smooth line through the other Edwards and Kerst points and the N. B. S. points. The values given for the bass drum calibration of October, 1960 using the Edwards and Kerst chamber include corrections for both these effects. They agree quite well with the calibration obtained using the N. B. S. dural chamber.

It is useful to tabulate the ratio of charge output for the chambers in order to avoid complications due to improvements in the primary calibrations. Table XIV gives such ratios for several combinations of chambers. The values for runs prior to October, 1960 are reconstructions made after the runs and consequently may not include some important corrections.

The bass drum calibration of October, 1960 is shown in Fig. 34. Several of the earlier calibration points have also been included. Some care must be used in reinterpreting old results since the small changes in the "sacred ratios" were sometimes used as corrections on the most recent absolute calibration. In addition, slight measured changes in the charging capacitors also were interpreted as changes in the absolute calibration because of the definition of the standard milliamp. Some typical values of the capacitors over the years are given in Table XV. In most cases the deviations are small and probably less then the accuracy of the measurements.

In placing limits on the experimental errors several things need to be considered. One is the accuracy of the original calibration. Edwards and Kerst assigned standard deviations of

TABLE XIV: RATIO OF CHARGE PRODUCED BY THE BASS DRUM TO CHARGE PRODUCED BY THE STANDARD CHAMBER FOR RECENT 300 Mev BETATRON MONITOR CALIBRATION RUNS.

Edwards and Kerst Chamber Used as Standard

	June 1954	June 1958	Nov. 1959	July 1960	Oct. 1960
Edwards and Kerst Chamber Number	3	6		6	6
E_γ(Mev)					
125					1.109
150	1.105	1.13		1.12	1.141
200	1.13	1.19		1.190	1.202 (av.)
225				1.188	
250	1.19	1.22			1.229
282.7					1.256
290		1.25			
300	1.19				
N. B. S. Dural Replica Used as Standard					
125					.08109
130			.0811		
150			.0779	.0776	.0778
170			.0760	.0756	
200			.0730	.0742	.0734 (av.)
250			.0710	.0700	.07022 (av.)
282.7					.06826

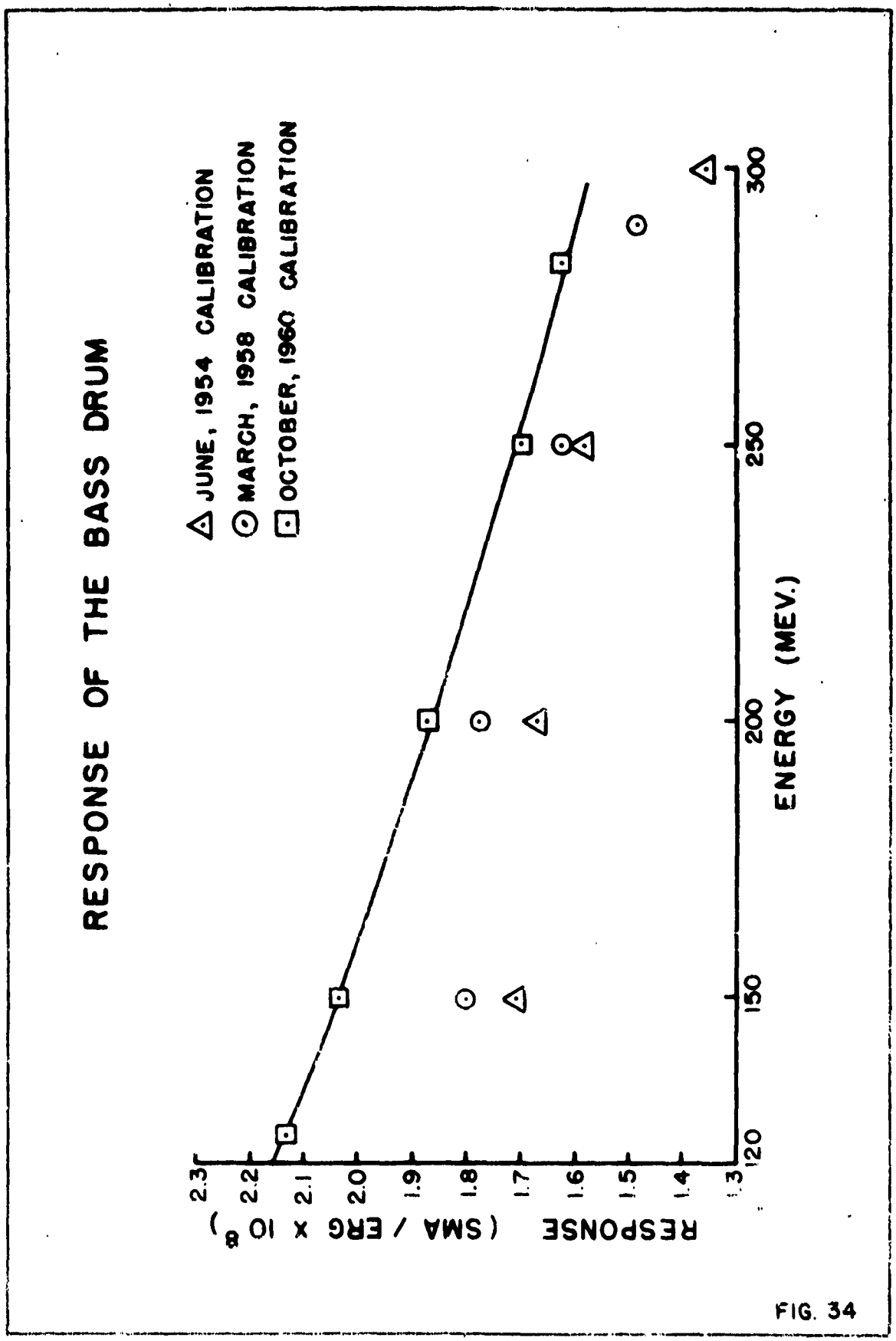
RESPONSE OF THE BASS DRUM
△ JUNE, 1954 CALIBRATION
⊙ MARCH, 1958 CALIBRATION
⊡ OCTOBER, 1960 CALIBRATION
RESPONSE (SMA / ERG x 10⁸)
2.3
2.2
2.1
2.0
1.9
1.8
1.7
1.6
1.5
1.4
1.3
120
150
200
250
300
ENERGY (MEV.)

FIG. 34

TABLE XV: CHARGING CAPACITORS

Capacitor	March, 1956	Jan.-Jun., 1958	October, 1960
300 Mev V.R. "Z" (defines sma)	1.021 μf	1.019 μf	1.021 μf
300 Mev V.R. "X"	1.013 μf	1.011 μf	
300 Mev V.R. "Y" (X + Y = 2μf)	1.010 μf	1.009 μf	
300 Mev V.R. "A"	5.368 μf	5.344 μf	
300 Mev V.R. "C"	10.51 μf	10.45 μf	10.47 μf

2.5 to 3% to their calibration. The N. B. S. errors are about 1 1/2% for calorimeter runs and 3% for the spectrometer points. A second consideration is the accuracy of transfer of calibration of the secondary standard to the bass drum. Fluxuations in the 1958, 1959, and 1960 calibrations indicate that it is on the order of one percent. This is slightly higher than might be expected. However reading errors as well as the corrections due to changes in vibrating reed gains and responses, leakage currents, and recombination are all not too much smaller than one percent.

In the runs of October, 1960 some measurements were made of recombination effects primarily by lowering the voltages on the various chambers. Such measurements are not accurate because the quantity of interest is the small difference between two responses. In general it appeared that the inefficiency due to recombination for the bass drum and the Edwards and Kerst chamber was roughly half of that predicted by the recombination formula 3, while the inefficiency of the N. B. S. chamber was one-fifth of the predicted value. The functional dependence of the formula on pulse length, ion density, and ion chamber voltage followed the trend of the experimental data. The results indicated that for normal, long-pulse operation the bass drum would suffer less than .1% recombination.

APPENDIX C. ENERGY CALIBRATION

Introduction

The π^+ photoproduction cross section varies rapidly with energy near threshold. As a result a small error in assigning the energy to a particular cross section measurement can result in a large error in the experimental value obtained for the matrix element. This has been illustrated in Fig. 35 by dividing the total cross section given by Robinson[77], $\sigma(E)$, by $4\pi\chi''(E+\Delta E)$ for ΔE = -2, -1, 0, 1, and 2 Mev ($\chi'' = \frac{q}{k(1+\omega/M)^2}$)

The points are plotted at E + ΔE. Below 160 Mev the effect of the energy shift is very pronounced.

Experimental measurements of cross sections by activation methods are also affected by the distribution of peak gamma ray energies. Several processes occur which result in a distribution of peak gamma ray energies. For instance the electrons can lose energy in the target before they radiate. Beam photographs indicate that the effective thickness of the platinum internal target is of the order of 3 mils. This causes a spread in energy from ionization loss of about .16 Mev. The finite length of the yield pulse causes an energy spread of .3 Mev. There is also an additional energy spread on the order of one Mev due to pulse-to-pulse variations in the peak betatron field. As a result an energy spread of 1.5 Mev is not at all unlikely.

As an example of the effect of a distribution of peak gamma ray energies, consider a cross section of the form $\sigma = A(E-E_T)^{1/2}$

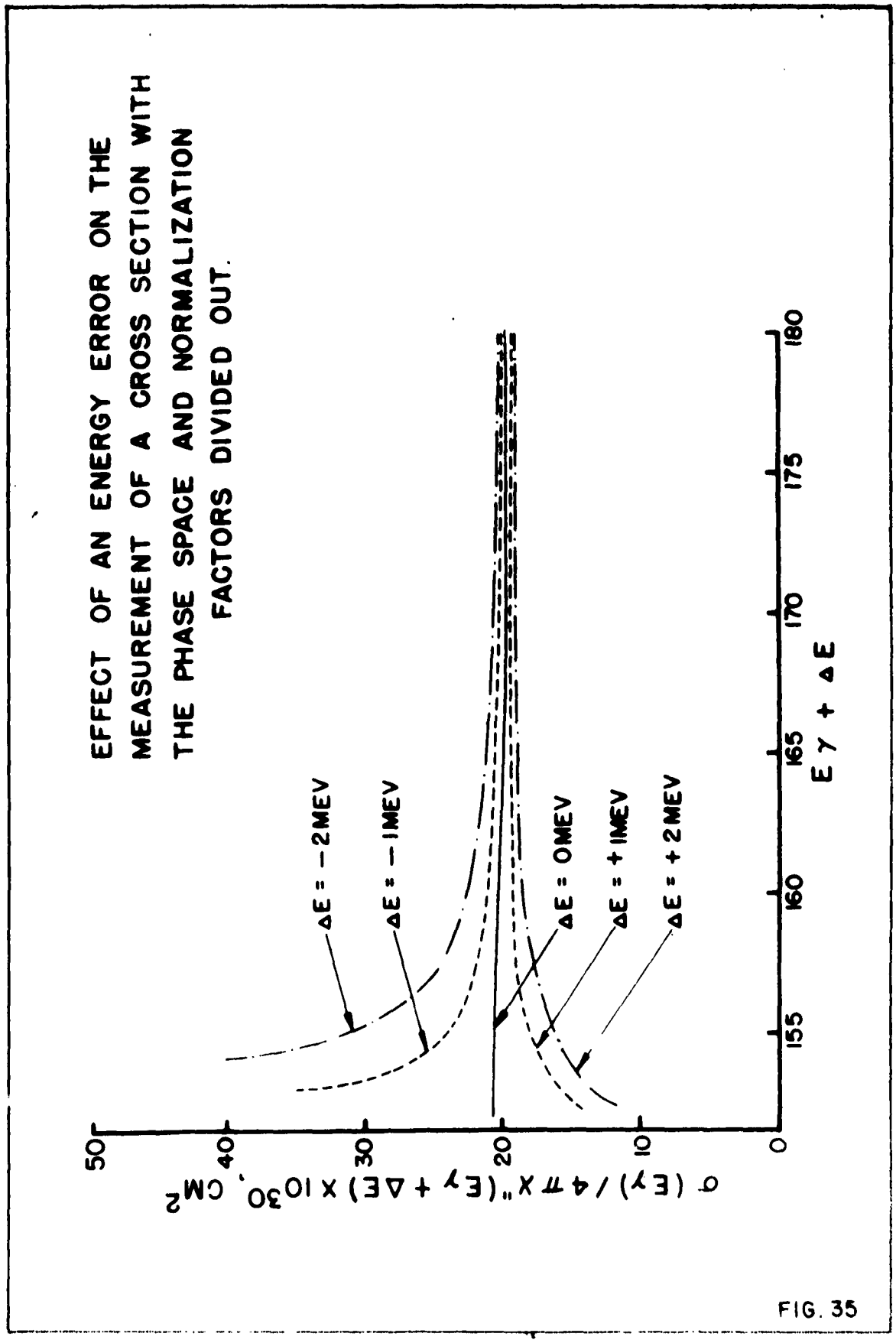
EFFECT OF AN ENERGY ERROR ON THE
MEASUREMENT OF A CROSS SECTION WITH
THE PHASE SPACE AND NORMALIZATION
FACTORS DIVIDED OUT.
ΔE = −2MEV
ΔE = −1MEV
ΔE = 0MEV
ΔE = +1MEV
ΔE = +2MEV
σ (Eγ) / 4π X = (Eγ + ΔE) X 10³⁰, CM²
Eγ + ΔE
0
10
20
30
40
50
155
160
165
170
175
180

FIG. 35

(a fair approximation to the π^+ cross section near threshold) and a uniform distribution of peak gamma ray energies of width $\Delta E'$ centered at $\bar{E}$.

$$Y(\bar{E}_\gamma) = \frac{A\int_{\bar{E}_\gamma - \Delta E'/2}^{\bar{E}_\gamma + \Delta E'/2} \int_{E_T}^{E} N(k,E)\,\sigma(k)\,dk\,dE}{\int_{\bar{E}_\gamma - \Delta E'/2}^{\bar{E}_\gamma + \Delta E'/2} dE} \qquad \text{(C-1)}$$

Near threshold $N(k)$ is approximately constant and (C-1) is easily integrated to give:

$$Y(\bar{E}_\gamma) = \frac{4}{15}\,\frac{A}{\Delta E'}\left[\left(\bar{E}_\gamma - E_T + \Delta E'/2\right)^{5/2} - \left(\bar{E}_\gamma - E_T - \Delta E'/2\right)^{5/2}\right] \qquad \text{(C-2)}$$

$$\text{for} \quad \bar{E}_\gamma - \frac{\Delta E'}{2} > E_T$$

$$Y(\bar{E}_\gamma) = \frac{4}{15}\,\frac{A}{\Delta E'}\left(\bar{E}_\gamma - E_T + \Delta E'/2\right)^{5/2} \qquad \text{(C-3)}$$

$$\text{for } \bar{E}_\gamma - E_T < \frac{\Delta E'}{2} \quad .$$

The apparent cross section is then:

$$\sigma'(\bar{E}_\gamma) = \frac{2}{3}\,\frac{A}{\Delta E'}\left[\left(\bar{E}_\gamma - E_T + \frac{\Delta E'}{2}\right)^{3/2} - \left(\bar{E}_\gamma - E_T - \frac{\Delta E'}{2}\right)^{3/2}\right] \qquad \text{(C-4)}$$

$$\text{for} \quad \bar{E}_\gamma - E_T > \frac{\Delta E'}{2}$$

$$\sigma'(\bar{E}_\gamma) = \frac{2}{3}\,\frac{A}{\Delta E'}\,\left(\bar{E}_\gamma - E_T + \frac{\Delta E'}{2}\right)^{3/2} \qquad \text{(C-5)}$$

$$\text{for } \bar{E}_\gamma - E_T < \frac{\Delta E'}{2} .$$

When $\bar{E}_\gamma - E_T$ is much larger than $\Delta E'/2$ the apparent cross section is a very good approximation to the true cross section. In Fig. 36 $\sigma'(\bar{E}_\gamma)/\sigma(\bar{E}_\gamma) \times \sigma_{CGLN}/4\pi\chi''$ has been plotted for $\Delta E'$ = 0 Mev, 2 Mev, 4 Mev, and 6 Mev to illustrate the effect of an energy spread in the peak gamma ray energy on the evaluation of the matrix element. For energy spreads of less than two Mev, the effect is only important for measurements within two Mev of threshold.

Since the effect of a small energy shift is so large it was important to include small perturbations ordinarily neglected in evaluating the energy. In addition some information about the peak energy spread was gained by considering the differences between the energies estimated by the various methods. For these reasons the three methods used to determine the peak energy are discussed in some detail below.

Mark II Integrator Calibration

The primary 300 Mev betatron integrator, Mark II, was calibrated during the 1958 betatron field measurements[78]. The field measurements were made with a rotating probe coil. The probe coil itself was calibrated in a dc magnetic field measured with a proton resonance apparatus. At the time, integrator values

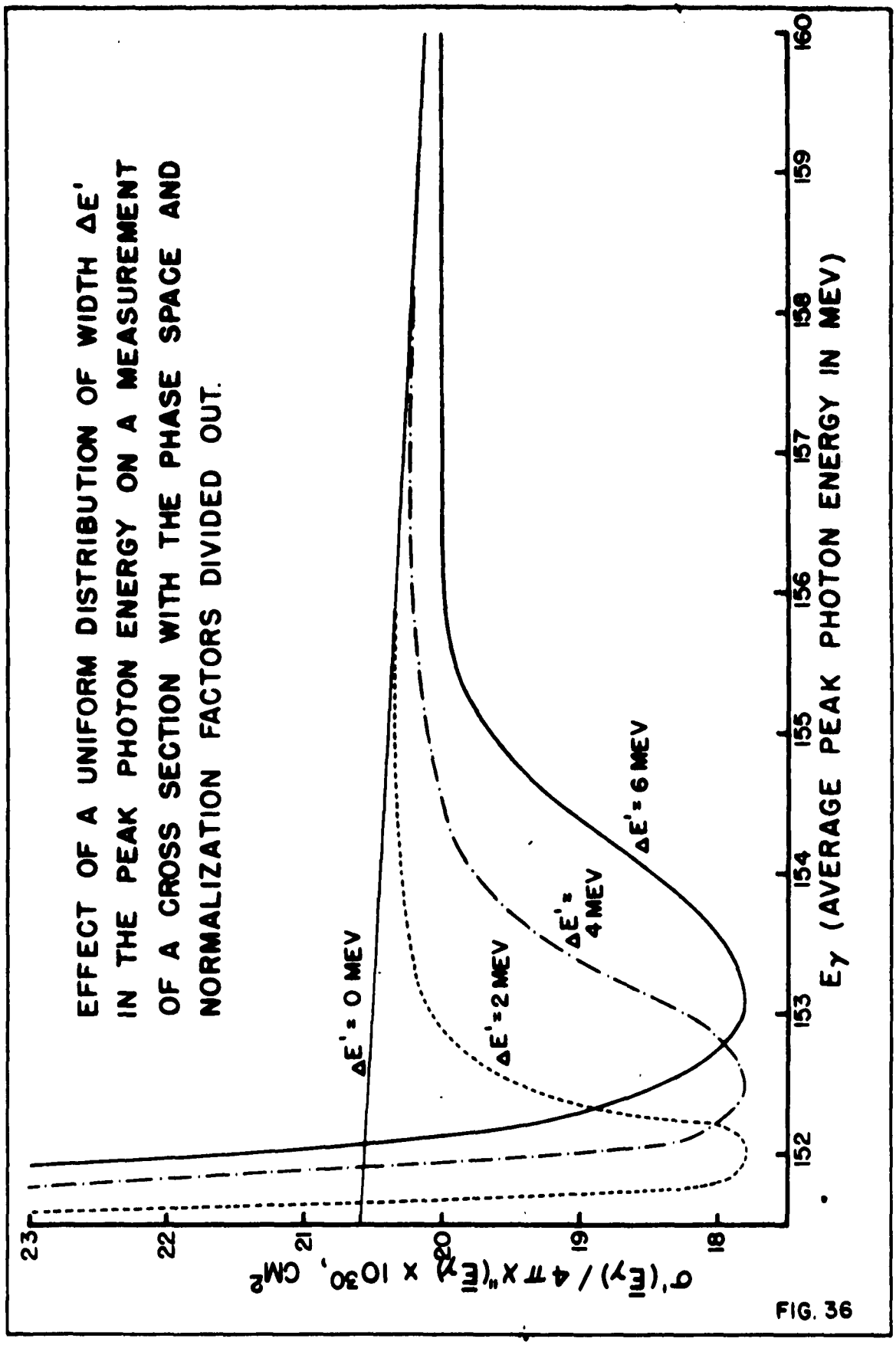
EFFECT OF A UNIFORM DISTRIBUTION OF WIDTH ΔE'
IN THE PEAK PHOTON ENERGY ON A MEASUREMENT
OF A CROSS SECTION WITH THE PHASE SPACE AND
NORMALIZATION FACTORS DIVIDED OUT.
ΔE' = 0 MEV
ΔE' = 2 MEV
ΔE' = 4 MEV
ΔE' = 6 MEV
σ'(Eγ) / 4π x''(Eγ) x 10³⁰, CM²
Eγ (AVERAGE PEAK PHOTON ENERGY IN MEV)
23
22
21
20
19
18
152
153
154
155
156
157
158
159
160

FIG. 36

for electron total energies were calculated. These values were based on field measurements taken on the target side of the betatron with a C-turn input to the integrator. In this experiment these energy values have been designated as the nominal energy values.

The integrator settings corresponding to the nominal energy values were reinterpreted for this experiment to include several additional effects. In the first place the measured field strengths at the opposite position on the assumed electron orbit were slightly higher than those on the target side indicating that the actual electron orbit was probably slightly larger. A value of r_{tar} = 48.70 inches was used rather than the 48.61 inches measured. (This was within the tolerance of the measurement.)

The field measurements indicated that the main bias caused a slight shift in the integrator settings. For the main bias current used in this experiment the correction was +.11% on the magnetic field for a particular integrator setting. The field measurements also indicated that the expander had some effect on the field strength. For this experiment the expander correction amounted to +.72%. It is difficult to understand the physical mechanism for such effects. This was realized at the time and some care was taken to confirm that they existed. Since there was some doubt on this point the energies have been calculated with and without the particular corrections.

No correction was made for the effect of the orbit position

transformer since the same taps were used in this experiment and the field measurements. Likewise no corrections were made for temperature effects, since evidence indicated that even on Mark I integrator they amounted to less than .1%/10°F.

The electron total energy was determined using E = .03708B (for E in Mev, and B in gauss). The maximum gamma ray energy was $E_{\gamma m} = E - mc^2$.

The capacitance of the integrator stack was remeasured at the time of the experiment and found to be .21% smaller than the value obtained during the field measurements. The energy values calculated from the Mark II settings were accordingly lowered by .21%.

The uncorrected magnetic field was 4060 gauss at a nominal energy of 150 Mev (tha' is a Mark II integrator setting of 418.6). With the expander and main bias corrections it was 4094 gauss. $E^{II}_{\gamma m}$ without the expander and main bias corrections was 149.7 Mev and with them it was 151.0 Mev. (Both cases include the -.21% effect of the capacitance change.)

Electron Resonance Field Measurements

An electron-spin resonance magnetometer was placed in the betatron field near the target at the time this experiment was performed. It provided a direct field measurement independent of the integrator calibration. The status of the apparatus has been covered in several reports by Stahlke[79, 80].

In the June, 1960 run the electron-spin probe was positioned at an assumed radius of 48.70 inches. The measured field was

4054.2 gauss for an integrator setting of 411.7 on Mark II (apparently the expander was not on). For a field index of n = 1/2 the field at the target would have been 3.8 gauss higher. Thus the integrator setting corresponded to $E^{ESR}_{\gamma m}$ = 149.7 Mev.

This value can be compared to the $E^{II}_{\gamma m}$ computed in the last section without an expander correction. The difference between the recomputed peak gamma ray energy and the nominal energy was -.3 Mev. A Mark II setting of 411.7 corresponds to a nominal energy of 147.6 Mev. Thus $E^{ESR}_{\gamma m} - E^{II}_{\gamma m} \simeq$ + 2.4 Mev. (This method of comparison assumes the capacitance of the Mark II integrator stack was the same during the magnetometer run and this experiment.) It should be pointed out that these were preliminary ESRM runs and were not intended as absolute field measurements. An earlier run intended as an absolute measurement indicated a difference between $E^{ESR}_{\gamma m}$ and the nominal energy that was smaller and negative.

The electron-spin resonance magnetometer runs also demonstrated graphically the change of the magnetic field over the time of the yield pulse. Typically 500 μs before 90° the field should be down by 1.8%. Experimentally it was found to be down by ~2.0%. In addition, random peak field variations were measured and found to be about .5%.

Threshold Calibration

If the π^+ photoproduction cross section has an energy dependence $\sigma = A(E-E_T)^{1/2}$ then the yield has an energy dependence

$Y = \frac{2}{3} A (E-E_T)^{3/2}$. As a result a plot of $Y^{2/3}$ versus energy should be a straight line intercepting the energy axis at threshold. In practice the cross section is not known. The shape of the yield curve is also dependent on the counter-target efficiency and the bremsstrahlung spectrum assumed.

Several theoretical activation curves were formed for different bremsstrahlung spectra, assumed cross sections, and efficiency functions. The breaks were calculated by fitting a line to $Y^{2/3}$ from 154 Mev to 170 Mev. This represents a portion of the curve that is nearly linear and neglects the points very near threshold where experimental measurements would be affected by an electron energy spread. In general the bremsstrahlung shape did not affect the threshold break point strongly (on the order of .1 Mev). Changing the form of the efficiency from a flat function to one which was higher near threshold (as in this experiment) tended to lower the threshold break point (on the order of .5 Mev). This effect was also observed experimentally. The threshold break for ABCDE, with a relatively steeper efficiency function, was found to be $\sim$.3 Mev lower than the break for ABCD. Similarly, when a cross section with a squared matrix element (with $1/k\omega$ stripped out) which increased near threshold was assumed the threshold break point tended to be lower ($\sim$.2 Mev). A compromise, extrapolated threshold break was chosen at 152.3 Mev. It was based mainly on a yield curve which employed a cross section that neglected terms of order v^2; a Schiff, integrated-over-angles spectrum; and the experimental, ABCD efficiency

function. The extrapolated break was about 1 Mev above the true threshold point.

Experimental values of the threshold break point were obtained by making a weighted, linear, least-squares fit to the two-thirds power of the reduced yield curve for the nominal energy region from 156 to 170 Mev. The nominal energy at which the break occurred (E^T = 153.8 Mev) was then considered to be $E^T_{\gamma m}$ = 152.3 Mev. Based on this difference all nominal energy values were lowered by 1.5 Mev. An alternative method would have been to make a shift that was proportional to energy. Such a shift would have been 20% larger at 180 Mev. The straight 1.5 Mev shift was chosen since it was felt that at least some of the difference was due to effects such as energy loss in the target which would have been independent of the peak gamma ray energy.

The two yield curves used to set the energy are shown in Fig. 37. The experimental values are plotted as a function of nominal energy while the theoretical curve is plotted against $E_{\gamma m}$.

Summary

Each of the three methods of energy calibration indicated different corrections on the nominal energies suggested for the Mark II integrator to obtain the peak gamma ray energy.

1) According to the threshold break assumption they should have been lowered 1.5 Mev.

2) If no correction was made for the effect of the expander, the Mark II integrator calibration indicated

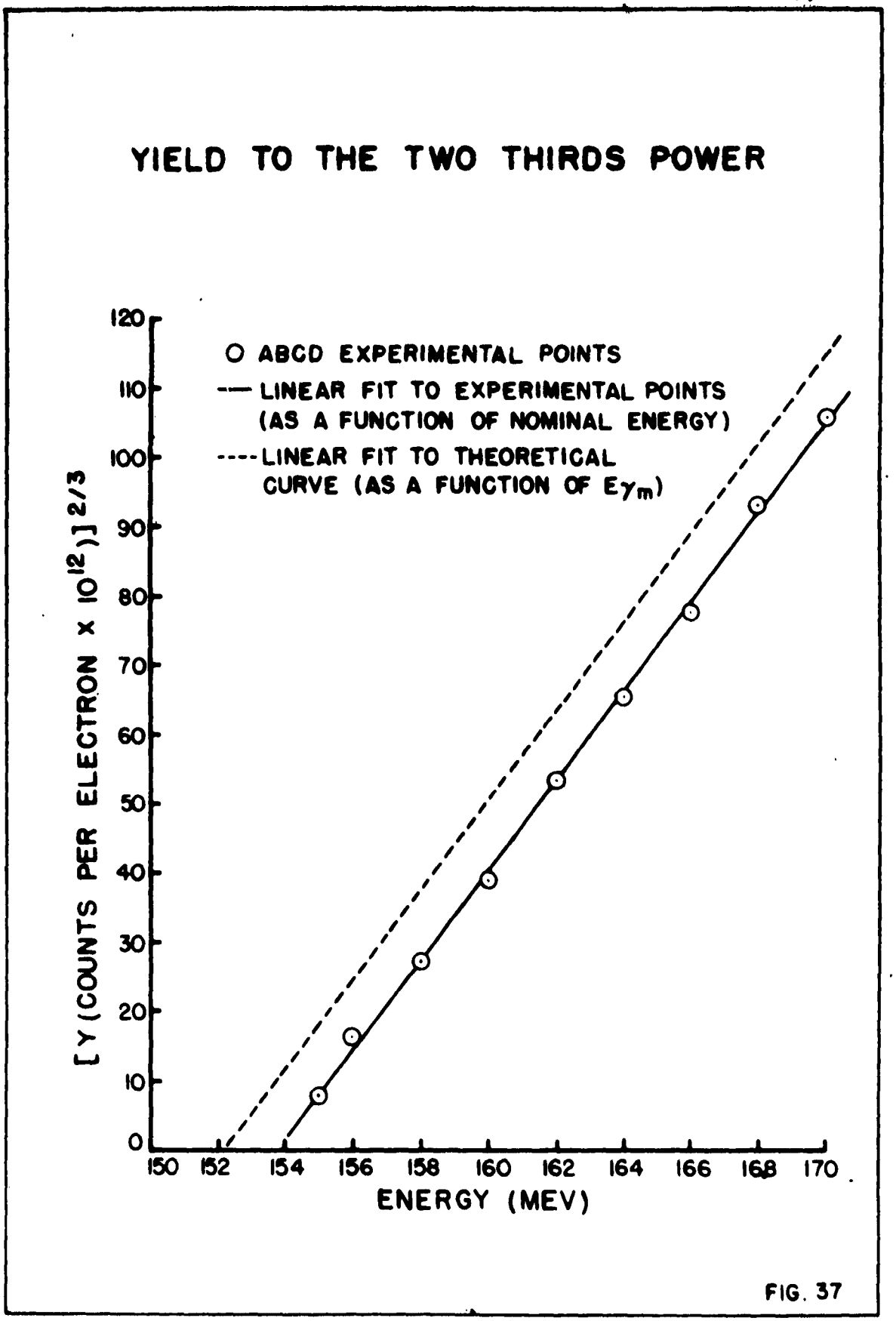
YIELD TO THE TWO THIRDS POWER
O ABCD EXPERIMENTAL POINTS
— LINEAR FIT TO EXPERIMENTAL POINTS (AS A FUNCTION OF NOMINAL ENERGY)
---- LINEAR FIT TO THEORETICAL CURVE (AS A FUNCTION OF Eγm)
[Y (COUNTS PER ELECTRON x 10^12)] 2/3
0
10
20
30
40
50
60
70
80
90
100
110
120
150
152
154
156
158
160
162
164
166
168
170
ENERGY (MEV)

FIG. 37

that they should have been lowered .3 Mev.

3) If a correction was made for the expander, they should have been raised 1.0 Mev.

4) Information from the electron-spin resonance indicates that they should have been raised 2.1 Mev.

Several of the effects which cause a distribution of energies make the difference between 1) and 2) quite reasonable since 1) measured the average peak gamma ray energy while 2) actually measured the total energy of the electron at peak field and then subtracted its rest mass. If expander corrections are included, the difference is larger than expected. The electron-spin resonance information was preliminary so that it does not cast much doubt on the close agreement between 1) and 2).

For this experiment 1) was used to set the energy scale.

APPENDIX D. ACCIDENTALS

Accidentals can occur in several ways in the type of counting system employed for this experiment. Pairs of doubles can form accidental coincidences in a multifold, slow-coincidence circuit. Accidentals also occur when true triples (or doubles) make fast coincidences with single counts. In many counting systems the second process occurs infrequently because most true triples (or doubles) are part of a true quadruple (or triple). However such was not the case in this experiment. For example, consider ABCD. Since B was much smaller than A the triples rate for ACD was roughly three to four times the quadruple rate. Similarly, the triples rate for ABC was much larger than ABCD because of the decreased counter thickness. As a result a single in D or B had an appreciable chance of forming a quadruple count.

The accidental count rate/monitor, N_A, for a perfect "and" circuit receiving square pulses of length τ is:

$$N_A = N_i N_j \frac{2\tau}{k T t} \qquad \text{(D-1)}$$

where N_i and N_j are the input channel count rates/monitor, T is the length of a monitor, t is the length of the betatron pulse, and k is the number of betatron pulses per second. In this experiment typical counting rates were on the order of 10^3 counts/sma for a multifold, 10^4 counts/sma for a doubles channel, and 10^6 counts/sma for a single channel. For the slow coincidence circuit τ was roughly five times τ for the fast circuit. In that case the two processes should contribute roughly the same

amount of accidentals. In practice coincidences of triples with fast singles were the dominant source of accidentals.

Accidentals were measured in the experiment by placing delays in individual channels and by narrowing the betatron pulse to increase the effective yield rate.

When delays were used the accidentals rose sharply as a function of energy for ABCD but were usually nearly constant with energy for the triples. This is the behavior expected from formula (D-1) since the triples in this experiment were due in large part to mesons while the doubles and singles were due mostly to the background and did not change rapidly with energy. The counting rates obtained with delays were very low and consequently such measurements were poor. However they did offer substantial evidence that the energy dependence of the accidentals could be predicted.

When a delay was placed in an individual channel all of the corresponding triples counts could produce accidentals (including those associated with true quadruples). As a result the number of accidentals was not the sum of those in the individual channels but some smaller number. For instance for ABCD the number of accidentals/sma was:

$$Q_T^{ABCD}(E) = \frac{K}{T} \left\{ Q_A^{ABCD}(E) \left(1 - \frac{N_{ABCD}(E)}{N_{BCD}(E)}\right) + Q_B^{ABCD}(E) \left(1 - \frac{N_{ABCD}(E)}{N_{ACD}(E)}\right) + Q_C^{ABCD}(E) \left(1 - \frac{N_{ABCD}(E)}{N_{ABD}(E)}\right) + Q_D^{ABCD}(E) \left(1 - \frac{N_{ABCD}(E)}{N_{ABC}(E)}\right) \right\} \qquad \text{(D-2)}$$

where K was the length of the accidentals run and $Q_A^{ABCD}(E)$ was the number of accidentals counted/sma when A was delayed in ABCD at a particular energy E, etc. Since the various counting rates, N_i were known, $Q_T(E)$ could be obtained directly from the experimental $Q_i(E)$.

If the normal betatron pulse was a rectangle of length L and the high yield pulse was a spike in the form of a triangle with base length Δ then the ratio of the accidentals for the two cases would have been:

$$\frac{Q_\Delta}{Q_L} = \frac{4}{3}\ \frac{L}{\Delta} \qquad \text{(D-3)}$$

(provided a monitor took the same length of time in both cases). This factor was theoretically about 9.0 for the yield pulses used in the experiment. It was measured experimentally using doubles accidentals (which produced higher counting rates) and found to be about .8 of the predicted value. The difference was due to the difficulty in knowing the exact yield pulse shape. The number of accidentals for normal yield rates based on the difference between the normal and spike runs would have been:

$$Q_L\ (E) = \frac{N_i\ (E,\ \text{spike}) - N_i\ (E,\ \text{normal})}{\left[\frac{Q_\Delta}{Q_L}\right] - 1} \qquad \text{(D-4)}$$

Theoretically $Q_L\ (E)$ from formula (D-4) should have been equal to $Q_T\ (E)$ from formula (D-2). Reasonable agreement was obtained experimentally particularly at higher energies except in

the case of ACD. The relatively poorer agreement at low energies was not an important factor since at energies near threshold the corrections tended to cancel when the below-threshold counting rate was subtracted.

In the case of ACD the accidental counting rate found from delay information was three to ten times higher than that found from the increased yield runs. No reason was found for the effect. However the correction would have been at most .3% of the observed count rates. For that reason no accidental correction was made on ACD.

No delay information was obtained on ABCDE. The high yield runs indicated that accidental corrections would be .3% at most. Hence no correction was applied to ABCDE either.

Accidental corrections were made on the experimental data in the following way. Each triple or double was assigned an energy dependence

$$N_i(E) = \alpha_i \left[1 + \beta_i (E-E_T)^{3/2}\right] . \qquad (D-5)$$

These energy dependences were substituted in formula (D-2) with a smoothed set of Q_i based on the experimental delay measurements. Then K was adjusted so that Q_T (180) was equal to Q_L (180) (that is the value obtained from the increased yield measurements). Q_L (180) was obtained using the experimental value of Q_Δ/Q_L from the doubles accidental measurements.

The accidental correction factor for a two-sma run was:

$$2Q_L^i(E) = \frac{A^i}{2T}\left[1 + B^i (E - 151.5)^{3/2}\right] \qquad \text{(D-6)}$$

where T is the length of a sma in minutes and E is the energy in Mev. The values of A and B are tabulated in Table XVI. The change in percent represented by the correction is also tabulated.

The accidentals were measured using the carbon absorber with the hydrogen target filled. The corrections for the copper absorber were found assuming that the singles and doubles count rates increased by the ratio of the copper below-threshold counting rate divided by the carbon below-threshold rate. (In both cases the cosmic ray background was subtracted.)

The empty target rates were also obtained on that basis. In addition the energy dependence was assumed to be the actual energy dependence of the count rate. The empty target correction had the form:

$$2\,Q_L^i(E) = \frac{A'\,N^i(E)}{2T} \qquad \text{(D-7)}$$

These corrections are also tabulated in Table XVI.

TABLE XVI: TABLE OF A AND B FOR ACCIDENTAL CORRECTIONS

Absorber	Target	Multifold Coincidence	A (or A')	B	% change at 180 Mev	% change at 150 Mev
Carbon	Filled	ABCD	293	0.017	1.13	2.37
	"	AD+BC	211	0.020	0.96	1.76
	"	ABC	4640	0.00236	2.24	3.70
	Empty	ABCD	0.600		1.45	0.99
	"	AD+BC	0.434		1.05	0.71
	"	ABC	1.93		4.63	2.80
Copper	Filled	ABCD	407	0.0078	1.81	2.91
	"	AD+BC	293	0.0092	1.42	2.10
	"	ABC	6360	0.00142	3.80	4.79
	Empty	ABCD	0.915		1.90	1.20
	"	AD+BC	0.648		1.34	0.85
	"	ABC	2.58		5.27	3.09

APPENDIX E. EFFICIENCY CALCULATIONS

Introduction

In order to obtain the absolute value of the cross section it was necessary to know the efficiency of the counter-target system. For this experiment the efficiency function consisted of the product of several effects. Some of the mesons (on the order of 5%) were not stopped by the hydrogen or carbon in the target and consequently did not count. Of those that did stop only a small fraction (2 1/2%) decayed into positrons the paths of which intercepted the counter telescope. Because of range straggling and the initial Michel spectrum only a fraction of those positrons penetrated the telescope. (The fraction varied over a wide range depending on the depth of the counter system.) Finally some positrons (abc t 10%) annihilated in flight and consequently did not count.

The efficiency function can be evaluated in several ways. One possibility is the evaluation of a very difficult numerical integral. Parker[44] has treated a problem somewhat similar to this in K^{o} production. The time for the evaluation of the necessary integrals was on the order of 10 hours for a digital computer with a multiplication time of 100 μs.

A second possibility, and the technique used in this experiment, is to employ a Monte Carlo method. (Cashwell and Everett[81] contains a useful review of the application of the Monte Carlo technique to nuclear detection problems.) Since Monte Carlo calculations attempt to reproduce the physical process

they are often relatively easier to visualize. However they also use enormous blocks of computer time. (The calculation discussed here took on the order of fifty hours to obtain 3% statistics using a University of Illinois computer, the "Illiac", with a multiplication time of 700 μs.)

Several groups have discussed Monte Carlo calculations in connection with the detection of positrons from pion decays. When this type of experiment was first performed by Leiss et al.[5] the calculation was broken into two parts. One Monte Carlo calculation stopped pions in the target and tested the positron directions for intersection with a counter[19]. The second calculation determined range straggling distributions for electrons of various energies in carbon[82]. In another recent experiment Ashkin et al.[37] used a Monte Carlo calculation to determine the efficiency of detection for 70 Mev positrons in a thick telescope. In order to estimate their errors they also did auxiliary calculations in which the energy loss parameters were varied.

In this experiment, unlike the Leiss et al. case, the final counter-target efficiency was determined by one code. The same general plan was used for the target portion. Then if the positron struck the counter it was assigned an energy using a Michel spectrum and allowed to travel through the counter telescope losing energy in nearly the same manner as in the Leiss et al. carbon calculation. The single code was a closer approach to the physical process because it accounted for the correlation between the thickness of the carbon absorber through

which the positron had to pass and the solid angle subtended by the telescope.

A second code was also used to compare the theoretical efficiency predicted with the energy loss parameters to the experimental efficiency using the positron beam. In that case monoenergetic positrons first lost energy in the thin telescope defining the beam and then traveled through the counter in the same way as they did in the main efficiency calculation.

Counter Efficiency

In the Monte Carlo calculation the positron tracks were formed by breaking the path of the positron into many small segments. The positron started at the first segment with an initial energy and then traveled a small distance through the material. In that distance it lost energy by ionization and radiation. The direction of the track was then changed on the basis of a multiple scattering distribution. The process was repeated again with the new energy, angle, and position. Finally, after many such segments, the positron had lost enough energy so that it was effectively stopped or had scattered out of the system.

In low Z materials positrons of less than 50 Mev lose energy mostly by ionization. The most probable energy loss due to ionization in a thin slab of material is nearly constant with energy down to 5 Mev. However individual positrons will lose more or less energy because of the statistical distribution of impact parameters. The distribution in energy loss is satisfactorily described by the Landau distribution for ionization straggling[83].

For positrons a small correction (about -3%) must be applied to the ionization loss formula derived for electrons. The correction comes about because the particles are no longer identical and results in a lowering of the energy loss.

Positrons also lose energy by radiating. This mechanism produces only 40% as much energy loss as that due to ionization at 50 Mev in carbon and decreases as the reciprocal of the energy. However the radiation losses produce a great deal of straggling since the energy lost in the bremsstrahlung process is uniformly distributed from the initial positron kinetic energy to zero energy.

In addition to losing energy, the positrons can also multiply scatter. For positrons of the energy under consideration the projected root mean square angle of multiple scattering increases linearly with decreasing energy. For this reason the positron direction can change drastically near the end of the track.

Finally the positrons can annihilate in flight. The probability for annihilation per unit path length is inversely proportional to energy. As a result counters which detect positrons with low average energy are rather strongly affected by annihilation corrections.

All of these effects depend in some way on the thickness of the incremental slab through which the positron passes. It is desirable for the slab to be thin enough so that in most cases the energy change is slight. Otherwise the radiation loss and multiple scattering parameters change appreciably in the segment.

A thin slab is also useful from the standpoint of calculations since the geometrical effects due to multiple scattering can be treated in the small-angle approximation. However the slab must be thick enough so that many atomic collisions occur. Most important of all from a coding standpoint, computing time depends inversely on the thickness of the slab. In this calculation, segment lengths of 1 cm above 10 Mev and 1/4 cm below 10 Mev were chosen. These values were lower than those chosen by Ashkin et al. and Modesitt[55] but larger than those of Leiss et al.

Ionization losses were treated using the method outlined in the thesis of Mills[41] with slight modifications. Mills relied on the experimental demonstration by Goldwasser et al.[84] that ionization losses in light elements for 10 to 15 Mev electrons are adequately described by the Landau straggling distribution modified by corrections for the density effect. (They found predicted and experimental most probable energy losses agreed to within 2 to 4 percent.) The Landau form with corrections for the density and positron effects is:

$$\Delta = S_o \quad \alpha + \Delta_p \qquad \text{(E-1)}$$

where

$$S_o = .1537 \frac{\sum Z}{\sum A} \rho t \quad \frac{1}{\beta^2} \quad (1 - \epsilon) \quad \text{(in Mev)} \qquad \text{(E-2)}$$

and Δ is the energy lost in Mev, Δ_p is the most probable energy

loss and is equal to $S_o \left[\ln t + 19.43\right]$, α is the universal distribution variable defined by the Landau distribution, ϵ is the fractional correction for positrons, and t is the thickness in cm. (This form applies, strictly speaking, to the extreme relativistic case. The $1/\beta^2$ has been added to make it correspond more closely with the conventional form. However at energies where this correction is important, the form of the density correction is no longer exact.) Mills tabulated the values of α at the edge of 64 bins of equal probability. The last bin was adjusted so that the distribution was truncated at $\alpha = 100$. As a result the relatively improbable large energy losses were treated incorrectly. (Leiss et al. used a better approach by treating the high energy loss tail in terms of an analytic function, but their procedure leads to a more difficult computer calculation.) The positron correction was found from Rossi[85]. In the calculation it was considered a constant although it is a weak function of energy. The constant was determined by averaging the correction from 10 to 40 Mev. In the actual program to determine ionization losses the table of α's was linearly interpolated on the basis of a random number. (Modesitt has given a useful discussion of the interpolation of probability distributions with random numbers.) Separate constants evaluated for 1 cm and 1/4 cm were used for each of the three different materials present (carbon or copper, Pilot B, and Lucite). In cases where the segment length was not 1 cm or 1/4 cm the constants were multiplied by the appropriate thickness in units

of 1 or 1/4 cm.

Radiation straggling was treated by using a probability distribution due to Eyges[86]. The particular form chosen (π_{02} with a = .25, b = 3/4) uses an approximation for the bremsstrahlung spectrum which seems to fit the more exact treatments in the region of 10 to 50 Mev better than the other available approximations. (For small thicknesses and small energy losses this distribution is very similar to that given by Heitler[87].) At 40 Mev the Eyges distribution gives less radiation loss than a theory employing a Bethe-Heitler bremsstrahlung spectrum, while at 10 Mev the Eyges distribution gives more radiation loss. (For the low Z materials of the counter-target system the coulomb corrections of Davies, Bethe and Maximon are not important.) The net effect is to give about the same total radiation loss as a more exact treatment based on a Bethe-Heitler spectrum. Actually the function that was used is more complicated than necessary since it makes allowances for several bremsstrahlung collisions in passing through the segment. In this calculation the segment was a small fraction of a radiation length thick so that multiple radiative collisions occurred infrequently. In the actual distribution, a further approximation is made by assuming that bt is small (t is the thickness in radiation lengths). The distribution is:

$$\pi_{02}(\nu)d\nu = bt \frac{(1.25)^{bt}(1-\nu)^{1/4}}{-\ln(1-\nu)} \left[1 + bt \ln\left\{-\ln(1-\nu)\right\}\right] d\nu \qquad \text{(E-3)}$$

where ν is the fractional energy lost by radiation and $\pi_{02}(\nu)\, d\nu$ is the probability that a positron loses from ν to $\nu + d\nu$ of its initial energy. A reduced probability was formed by dividing the distribution by bt and multiplying it by a standard value $(bt)_1$. The cumulative reduced probability was then:

$$Y_i = (bt)_1 \int_0^{\nu_i} \frac{\pi_{02}(\nu)\, d\nu}{bt} \qquad \text{(E-4)}$$

This had the effect of producing an integral that was very weakly dependent on the length of the segment. The integrals were evaluated for $(bt)_1 = .02588$ (based on .75 cm of carbon of density 1.1) and ν_i was found by setting $P_i = 1 \times 2^{-10}$, 2×10^{-10}, ..., 4×2^{-10}, 2×2^{-8}, ..., 4×2^{-8}, 2×2^{-6}, ..., 16×2^{-6}. (Energy losses less than about $10^{-5}E$ were considered to be zero.) The nonuniform P_i were chosen because the integral changed rapidly for values of ν close to one. ν was found by dividing a random number in the interval 0 to 1 by $bt/(bt)_1$. This gave the reduced probability which was used to linearly interpolate the table of ν_i to obtain a value ν. Finally the energy loss was found by multiplying the energy by ν. The radiation lengths quoted by Bethe and Askin[88] (which include screening effects) were used to evaluate bt for each of the three materials.

Multiple scattering angles were computed using an approximation to the Moliere multiple scattering distribution suggested

by Hanson et al.[89]. They pointed out that the more complicated Moliere distribution could be approximated by a Gaussian with a width slightly reduced in relation to the older theories. They found reasonable agreement between the predictions of the Moliere theory and experiment. (The experimental values for $\theta_{1/e}$ were about 5% lower than the theoretical ones.) Their approximation breaks down at angles greater than 2 $\theta_{1/e}$. Such angles come about because of single scatterings and occur infrequently. Recently Nigram et al.[90] reinvestigated the Moliere formula and suggested second Born approximation corrections which have a strong effect on the large angles. Their formulation gives better agreement with the experimental work of Hanson et al. provided certain assumptions are made concerning screening. Because of such theoretical uncertainties and the additional calculation difficulties the problem of large angles was ignored in the efficiency calculation by assigning an angle of roughly 2 $\theta_{1/e}$ to the last 1/2% of the probability in the distribution. This was also useful from a computational standpoint since it helped to avoid a breakdown in the sin $\theta = \theta$ approximation. The cumulative distribution function was obtained by integrating a Gaussian distribution. Several different probability step sizes (68 bins total) were used to provide better interpolation in the tails. For projected angles the cumulative distribution function (normalized to 1 in the interval 0 to 1) is:

$$P(\alpha_i) = \frac{2}{\sqrt{\pi}} \int_0^{x_i} e^{-x^2} \, dx \qquad \text{(E-5)}$$

where $x = \frac{\alpha}{\theta_{1/e}}$ and $\theta_{1/e} = \chi_c (B-.7)^{1/2}$. ($\chi_c$ and B are defined in Hanson et al.) Typically for Pilot B (ρ = 1.02, H/C = 1.10), $\theta_{1/e}$ proj (radians) = $\frac{2.409\sqrt{t}}{E}$, (E in Mev, t in cm). In the program a table of x_i was interpolated with the absolute value of a random number in the interval $-1 \leq R < 1$. The sign of the random number determined the sign of the angle. α was found by multiplying x by E $\theta_{1/e}$, and dividing by the energy. Values of E $\theta_{1/e}$ were tabulated for each of the substances in the counter at 1 cm and 1/4 cm.

For both Lucite and Pilot B, where more than one element was involved, χ_a^2 was found for carbon. (See Hanson et al. for the definition. χ_a^2 is only weakly dependent on Z.) χ_c^2 was found for carbon in terms of the thickness in radiation lengths. Then the actual thicknesses used in the constants were divided by the radiation lengths for the appropriate substances. (Rossi[85], p. 53, gives the method for evaluating a radiation length for a mixture of elements.)

The probability of annihilation in flight was treated as a correction rather than using a Monte Carlo technique. If $\varphi(E)$ is the cross section for annihilation at a particular energy (see Heitler[87], p. 269) then $E\varphi(E)$ is a weak function of energy. In the program $E\varphi(E)$ was tabulated as a function of energy at 46 discrete energies. $\varphi(E)$ was obtained by interpolating the table with the energy and then dividing by the energy. The probability of annihilation in a segment of length t is $dP = \varphi(E) \frac{N_o \rho \Sigma Z}{\Sigma A} t$.

The probability was accumulated for each segment as the positron passed through a particular counter. The total was assigned as the annihilation probability in that particular counter. At the end of each event the annihilation probabilities for the counters were summed to the front face of the last counter in the coincidence. If the coincidence counted for the event the value was added to a grand total which was averaged at the end of the program to give an average annihilation probability, P_{ijkl}, for a coincidence count. Then the overall efficiency was multiplied by a factor $(1 - P_{ijkl})$ to correct for the possibility of annihilation. This method was used rather than the formula in Heitler (p. 385) because it automatically included the effect of radiation losses.

The positrons were advanced through the counter telescope, segment by segment, using the "segment" subroutine. This routine was central to the entire counter portion of the efficiency calculation. Typically one turn through it took 50 msec and a typical positron track required twenty such loops. When the routine was entered the energy loss constants were set for 1 cm or 1/4 cm depending on whether the positron energy was above or below 10 Mev. Then a test was performed to see if less than 1 cm (or 1/4 cm) remained to the end of the counter. If the remaining distance was less than 1 cm (or 1/4 cm) the energy loss constants were re-evaluated for the decreased length. The position of the positron was advanced using a set of direction cosines generated on the last segment loop. (Thus $x' = x + at$, $y' = y + bt$, $z' = z + ct$ where primes indicate values at the end of the loop

and a, b, c are direction cosines. z is perpendicular to the face of the counter telescope and x is perpendicular to the plane defined by the x ray beam and the perpendicular to the counter telescope) Then the routine computed an ionization and radiation energy loss for the segment, each time testing to see if the total energy had dropped below 1.5 Mev. If the energy was less than 1.5 Mev the event was terminated. After that the annihilation probability for the segment was computed. Then the program computed χ and Ψ, the projected multiple scattering angles. (χ and Ψ are defined in a coordinated system with its z axis along the direction of motion and its y axis perpendicular to the z axis of the counter.) χ and Ψ were small angles except occasionally at very low energies near the end of the track. The same equations were still applied even when the small-angle approximation no longer held, since such cases rarely occurred and were very close to the end of the event. Because of scaling difficulties it was necessary to turn off the multiple scattering in these cases if χ and Ψ or the overall change in angle exceeded 60°.

Under normal conditions the situation mentioned above did not occur and the direction cosines were advanced by the equations:

$$a' = a \cos \theta' - \frac{\{\chi ca - \Psi b\}}{\sqrt{1 - c^2}} \qquad \text{(E-6)}$$

$$b' = b \cos \theta' - \frac{\{\chi cb + \Psi a\}}{\sqrt{1 - c^2}} \qquad \text{(E-7)}$$

$$c' = c \cos \theta' + \chi\sqrt{1-c^2} \qquad \text{(E-8)}$$

where $\cos \theta' = 1 - 1/2\,(\chi^2 + \psi^2)$

Except that if $c = .25$ $(\theta = 0)$

$$a' = -\chi$$

$$b' = -\psi$$

This set of equations was based on a second order approximation. If a first order approximation had been used, c would not have advanced. If c alone had been taken to the second order the sum of the squares of the direction cosines would have exceeded 1 by a larger and larger amount as further segments were considered. The exact equations were not used because the evaluation of the trigonometric function would have required too much computer time. (Cashwell and Everett, p. 103, develops the exact equations.) After the direction cosines were advanced, the angle relative to the z axis was tested to determine if it was greater than 75°. If it was, the event was terminated. The flow chart for the segment subroutine is illustrated in Fig. 38.

The end tests employed were similar to those used by Leiss et al. Trial calculations indicated that the efficiency determination was relatively insensitive to the particular values chosen.

At the beginning of each counter the positron x and y coordinates were tested to see if they exceeded the boundaries of the counter. If the positron was in the boundaries of the

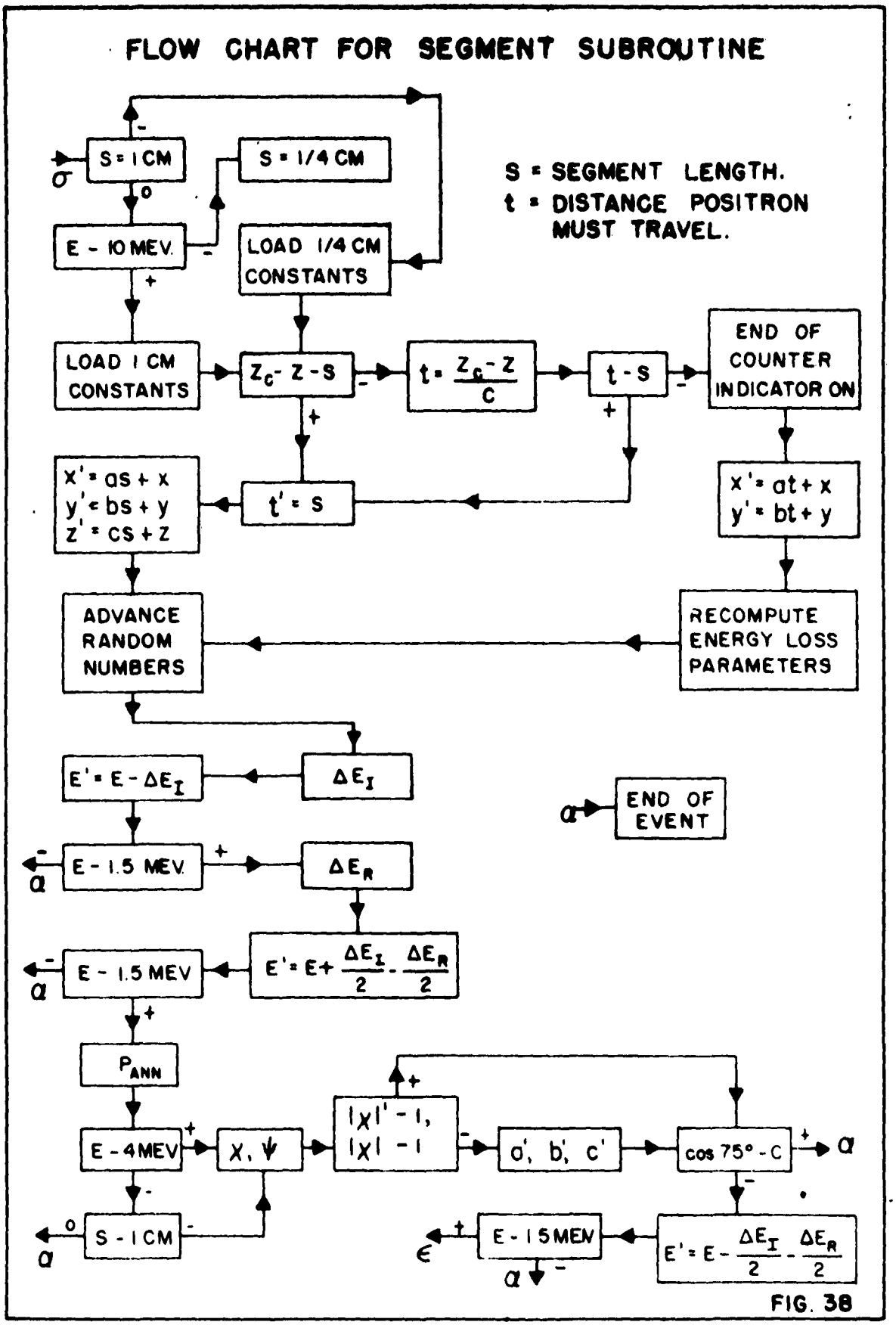
FLOW CHART FOR SEGMENT SUBROUTINE
S = SEGMENT LENGTH.
t = DISTANCE POSITRON MUST TRAVEL.
S = 1 CM
S = 1/4 CM
E - 10 MEV.
LOAD 1/4 CM CONSTANTS
LOAD 1 CM CONSTANTS
$Z_c - Z - S$
$t = \frac{Z_c - Z}{c}$
t - S
END OF COUNTER INDICATOR ON
$x' = as + x$
$y' = bs + y$
$z' = cs + z$
t' = S
$x' = at + x$
$y' = bt + y$
ADVANCE RANDOM NUMBERS
RECOMPUTE ENERGY LOSS PARAMETERS
$E' = E - \Delta E_I$
ΔE_I
END OF EVENT
E - 1.5 MEV.
ΔE_R
E - 1.5 MEV
$E' = E + \frac{\Delta E_I}{2} - \frac{\Delta E_R}{2}$
P_{ANN}
E - 4 MEV
χ, ψ
$|\chi|' - 1, |\chi| - 1$
a', b', c'
cos 75° - C
S - 1 CM
E - 1.5 MEV
$E' = E - \frac{\Delta E_I}{2} - \frac{\Delta E_R}{2}$

FIG. 38

front face it was considered to have counted in that counter. Therefore, from the standpoint of the efficiency calculation, the solid angle was determined by the front face of the counter. In the case of A such a procedure was dangerous because the counter was two inches thick. Consequently the solid angle portion of the ACD efficiency calculation was probably not reliable. However in the case of coincidences employing B as the counter determining the solid angle a reasonable estimate of the possible error in the cross section due to such considerations is two times half the thickness of B divided by the distance to B or roughly 2% .

A small additional thickness was added to the original thickness of each counter to include the effect of the counter wrapping. An equivalent thickness was assigned to the wrapping based on equating the sum of the losses from ionization and radiation for a 20 Mev electron in the wrapping and the original material. In practice the correction was nearly equivalent to adding an additional thickness based on thickness of the wrapping in g/cm^2.

At the end of each event all of the coincidences were tested to see if their respective counters had fired. If they had, the event was scored as a count for the particular coincidence.

Target Efficiency

The target portion of the Monte Carlo calculation was similar to the method used by Leiss et al. and has been described by Penner[19]. Initial meson coordinates were given in a cylindrical coordinate system located at the center of the appendix with the

z_0 axis along the beam and the x_0 axis perpendicular to the plane defined by the beam-counter plane. The meson coordinates were assigned at random in the region defined by the appendix end windows and the beam by letting $r_0 = \sqrt{|R_1|}\ r_b$, and $z_0 = R_0\ l_a/2$, and $\varphi_0 = \pi R_2$ (where R_0, R_1, and R_2 are random numbers in the interval $-1 \leqslant R_1 < 1$).

The meson direction was given in a spherical coordinate system located at the meson origin (with its z axis parallel to the beam) by assuming an isotropic photoproduction cross section in the center of mass. For an isotropic cross section $\cos \theta^* = R_4$ and $\Phi^* = \Phi = \pi R_3$. $\cos \theta^*$ was used to interpolate the revised Malmberg and Koester[91] dynamics tables at the particular gamma ray energy in order to obtain the range of the meson in carbon and liquid hydrogen and its angle to the z axis in the laboratory system.

The ranges had previously been obtained at the kinetic energies tabulated in the Malmberg and Koester tables by using three empirical range formulas:

$$R\ (\text{hydrogen}) = .00369\ T^{1.830}$$

$$R\ (\text{carbon}) = .0103\ T^{1.769}$$

$$R\ (\text{copper}) = .0141\ T^{1.778}$$

(Where the kinetic energy is in Mev and the ranges are in g/cm^2.) These formulas were chosen to closely match the ranges given in UCRL 2426 (Rev.) II[92] over the energy region from one to thirty Mev.

The kinetic energies at particular photon energies and angles in the revised Malmberg and Koester tables are several Mev larger than those given in the original tables (used by Leiss et al.).

The stopping point of the meson was determined assuming it had traveled only in hydrogen. If the point was outside the hydrogen appendix, the distance the meson traveled in hydrogen was converted to an equivalent carbon (or copper) thickness and subtracted from the carbon (or copper) range. The equivalent thickness was computed on the basis of relative ionization losses at 14 Mev. The stopping point was recomputed using the carbon (or copper) range and tested to see if it was within the absorber. If it was outside, the event was rejected and a new meson was started. Fig. 39 is the flow chart for this portion of the process.

The range of the muon was neglected. In hydrogen it is about 1 cm. Similarly, small perturbations due to pion decays in flight were neglected.

A spherical coordinate system was located with its origin at the meson stopping point and its z axis perpendicular to the face of the counter telescope. The positrons were confined to a cone of angles $\theta' < \theta'_{max}$ in order to utilize a smaller number of events. θ'_{max} was large enough (35°) so that the A counter was always fully illuminated. The positron angles were assigned using $\cos \theta' = 1 - N|R_7|$, $\Omega' = \pi R_6$ ($N = 1 - \cos \theta'_{max}$). The final raw value of the efficiency for a particular coincidence, given by the number of such coincidences in the counter system divided by the number of mesons started, was multipled by N/2 to compensate

CONDENSED FLOW CHART FOR TARGET SUBROUTINE

$\beta \longrightarrow$ NEW EVENT

$$d_H^{(1)} = \frac{-r_0 \cos(\phi_0 - \Phi)}{\sin\Theta} + \frac{1}{\sin\Theta}\sqrt{r_a^2 \; r_0^2 \sin^2(\phi_0 - \Phi)}$$

$$d_H^{(2)} = \frac{L_a/2 - Z_0}{\cos\Theta}$$

p = DISTANCE MESON TRAVELS TO ABSORBER.

d = DISTANCE MESON TRAVELS IN HYDROGEN.

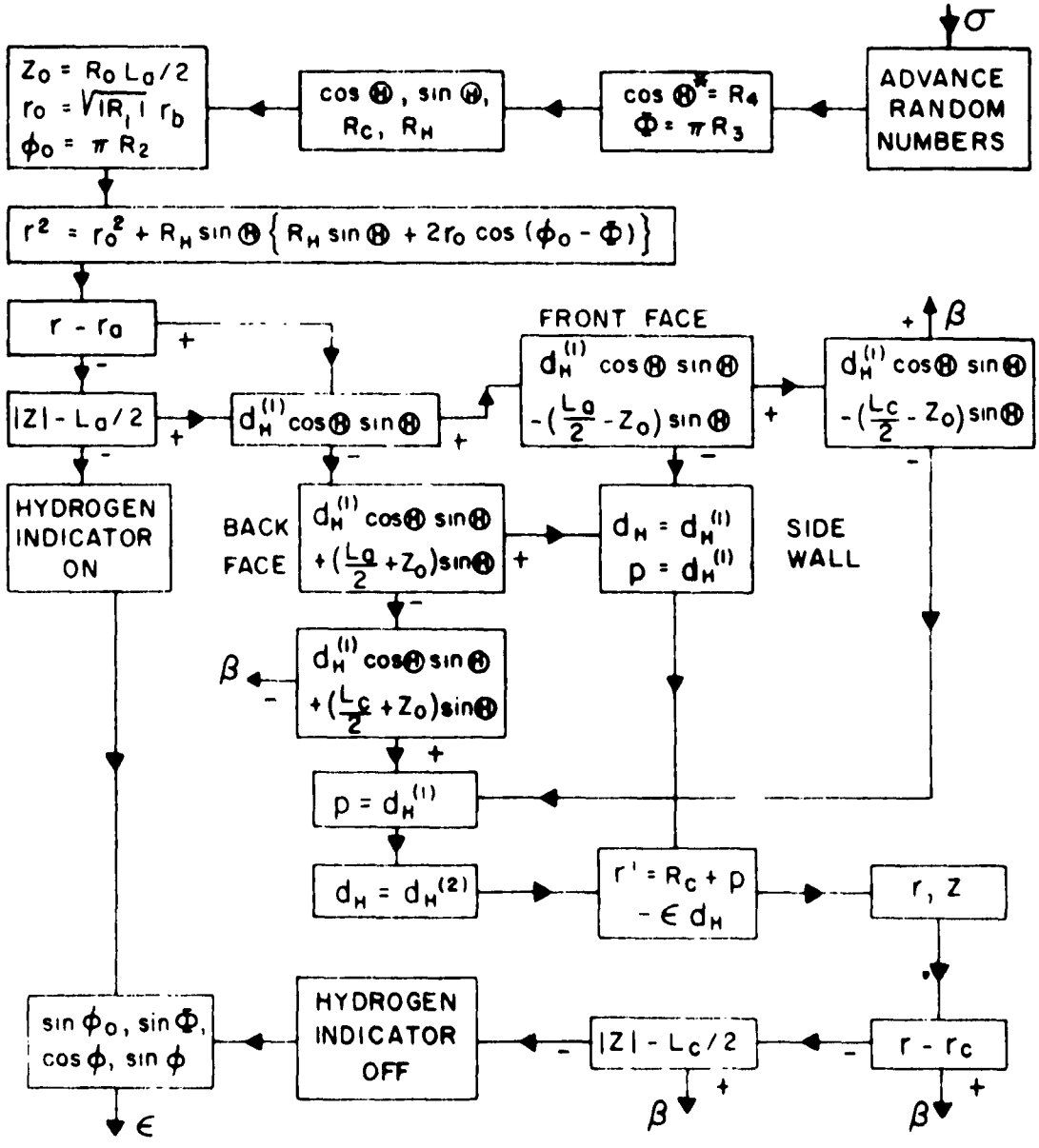

FIG. 39

the restriction on the solid angle.

Then θ' and ϕ' were used to find the intersection of the positron direction with the plane of the front face of A. The coordinates of the intersection were tested to see if they were within the A boundaries. If they were not the event was rejected and a new meson was started. If the positron direction intercepted the front face of A, the distance the positron traveled through the absorber was computed. (Cashwell and Everett, p. 43, outlines the method used in this calculation.) An equivalent thickness correction was also made for any hydrogen the positron passed through. In addition, a small, constant, equivalent thickness was added to account for the vacuum jacket, radiation shields, and the front wrapping on A.

At that point the positron was assigned an energy using the form of the Michel distribution given by Dudziac et al[38]. The distribution was handled in the same manner as those employed for the energy loss parameters. It was integrated to obtain values of the energy at the edge of 32 bins of equal probability. These energies were linearly interpolated with a random number to obtain the positron energy for a particular event.

The positron then lost energy by ionization and radiation and accumulated some probability of annihilation based on the thickness of the absorber through which it had passed. Multiple scattering was not included at this point because the original positron distribution was isotropic and no net change would have resulted (at least to first order). From that point on, the positron was handled by the counter portion of the code.

Computing Factors

Illiac library subroutine V9 was used as the pseudo-random number generator. It employs a complicated algorithm based on convenient machine operations to rearrange the bits of five starting numbers without resorting to multiplication. It is capable of producing 5 random numbers in 3 ms (roughly four equivalent multiplications). The sequence of numbers has been found not to repeat within the first 10 million numbers. In these calculations essentially all of the first 10 million numbers were used.

The two final efficiency calculations required roughly six man months to program (including the time to formulate the necessary equations). The final target-counter efficiency program was about 1800 words long, making it necessary to store portions of the program on the magnetic drum. The 1800 words were broken down into 250 words of library routines, 450 words of stored tables, 100 words of constants, and 1000 words of order pairs. In addition 170 words were required for temporary storage.

Summary

The efficiencies, $F_1(E)$ for the counter-target system as determined by the Monte Carlo program are tabulated in Table XVII as a function of coincidence, gamma ray energy, and absorber. The actual efficiencies used in the experimental analysis were obtained by smoothing the Monte Carlo values with least-squares fits.

Also tabulated in Table XVII are:

1) H(E) = the percentage of mesons stopped in the target.

2) SA(A) = the effective solid angle subtended by A.

3) SA(B) = the effective solid angle subtended by B.

4) P_A = the correction applied for annihilation.

The uncertainty given is $\epsilon = 100/\sqrt{n}\,\%$ where n was the total number of counts in the Monte Carlo evaluation for the particular coincidence at the energy.

The efficiency for ABCD with a carbon absorber as a function of energy is illustrated in Fig. 40. The solid line is the least-squares fit to the Monte Carlo points.

The efficiency for ABCD was also calculated using the method of Leiss et al. as a check. Penner's distribution of positron paths in carbon was renormalized to the new absorber. In addition annihilation corrections were included. These values are also shown in Fig. 40. They agree quite closely with the values calculated using the new method.

The predicted efficiencies, $F_1(E)$, for the experimental measurement of the counter-telescope efficiency with a positron beam are tabulated in Table XVIII. The particular set is for the case of the beam striking the center of the counter telescope.

TABLE XVII: EFFICIENCY FACTORS FOR THE COUNTER-TARGET SYSTEM.

Absorber	Copper	Carbon					
Energy (Mev)	178	178	174	170	166	162	158	154
H(E)	.9288	.9028	.9151	.9244	.9296	.9317	.9531	.9714
SA(A)x10^2	2.664	2.617	2.588	2.595	2.556	2.631	2.650	2.696
SA(B)x10^2	.7114	.6989	.7125	.7160	.7082	.7319	.7327	.7239
ABC								
F(E)x10^3	2.232	3.588	3.694	3.610	3.620	3.928	4.084	4.197
ϵ(%)	3.59	2.27	2.24	2.28	2.32	2.28	2.26	2.27
P_A	.0924	.0862	.0872	.0897	.0897	.0887	.0855	.0837
ACD								
F(E)x10^3	1.838	3.806	3.669	3.557	3.408	3.848	4.178	4.369
ϵ(%)	3.88	2.15	2.19	2.24	2.34	2.24	2.18	2.17
P_A	.1274	.1274	.1298	.1322	.1332	.1334	.1306	.1282
ABCD								
F(E)x10^3	0.658	1.332	1.369	1.258	1.234	1.396	1.505	1.577
ϵ(%)	6.47	3.63	3.58	3.75	3.87	3.72	3.62	3.60
P_A	.1314	.1320	.1353	.1362	.1388	.1369	.1341	.1321
ABCDE								
F(E)x10^3	0.380	0.824	0.836	0.778	0.735	0.889	0.956	1.016
ϵ(%)	8.49	4.59	4.55	4.74	4.98	4.62	4.50	4.45
P_A	.1398	.1403	.1465	.1483	.1486	.1514	.1471	.1448

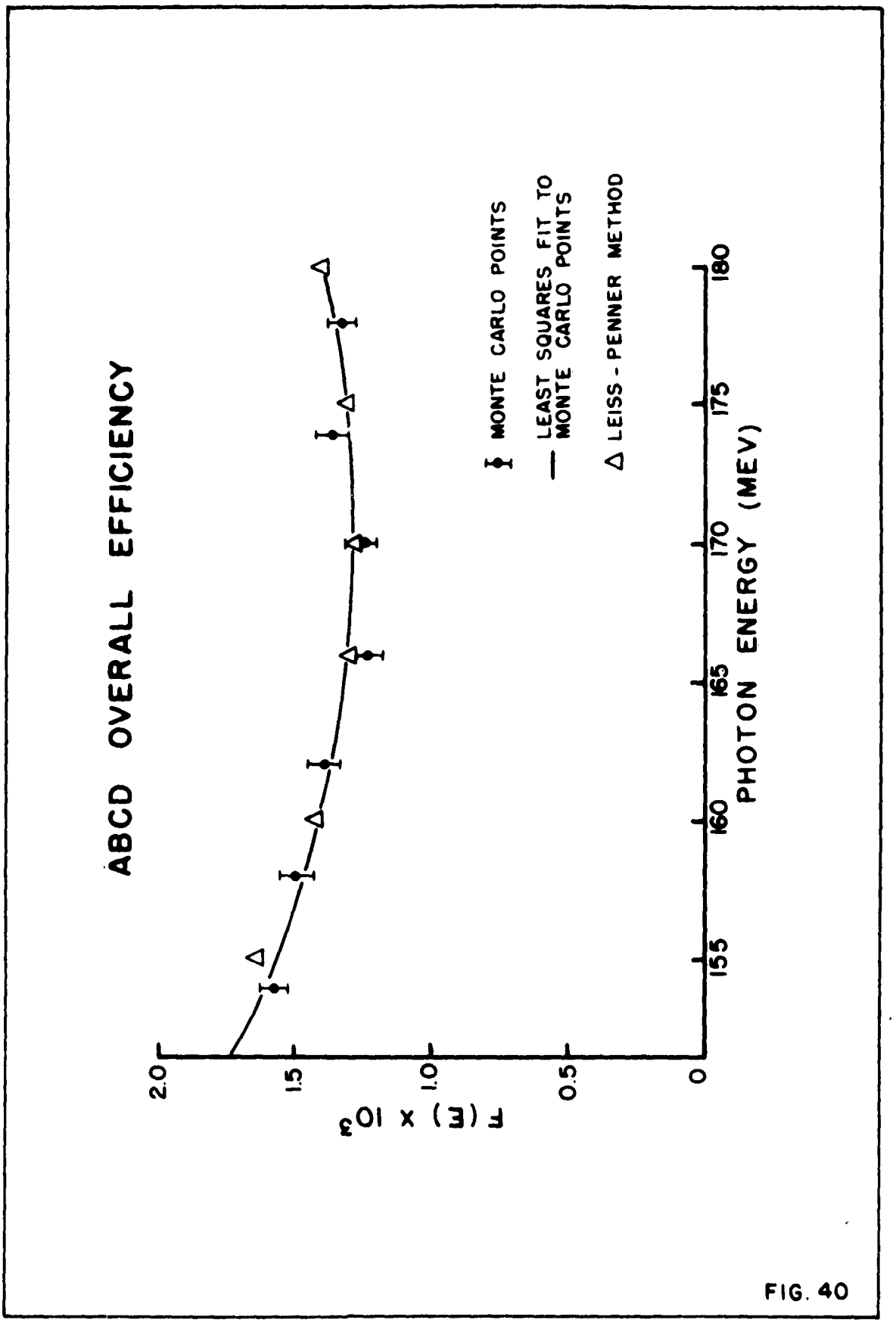
ABCD OVERALL EFFICIENCY
MONTE CARLO POINTS
LEAST SQUARES FIT TO MONTE CARLO POINTS
LEISS - PENNER METHOD
T (E) x 10³
2.0
1.5
1.0
0.5
0
155
160
165
170
175
180
PHOTON ENERGY (MEV)

FIG. 40

TABLE XVIII: THEORETICAL EFFICIENCY FACTORS FOR THE POSITRON BEAM CALIBRATION OF THE COUNTER TELESCOPE EFFICIENCY.

Energy (Mev)	61.9	50.8	39.6	28.0
ABC				
$F_1(E)$	.964	.951	.920	.850
ϵ(%)	2.68	2.69	2.72	2.80
P_A	.028	.034	.043	.064
ABCD, ACD				
$F_1(E)$	.871	.798	.652	.097
ϵ(%)	2.78	2.88	3.14	7.84
P_A	.062	.076	.104	.163
ABCDE				
$F_1(E)$	.829	.727	.490	.002
ϵ(%)	2.83	2.99	3.58	15.80
P_A	.072	.089	.121	.189

BIBLIOGRAPHY

1. H. L. Anderson and E. Fermi, Phys. Rev. 86, 794 (1952).
2. M. Beneventano, G. Bernardini, D. Carlson-Lee, G. Stoppini, and L. Tau, Nuovo Cimento 4, 323 (1956).
3. M. Cini, R. Gatto, E. L. Goldwasser, and M. Ruderman, Nuovo Cimento 10, 243 (1958).
4. A. Barbaro, E. L. Goldwasser, and D. Carlson-Lee, Bull. Am. Phys. Soc. Ser. II, 4, 23 (1959).
5. J. E. Leiss, S. Penner, and C. S. Robinson, Phys. Rev. 98, 1188 (1955).
6. S. Penner and C. S. Robinson, Bull. Am. Phys. Soc. Ser. II, 1, 173 (1956).
7. J. E. Leiss and S. Penner, Bull. Am. Phys. Soc. Ser. II, 4, 273 (1959).
8. W. P. Swanson, Ph.D. Thesis, UCRL-9194 (1960), p. 96.
9. R. C. Miller, Phys. Rev. 95, 796 (1954).
10. E. L. Goldwasser, Lecture Notes on Mesons and High Energy Nuclear Physics (Unpublished).
11. É. G. Gorzhevskaya, V. M. Popova, and F. R. Yagudina, Soviet Physics, JETP 11, 200 (1960).
12. M. I. Adamovich, É. G. Gorzhevskaya, V. G. Larionova, V. M. Popova, S. P. Kharlamov, and F. R. Yagudina, Soviet Physics, JETP 11, 779 (1960).
13. G. M. Lewis and R. E. Azuma, Proc. Phys. Soc. (London) 73, 873 (1959).
14. J. G. Rutherglen, J. Walker, D. Miller, and J. M. Patterson, Proceedings of the 1960 Annual International Conference on High Energy Physics at Rochester.
15. R. R. Wilson, Nuclear Instruments 1, 101 (1957).
16. D. C. Gates, R. W. Kenney, D. A. McPherson, and W. P. Swanson, Rev. Sci. Instr. 31, 565 (1960).
17. G. Bernardini and E. L. Goldwasser, Phys. Rev. 95, 857 (1954).

18. J. E. Leiss, Ph.D.Thesis, University of Illinois (1954).

19. S. Penner, Ph.D. Thesis, University of Illinois (1956).

20. G. F. Chew, M. L. Goldberger, F. E. Low, and Y. Nambu, Phys. Rev. 106, 1345 (1957).

21. G. F. Chew, Phys. Rev. 94, 1748 (1954).

22. G. F. Chew, Phys. Rev. 94, 1755 (1954).

23. G. F. Chew, Phys. Rev. 95, 1669 (1954).

24. M. Gell-Mann and K. M. Watson, Ann. Rev. Nuclear Sci. 4, 219 (1954).

25. A. M. Baldin and B. B. Govorkov, Nuclear Phys. 13, 193 (1959).

26. E. Fermi, Sup. Nuovo Cimento 2, 17 (1955).

27. W. O. Lock, High Energy Nuclear Physics, Methuen, London (1960), p. 98.

28. M. J. Moravcsik, Phys. Rev. 104, 1451 (1956).

29. J. H. Malmberg and C. S. Robinson, Phys. Rev. 109, 158 (1958).

30. G, Bernardini, Sup. Nuovo Cimento 2, 104 (1955).

31. H. Bethe and F. de Hoffmann, Mesons and Fields, Row, Peterson, and Co., Evanston (1955), p. 174.

32. S. Gartenhaus and R. Blankenbecler, Phys. Rev. 116, 1305 (1959).

33. G. Höhler and K. Dietz, Z. Physik 160, 453 (1960).

34. G. Jona-Lasinio and H. Munczek, Phys. Rev. 117, 585 (1960).

35. J. Hamilton and W. S. Woolcock, Phys. Rev. 118, 291 (1960).

36. A. M. Baldin, Soviet Physics-JETP 39, 1151 (1960).

37. J. Ashkin, T. Fazzini, G. Fidecaro, A. W. Merrison, H. Paul, and A. V. Tollestrup, Nuovo Cimento 13, 1240 (1959).

38. W. F. Dudziak, R. Sagane, and J. Vedder, Phys. Rev. 114, 336 (1959).

39. J. H. Malmberg, Ph.D. Thesis, University of Illinois (1957).

40. E. A. Whalin, Jr. and R. A. Reitz, Rev. Sci. Instr. 26, 59 (1955).

41. F. E. Mills, Ph.D. Thesis, University of Illinois (1955).

42. R. S. Jones, Ph.D. Thesis, University of Illinois (1961).

43. H. K. Schoenwetter, Rev. Sci. Instr. 24, 515 (1953).

44. S. Parker, Ph.D. Thesis, University of California, UCRL-8754 (1959).

45. P. Baum, private communication.

46. R. S. Jones, private communication.

47. P. Cziffra and M. J. Moravscik, A Practical Guide to the Method of Least Squares, UCRL-8523 (1958).

48. A. S. Penfold and J. E. Leiss, Analysis of Photo Cross Sections, Physics Research Laboratory Report (1958).

49. H. W. Koch and J. W. Motz, Revs. Modern Phys. 31, 920 (1959).

50. U. Fano, H. W. Koch, and J. W. Motz, Phys. Rev. 112, 1679 (1958).

51. E. G. Fuller, E. Hayward, and H. W. Koch, Phys. Rev. 109, 630 (1958).

52. H. E. Hall, Ph.D. Thesis, University of Illinois (1961).

53. J. E. Leiss, private communication.

54. A. S. Penfold and J. E. Leiss, Phys. Rev. 114, 1332 (1959).

55. G. E. Modesitt, Ph.D. Thesis, University of Illinois (1958).

56. W. H. Barkas and A. H. Rosenfeld, UCRL-8030-rev. (1961).

57. R. J. Plano, Nevis Cyclotron Laboratory Report 87 (1960).

58. H. P. Noyes and D. N. Edwards, Phys. Rev. 118, 1409 (1960).

59. J. S. Ball, Phys. Rev. Letters 5, 73 (1960).

60. B. De Tollis, E. Ferrari, and H. Munczek, Nuovo Cimento 18, 198 (1960).

61. M. Gourdin, D. Lurié, and A. Martin, Nuovo Cimento 18, 933 (1960).

62. J. K. Walker, Nuovo Cimento 21, 577 (1961).

63. P. D. Edwards and D. W. Kerst, Rev. Sci. Instr. 24, 490 (1953).

64. J. E. Leiss, J. S. Pruitt, and R. A. Schrack, National Bureau of Standards Report 6149 (1958).

65. J. S. Pruitt and S. R. Domen, National Bureau of Standards Report 6218 (1958).

66. J. W. Boag, Brit. J. Radiol. 23, 601 (1950).

67. B. B. Rossi and H. H. Staub, Ionization Chambers and Counters, McGraw-Hill, New York (1949), p. 29.

68. C. S. Robinson, Further note on the NTP conditions referred to in the Edwards and Kerst article on the calorimetric calibration of the Illinois 300 Mev X ray beam, Physics Research Laboratory internal note (1958). First note dated Mar. 27, 1958 should be disregarded.

69. W. Blocker, R. W. Kenney, and W. K. H. Panofsky, Phys. Rev. 79, 419 (1950).

70. J. W. DeWire, Calibration Data for the Quantameter and the Cornell Thick-Walled Ionization Chamber, Cornell internal report (1959). The calibration referred to is one performed in 1952.

71. F. J. Loeffler, T. R. Palfrey, and G. W. Tautfest, Nuclear Instruments 5, 50 (1959).

72. A. P. Komar and S. P. Kruglov, Soviet Physics-Tech. Phys. 5, 1299 (1961).

73. E. M. McMillan, W. Blocker, and R. W. Kenney, Phys. Rev. 81, 455 (1951).

74. L. J. Koester, Jr., On the Response of Flat Ionization Chambers, Physics Research Laboratory internal report (1958).

75. R. R. Wilson, Phys. Rev. 86, 261 (1952).

76. "Bass Drum Calibration and Other Pertinent Data", a Physics Research Laboratory internal note, condensed information from the ion chamber log book from June 25, 1953 to February, 1957.

77. C. S. Robinson, Tables of Cross Sections for π^+ Photoproduction from Hydrogen, According to the Theory of Chew, Goldberger, Low and Nambu, University of Illinois (1959).

78. C. L. Rogers, Energy Calibration Report on University of Illinois 300 Mev Betatron, Physics Research Laboratory Internal Report (1959).

79. J. Stahlke, Engineering Report on Electron Spin Resonance Magnetometer (ESRM), Physics Research Laboratory Internal Report (1960).

80. J. Stahlke, Accuracy Tests on the ESR Magnetometer, Physics Research Laboratory Internal Report (1960).

81. E. D. Cashwell and C. J. Everett, A Practical Manual on the Monte Carlo Method for Random Walk Problems, Pergamon Press, New York (1959).

82. J. E. Leiss, S. Penner, and C. S. Robinson, Phys. Rev. 107, 1544 (1957).

83. L. Landau, J. Phys. (U.S.S.R.) 8, 201 (1944).

84. E. L. Goldwasser, F. E. Mills, and A. O. Hanson, Phys. Rev. 88, 1137 (1952).

85. B. B. Rossi, High-Energy Particles, Prentice-Hall, New York (1952).

86. L. Eyges, Phys. Rev. 76, 264 (1949).

87. W. Heitler, The Quantum Theory of Radiation, Third Ed., Oxford University Press, London (1954).

88. E. Segre, ed., Experimental Nuclear Physics, Vol. 1, Wiley, New York (1953).

89. A. O. Hanson, L. H. Lanzl, E. M. Lyman, and M. B. Scott, Phys. Rev. 84, 634 (1951).

90. B. P. Nigram, M. K. Sundaresan, and Ta-You Wu, Phys. Rev. 115, 491 (1959).

91. J. H. Malmberg and L. J. Koester, Tables of Nuclear Reaction Kinematics at Relativistic Energies, Second Ed., University of Illinois (1960).

92. J. H. Atkinson, Jr. and Beverly Hill Willis, UCRL-2426 II (Rev.) (1957).